IRON-FORMATION PROTOLITH AND GENESIS, CUYUNA RANGE, MINNESOTA

Peter L. McSwiggen, G.B. Morey, and Jane M. Cleland

UNIVERSITY OF MINNESOTA

Saint Paul — 1995

IRON-FORMATION PROTOLITH AND GENESIS,

CUYUNA RANGE, MINNESOTA

CONTENTS

ILLUSTRATIONS

TABLES

IRON-FORMATION PROTOLITH AND GENESIS, CUYUNA RANGE, MINNESOTA

By

Peter L. McSwiggen, G.B. Morey, and Jane M. Cleland

ABSTRACT

The Cuyuna iron range in east-central Minnesota is unique in the Lake Superior region because of its large manganiferous iron ore resource. The protolith to the ore has traditionally been considered a Lake Superior-type iron-formation similar to other Early Proterozoic iron-formations in the region. However, recent stratigraphic, mineralogical, and geochemical studies show that the Trommald Formation—the principal iron-formation of the Cuyuna North range—is not the product of a simple sedimentological regime. The presence of the minerals aegirine, barite, Ba-feldspar, and tourmaline within or associated with the iron-formation shows that hydrothermal and exhalative processes were very important during deposition of the iron-rich strata. This new interpretation has significant implications for mineral exploration in this part of Minnesota. It implies that parts of the Cuyuna range may be likely areas for exploration for sediment-hosted, submarine exhalative, Pb-Zn-Ag deposits.

INTRODUCTION

The Cuyuna range in east-central Minnesota (Fig. 1) was a major producer of iron ore for 80 years. Between discovery in 1904 and closing in 1984 the range shipped more than 106 million tons, much of which was manganiferous iron ore that contained more than 10 percent manganese. It is that manganese component that sets the Cuyuna range apart from other Early Proterozoic iron mining districts in the Lake Superior region. The range still contains an appreciable manganese resource (Lewis, 1951; Beltrame and others, 1981) that is approximately 46 percent of the identified resource in the United States (Dorr and others, 1973). Much of the resource is located on the Cuyuna North range where most of the mining took place and consequently where there is an extensive analytical data base. Beltrame and others (1981) have estimated that a minimum of 170 million metric tons of manganiferous iron ore, with an average grade of 10.46 weight percent Mn, can be found. These estimates have changed little over the past 20 years.

It has never been feasible, economically, to recover manganese from the North range, mainly because metallurgical methods could not effectively separate manganese from the iron without expending large quantities of energy. However, the U.S. Bureau of Mines has now developed mining techniques that apparently can extract manganese from associated iron in situ. In support of that effort, the Minnesota Geological Survey undertook to develop a better understanding of the protolith to the manganiferous iron ores on the North range (Fig. 1). This study chiefly analyzed drill core obtained by the Minnesota Geological Survey during an evaluation of the manganese potential of the range at the beginning of World War II (Grout 1941). From that evaluation, further detail was published ultimately in Grout and Wolff (1955). This study builds on that work.

REGIONAL GEOLOGIC SETTING

Our view of the stratotectonic evolution of the Cuyuna range has changed considerably from that of Grout and his generation (Southwick and others, 1988). The tectonic framework is now envisioned as the product of a collisional event—the Penokean orogeny of Goldich and others (1961)—between 1900 and 1760 Ma, with most activity in the interval between 1870 and 1850 Ma (Morey and Van Schmus, 1988). We now think that the zone of deformed rocks produced by the Penokean orogeny and earlier Early Proterozoic tectonic events, which includes the South range and contiguous areas to the south and east, consists of an allochthonous fold-and-thrust belt that contains several structural discontinuities which probably are zones of thrusting. The discontinuities bound discrete structural panels or enclaves that possess small-scale structural features consistent with large-scale north-northwest-
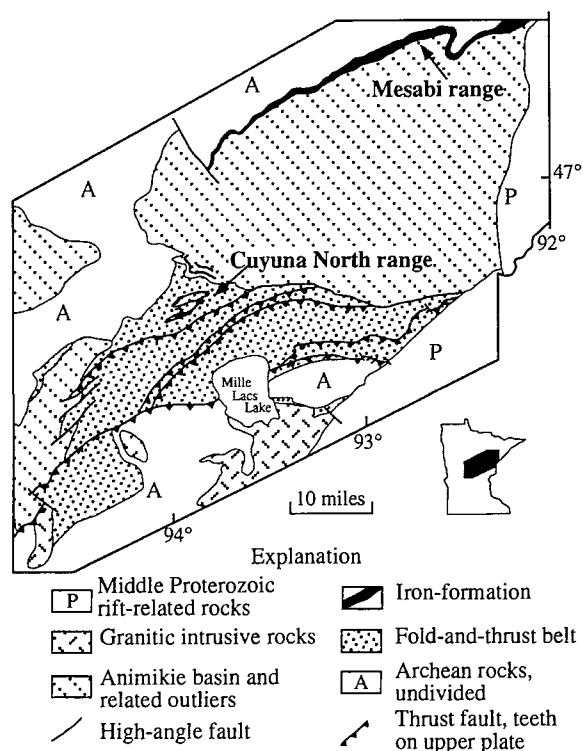
Figure 1. Generalized geologic framework of the Penokean orogen in east-central Minnesota (after Southwick and others, 1988).

Explanation

P	Middle Proterozoic rift-related rocks	▨	Iron-formation
	Granitic intrusive rocks		Fold-and-thrust belt
	Animikie basin and related outliers	A	Archean rocks, undivided
╱	High-angle fault	⫽	Thrust fault, teeth on upper plate

verging nappes (Holst, 1984; Southwick and Morey, 1991). The belt of strongly deformed rocks flanks a tectonic foredeep which extends to the Mesabi iron range in northern Minnesota where rocks of the well-known Animikie Group are exposed. Because the basin is filled with strata that can be assigned to the Animikie Group, Southwick and others (1988) have referred to the foredeep as the Animikie basin, a usage somewhat at odds with that in the earlier literature (Trendall, 1968; Morey, 1983).

The structural studies of Southwick and others (1988) also showed that iron-formation was deposited at different times in different parts of the Penokean orogen (Fig. 1). Thus earlier stratigraphic interpretations founded on the hypothesis of a single iron-rich interval are no longer valid. This change in stratigraphic thinking is important in understanding the origin of the manganiferous iron ores. We can no longer extrapolate sedimentological and mineralogical attributes from one part of the range to another. Therefore the geology of each district must be evaluated separately, because each can have its own unique stratigraphic and tectonic history, even though the deposits themselves may share many similar attributes.

The emphasis of this report is on the geologic factors that control the distribution of manganese in the North range. What follows is a brief description of the structural and stratigraphic attributes of the iron-rich host rocks, together with a summary of their principal sedimentological attributes. A description also is given of the extent, location, and origin of the manganese-bearing materials that occur within the iron-formation. Although preliminary in nature, this report provides some of the geologic data necessary for the ultimate economic utilization of the manganese deposits.

LOCAL GEOLOGIC SETTING

The stratigraphic sequence in the Cuyuna North range terranes includes the Mille Lacs Group of Morey (1978) and the North range group of Southwick and others (1988). The Mille Lacs Group is poorly documented, but the North range group consists of the three lithostratigraphic units that were originally named and defined by Schmidt (1963)—(1) the Mahnomen Formation, a lower quartz-rich sandstone-siltstone sequence; (2) the Trommald Formation, a middle iron-rich and locally manganese-rich sequence; and (3) the Rabbit Lake Formation, an upper black shale-graywacke interval. In addition, Southwick and others (1988) have recognized at least two other major iron-rich intervals in the middle part and a third smaller interval in the upper part of the Mahnomen Formation. The Trommald Formation is the main iron-formation of the North range. It was extensively drilled during exploration for iron ore in the early part of the century and as a result its map distribution is fairly well known (Schmidt, 1963; Morey and Morey, 1986). However, the underlying and overlying units, and especially the Mahnomen Formation, remain poorly understood.

Much of the following discussion is based on core data from the Merritt, Arko, Northland, and North Hillcrest mines (Fig. 2), supplemented by mine descriptions of Schmidt (1963). Composite logs of those sites are given in Figures 3-6.

Rabbit Lake Formation

The Rabbit Lake Formation is the uppermost lithostratigraphic unit in the North range group. Of the four cores studied, it was intersected only at the Merritt site (Fig. 3) where it consists of approximately 50 feet of gray phyllite. The more extensive descriptions of Schmidt (1963) show that this formation also contains intervals of metasiltstone and metagraywacke and may be more than 2000 feet thick. Others have reported that the Rabbit Lake Formation contains intervals of volcanic material and lean iron-formation (Melcher and others, 1996). A sharp contact separating the Rabbit Lake from the underlying Trommald Formation implies that chemical precipitation was abruptly overwhelmed by terrigenous sedimentation. Thin units of chert and iron-formation interlayered with the clastic sediments mark the periodic return to chemical
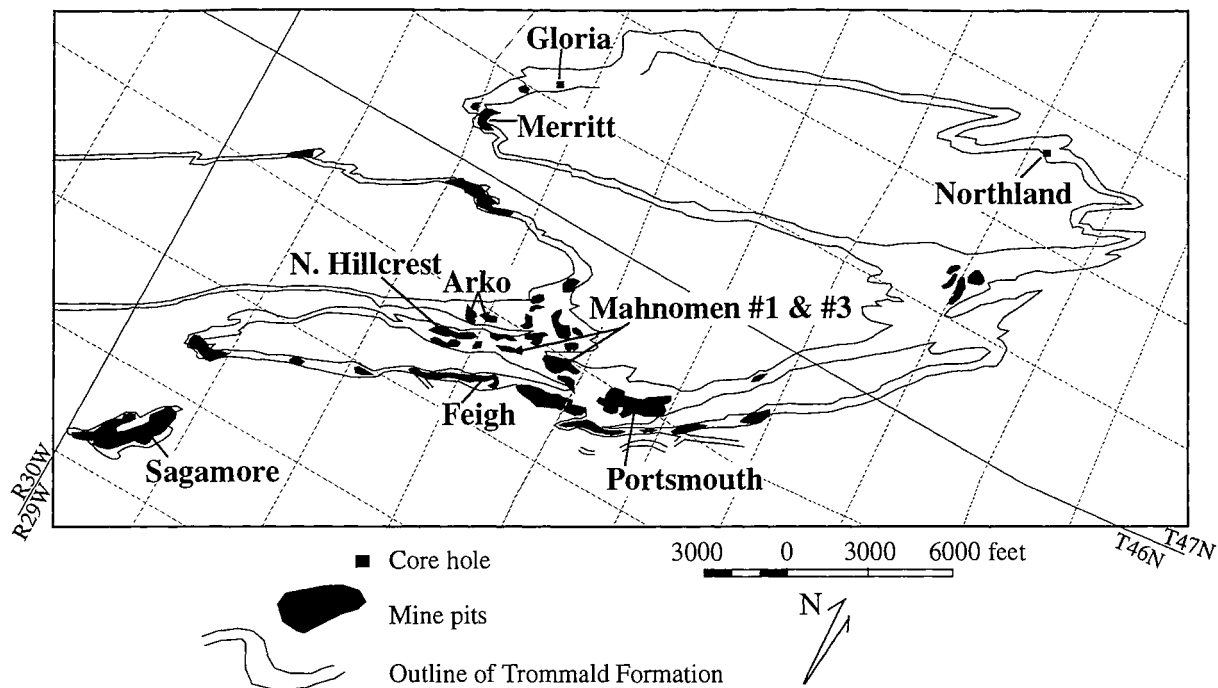
Figure 2. Locations of Cuyuna North range mines and drill holes.

sedimentation in early Rabbit Lake time. It is generally assumed that the influx of clastic detritus at the beginning of Rabbit Lake time corresponds to a period of pronounced foundering of the depositional basin (e.g., Morey, 1983).

Trommald Formation

The Trommald Formation is the principal iron-formation of the North range. Schmidt (1963) divided it into two units—a thick-bedded facies and a thin-bedded facies. Our upper member—a red, thick-bedded, manganese- and hematite-rich, oxide iron-formation—is equivalent to Schmidt's thick-bedded facies. However, we found it useful to divide Schmidt's thin-bedded facies into two informal units—a middle member composed of black, laminated, carbonate-silicate iron-formation and a lower member composed of gray, thin-bedded, carbonate-silicate iron-formation. The contact separating the upper and middle members is sharply defined over an interval of only a few centimeters, whereas the contact between the middle and lower members is gradational over several feet. The middle and lower members of this report together are roughly equivalent to the so-called green carbonate slate of Grout and Wolff (1955).

The three members are unevenly distributed across the North range. The Trommald Formation consists of only the laminated and thin-bedded carbonate-silicate iron-formation over a broad arc-shaped zone that extends from the north side of the range, around on the east to the south side (Fig. 7). Manganese- and hematite-rich oxide iron-

formation overlies the carbonate-silicate iron-formation in the central part of the range, and the Trommald Formation consists of only the hematite-rich iron-formation, which lacks manganese, in the western part of the range. These stratigraphic relationships imply that the two types of iron-formation were deposited in considerably different sedimentological regimes and that the boundary between these regimes migrated to the northeast through time.

Mixed with the iron-formation are a variety of rock types from sedimentary to igneous. Schmidt (1963) recorded the dominant host rocks in most of the mine pits of the North range. The data suggest that the southernmost part of the iron-formation contains the greatest abundance of igneous rocks (Fig. 8).

Upper Member

The upper member of the Trommald Formation was first described as a cherty iron-formation (Grout and Wolff, 1955). However, thick stratigraphic intervals lack appreciable chert, and consequently Schmidt (1963) preferred the term thick-bedded for this part of the iron-formation. We prefer "upper member" because thin beds of silicate- and oxide-rich iron-formation are intercalated within thick intervals of massive, granular iron-formation.

Much of the upper member in the Merritt core, previously described as chert or jasper, in fact consists of cryptocrystalline aegirine or rhodonite intergrown with hematite. The upper member also contains discrete grains of

3
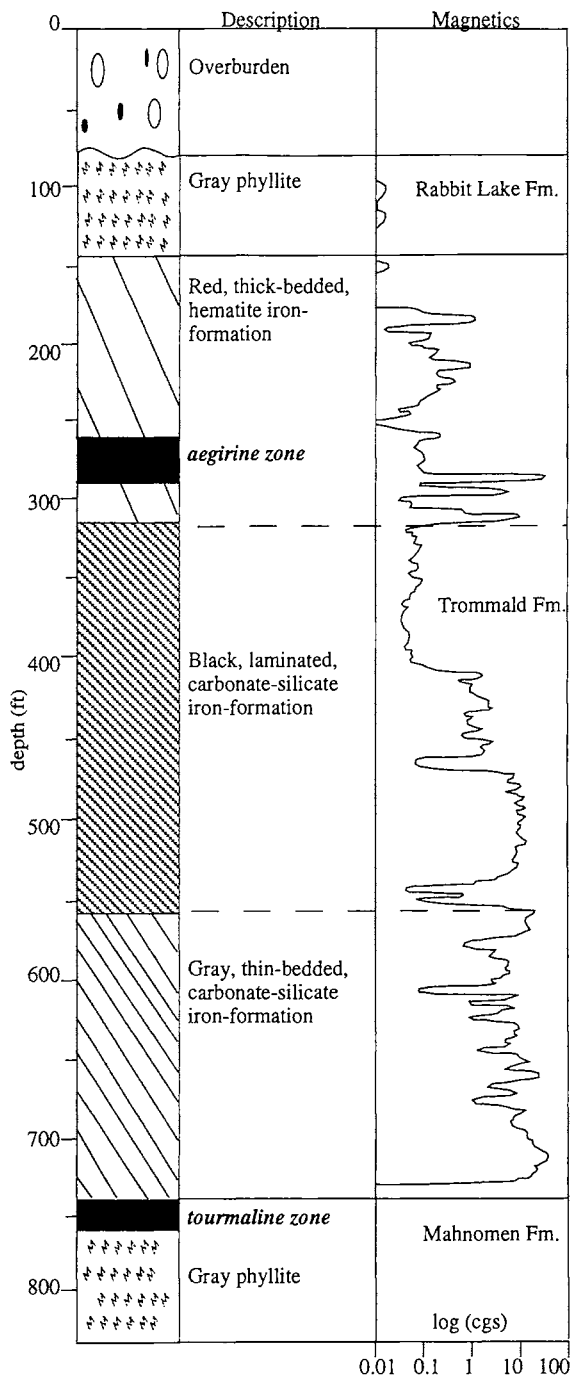
Figure 3. Stratigraphy of the Merritt drill hole. Core intersects the entire Trommald Formation, together with short intervals of the Rabbit Lake and Mahnomen Formations.

Figure 3 labels:
Description — Magnetics
Overburden
Gray phyllite — Rabbit Lake Fm.
Red, thick-bedded, hematite iron-formation
aegirine zone
Trommald Fm.
Black, laminated, carbonate-silicate iron-formation
Gray, thin-bedded, carbonate-silicate iron-formation
tourmaline zone
Gray phyllite — Mahnomen Fm.
log (cgs)
0.01 0.1 1 10 100
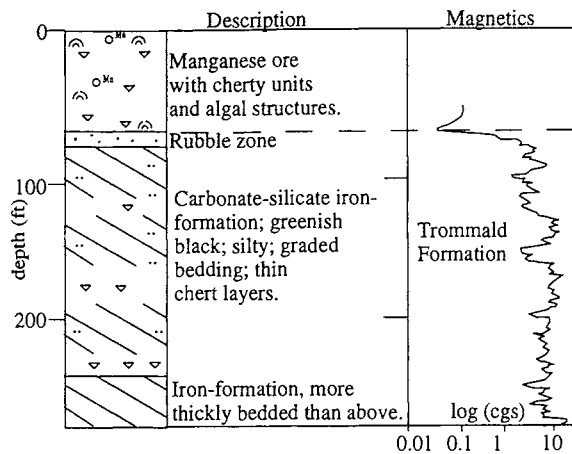
Figure 4. Stratigraphy of the Arko drill hole.

Figure 4 labels:
Description — Magnetics
Manganese ore with cherty units and algal structures.
Rubble zone
Carbonate-silicate iron-formation; greenish black; silty; graded bedding; thin chert layers. — Trommald Formation
Iron-formation, more thickly bedded than above. — log (cgs)
0.01 0.1 1 10
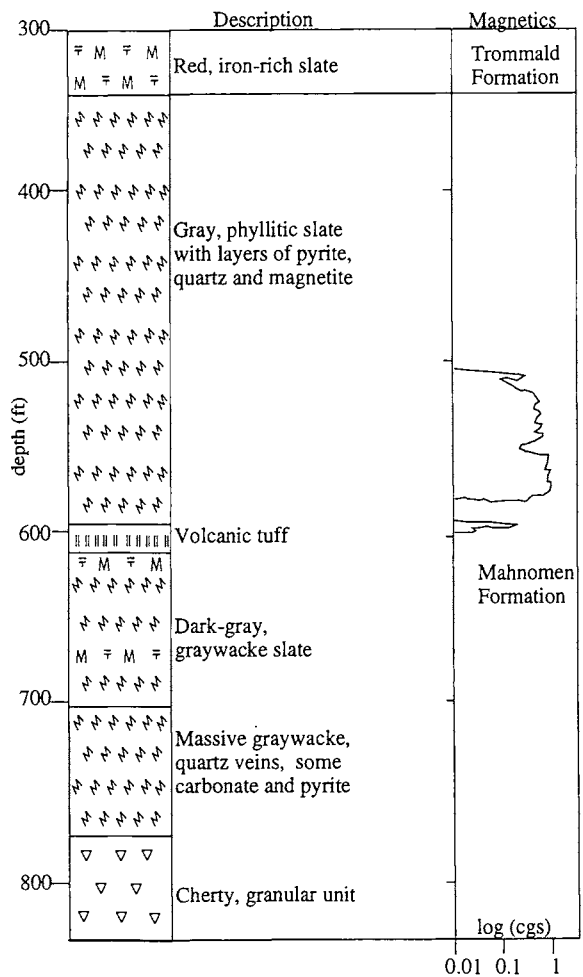
Figure 5. Stratigraphy of the Northland drill hole.

Figure 5 labels:
Description — Magnetics
Red, iron-rich slate — Trommald Formation
Gray, phyllitic slate with layers of pyrite, quartz and magnetite
Volcanic tuff
Dark-gray, graywacke slate — Mahnomen Formation
Massive graywacke, quartz veins, some carbonate and pyrite
Cherty, granular unit
log (cgs)
0.01 0.1 1

4
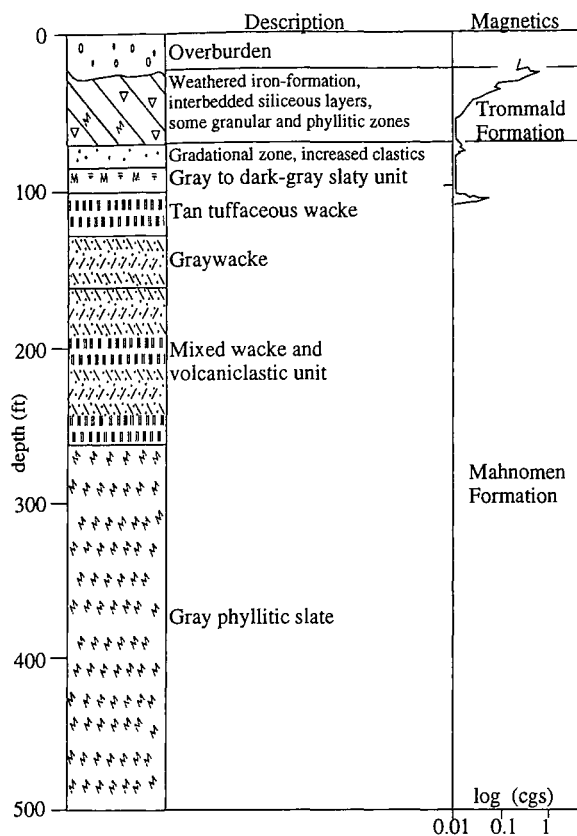
Figure 6. Stratigraphy of the North Hillcrest drill hole.

hematite, magnetite, various manganese oxides, hyalophane, rhodochrosite, calcite, and minor amounts of stilpnomelane, magnesioriebeckite and jacobsite. Thus parts of the upper member have mineralogical attributes that differ substantially from those associated with typical Lake Superior-type iron-formation.

Characteristic of the upper member are spheroidal structures that have been described as oolites (Grout 1946; Grout & Wolff, 1955) but have physical features similar to oncolites (Fig. 9a-d). Their actual origin is unclear, and we refer to them simply as micronodules of uncertain origin. They typically consist of rounded core grains surrounded by a number of quasi-concentric rims. The mineral assemblages in both cores and rims may contain any of the following phases: rhodonite, aegirine, rhodochrosite, hematite, Ba-feldspar, and calcite. In the example shown in Figure 9a, the core consists of rhodonite, which was successively surrounded by monomineralic rims of hematite, Ba-feldspar, and lastly rhodochrosite. The micronodules and their associated mineral assemblages have been described by McSwiggen and others (1994a, 1994b).

These micronodules also contain internal structures which shed some light on their origin. Some core grains contain internal structures, such as the internal layering

shown in Figure 10a. Less common examples include evidence of brittle deformation. As shown in Figure 10b, the core grain appears to be undeformed, whereas the surrounding rim material appears to have been compressed on the left side but pulled apart on the right side of the structure. Thus deformation apparently took place after the core grain had become rigid but before the enclosing sediment was completely lithified. This implies a paragenetic sequence that may involve significant gaps in time between successive periods of mineral growth or deposition. Some micronodules also have what appear to be shrinkage cracks like those illustrated in Figure 10c. However the shrinkage cracks do not necessarily indicate a period of subaerial desiccation, but more likely represent volume loss associated with the transformation of a phase or phases to a crystalline form (Heath, 1981). A few micronodules also contain rounded internal structures (Fig. 10d) that resemble the spherical microstructures in the Biwabik Iron Formation of the Mesabi range that Darby (1972) attributed to protoalgal activity.

The upper member also contains layers and crosscutting zones of aegirine, as well as veins composed of rhodonite, Ba-feldspar, aegirine, calcite, quartz, and various manganese oxides. The aegirine and Ba-feldspar occurrences have been discussed in more detail by McSwiggen and others (1994a, 1994b). Their presence both as an early phase in bedded sediments and as crosscutting vein material implies several periods of mineralization.

Middle and Lower Members

The middle and lower members of the Trommald Formation both consist of laminated to thin-bedded carbonate-silicate iron-formation. They differ mainly in color and bedding. The middle member is black and laminated, whereas the lower member is medium to dark gray and thin bedded. Both members contain ferroan kutnahorite, manganiferous siderite, stilpnomelane, minnesotaite, hematite, magnetite, quartz, and chamosite. Bedding is typically defined by intercalated layers of carbonates ($\pm$ iron silicates) and iron silicates ($\pm$ carbonates). The type of carbonate that occurs in these members is fairly consistent, and typically the ferroan kutnahorite and manganiferous siderite occur together in the carbonate-rich horizons. In contrast, the type of iron-silicate minerals varies from core to core. The stilpnomelane and chamosite occur in the Arko core, whereas stilpnomelane and minnesotaite occur in the Merritt core.

Magnetic susceptibility is a useful attribute for distinguishing the three members of the Trommald Formation. The magnetic susceptibility of the upper member is highly variable (Fig. 3); magnetic highs are related to thin beds that contain magnetite, whereas the lows are related to beds composed of hematite or iron silicates. The upper
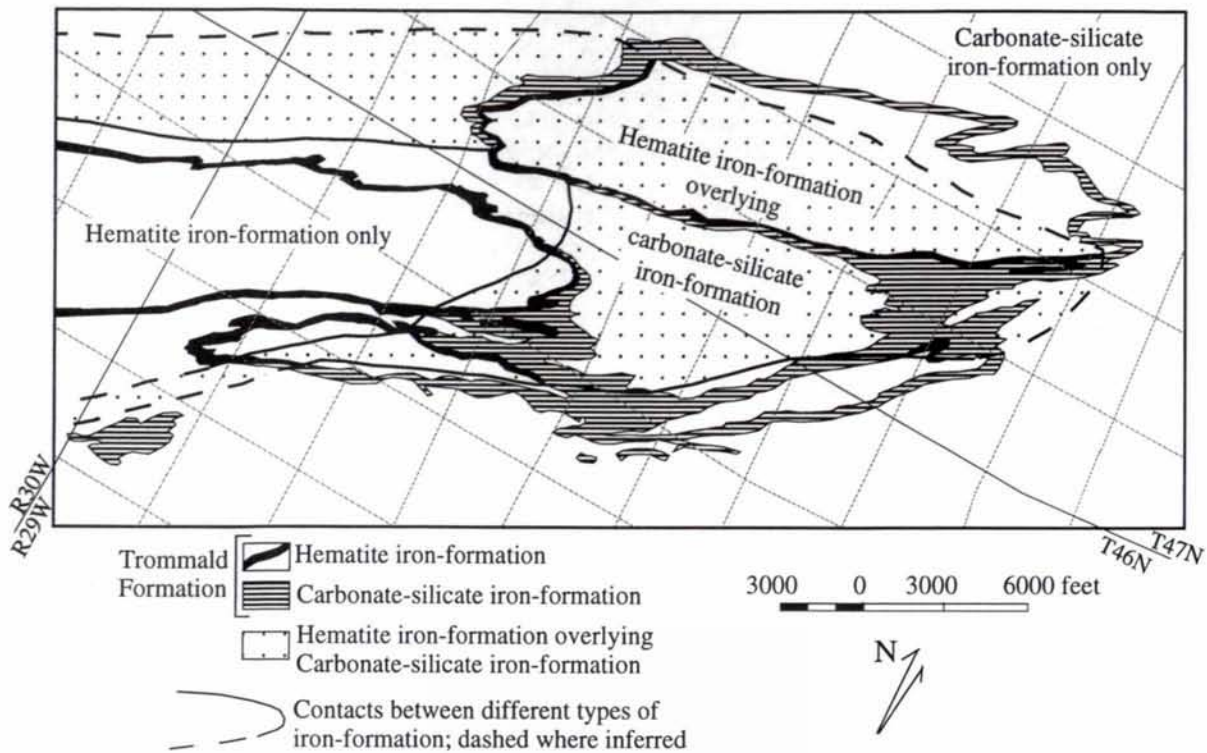
Figure 7. Lithofacies map of the Trommald Formation, Cuyuna North range (modified from Schmidt, 1963). Shown are the Trommald Formation outline, and the distribution of the hematite iron-formation—the upper member of this report—and the carbonate-silicate iron-formation—the middle and lower members of this report. Both are present in a central arcuate zone, outside of which only the carbonate-silicate iron formation is present, and inside of which only the hematite iron-formation is present.
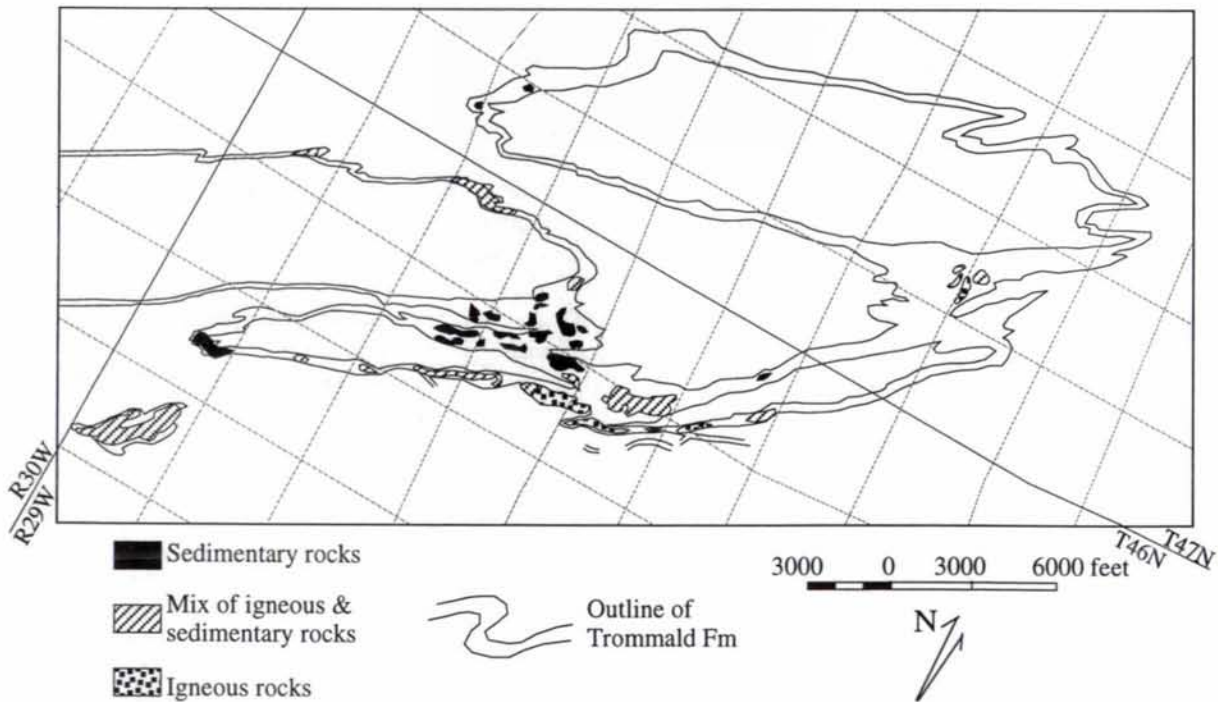
Figure 8. Map of the dominant rock types of the host rock in each of the mine pits in the Cuyuna North range (data from Schimdt, 1963). The data suggest that the southernmost limb contains the greatest abundance of igneous rocks.

6
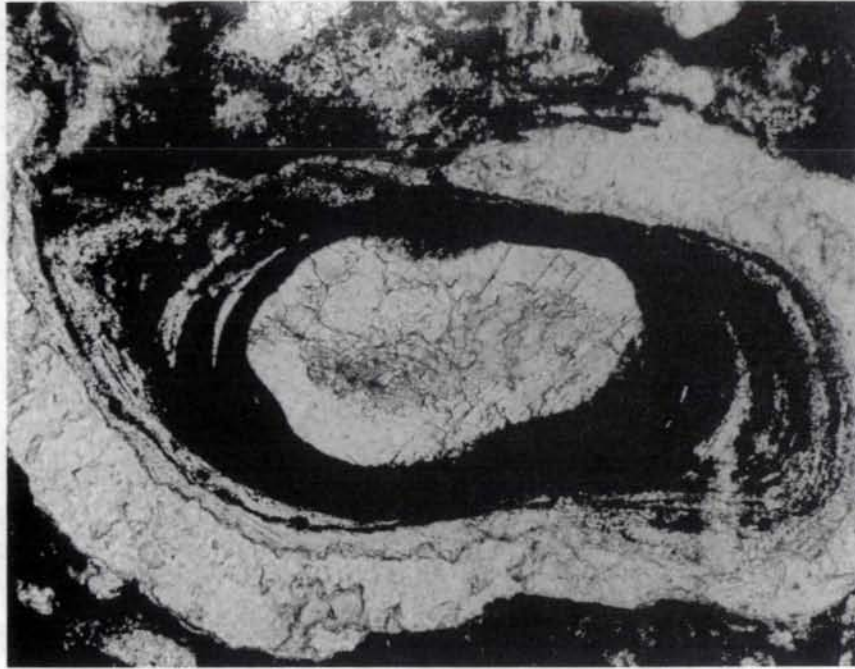
Figure 9a.

Figure 9b.

Figure 9. Examples of mineralogical variations within micronodules in the upper member of the Trommald Formation.
(a) Photomicrograph of rhodonite core surrounded sequentially by hematite, Ba-feldspar, and rhodochrosite.
(b) Photomicrograph of rhodonite core grain surrounded by intergrown cryptocrystalline rhodonite and hematite.
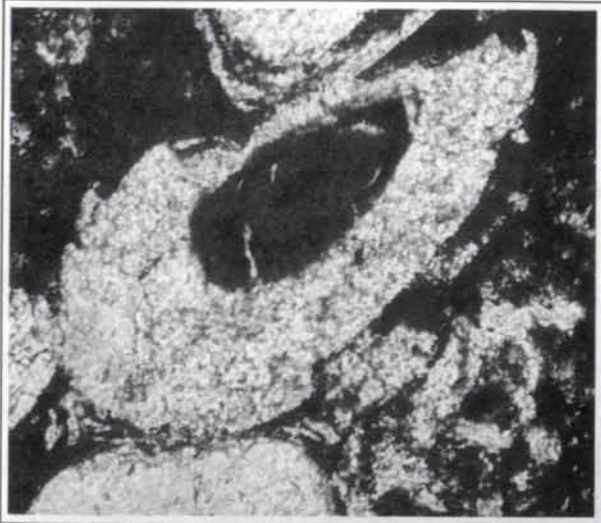
Figure 9 (continued). (c) Composite image of photomicrograph and backscattered electron image of micronodule cored by hematite and calcite surrounded by rhodochrosite.
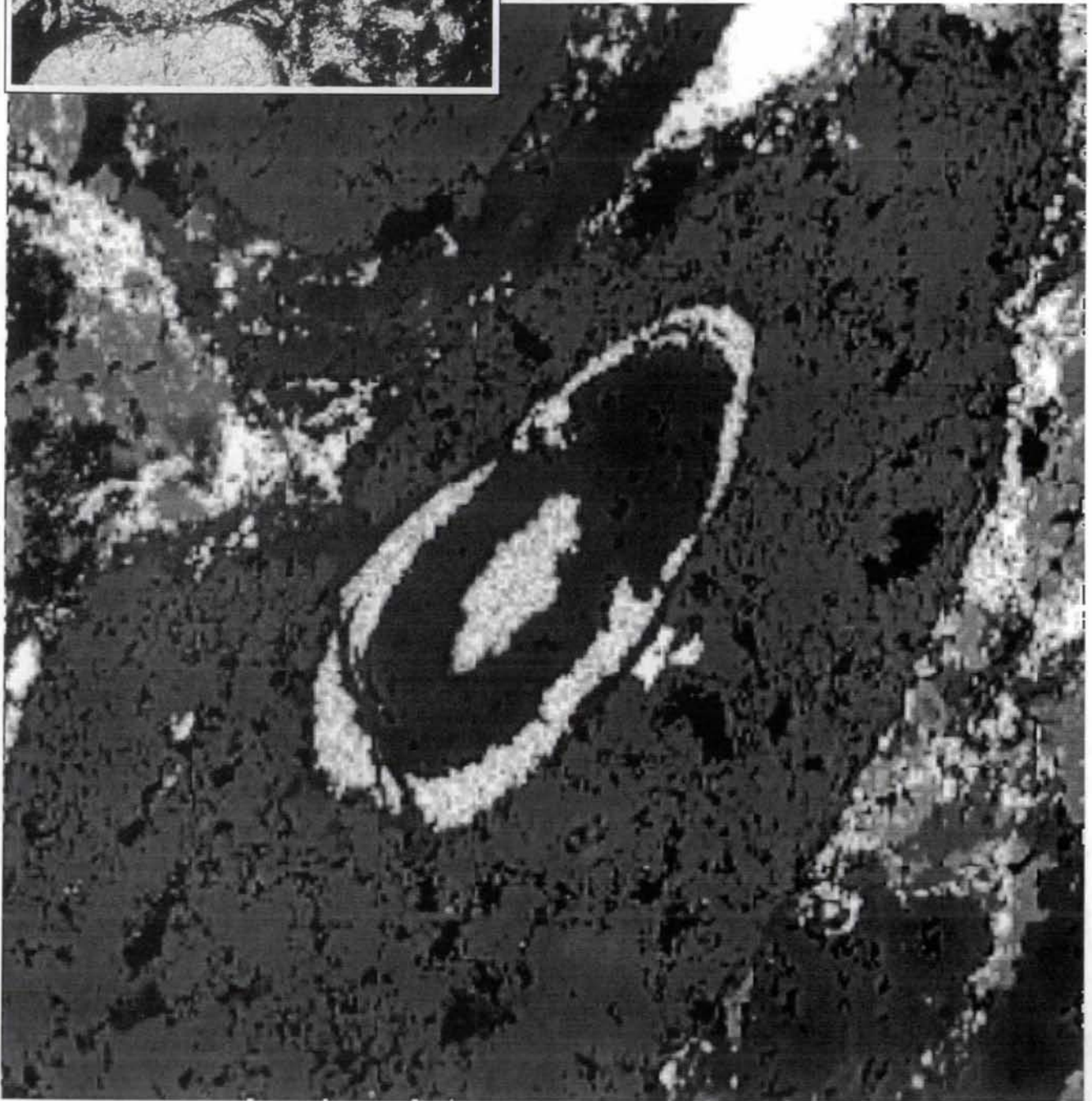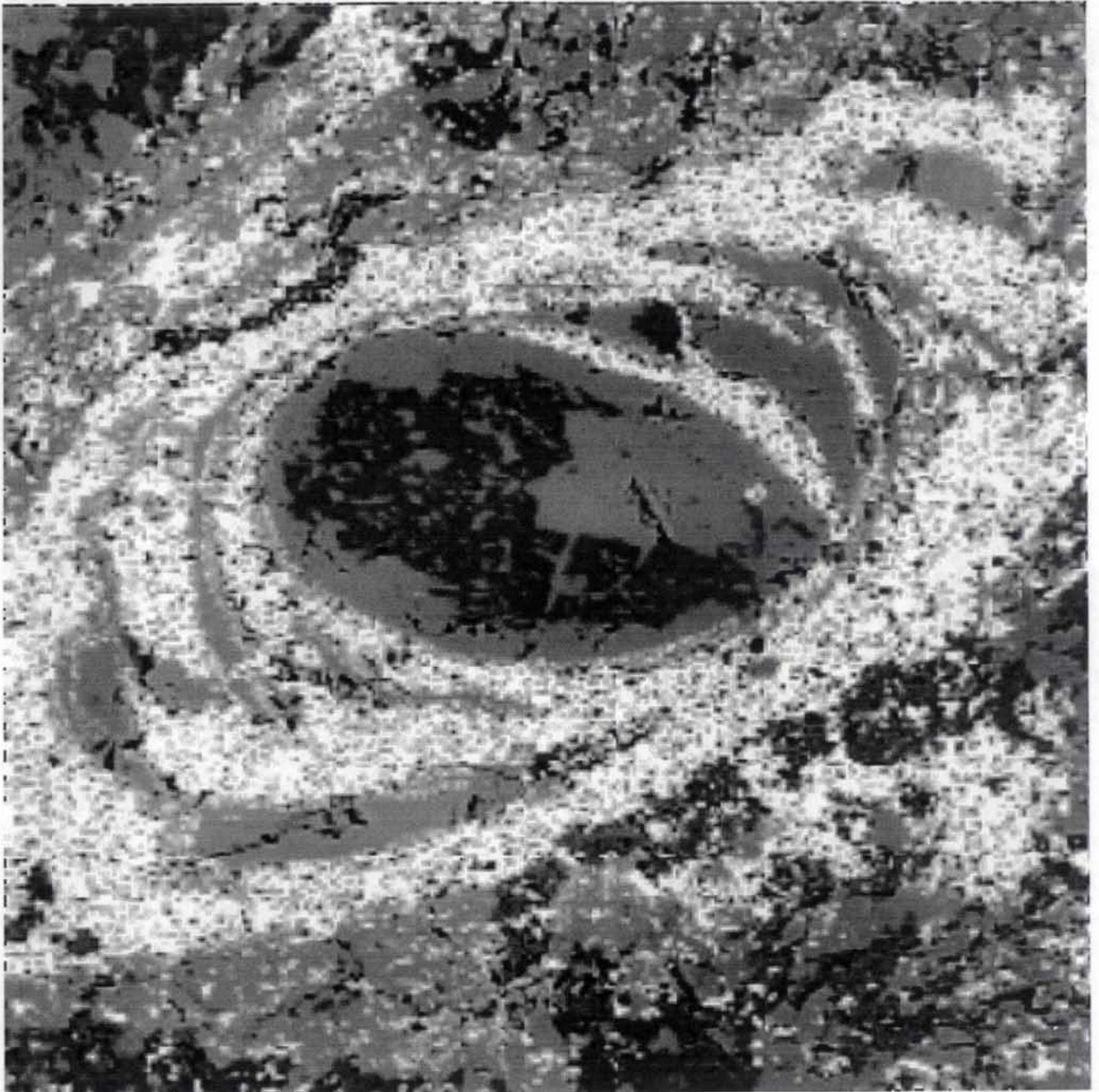
Figure 9 (continued). (d) Backscattered electron image of aegirine and rhodonite core grain surrounded by bands of hematite and rhodonite.
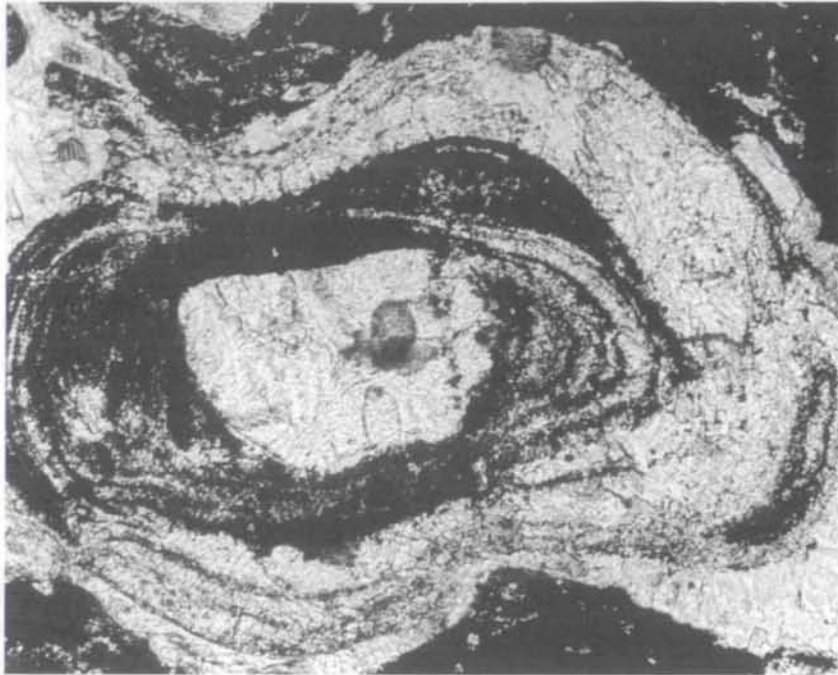
Figure 10a.
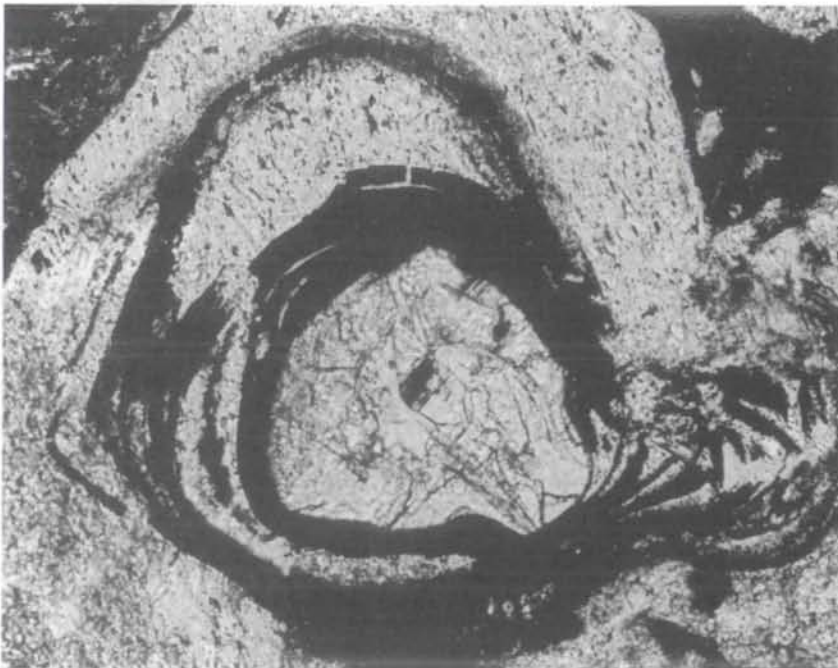
Figure 10b.

Figure 10. Examples of internal structures within micronodules in the upper member of the Trommald Formation.
(a) Internal banding within the core grain of rhodonite and hematite surrounded by rhodochrosite.
(b) Undeformed core grain surrounded by deformed layering.
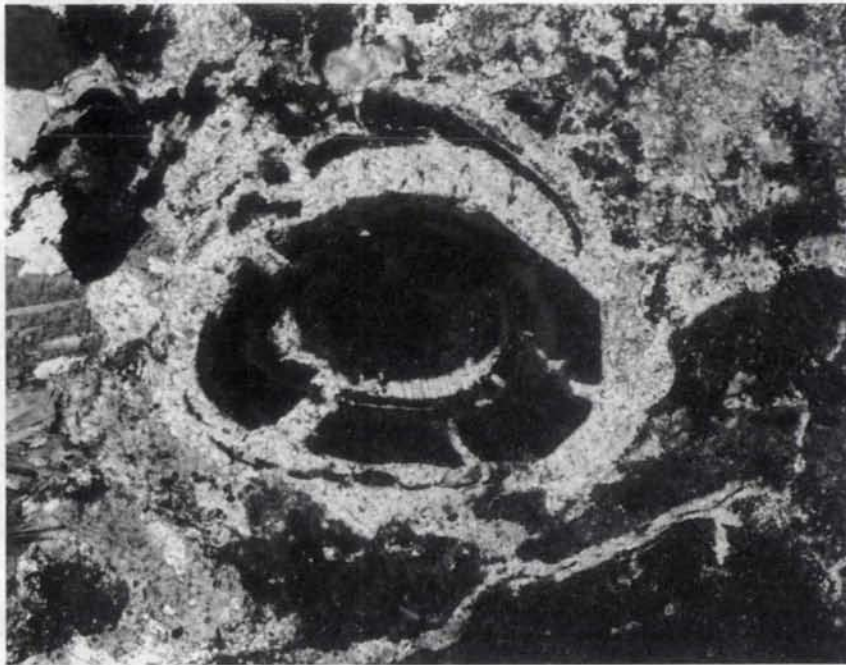
Figure 10c.

Figure 10d.

Figure 10 (continued). (c) Shrinkage cracks in a hematite core grain. (d) Spherical microstructures in a hematite core grain which may be protoalgal fossil material.

part of the middle member is weakly magnetic, in marked contrast to the lower part of the middle member and the entire lower member, which are strongly magnetic (Fig. 3). The differences in the magnetic properties of the units do not reflect significant differences in the total iron content, but rather reflect the presence of minor amounts of magnetite, which typically occurs as euhedral grains no more than 1 mm in diameter.

Mahnomen Formation

Epiclastic strata beneath the Trommald Formation are assigned to the Mahnomen Formation, a unit estimated to be at least 2000 feet thick (Schmidt, 1963). In the Northland, Merritt, and North Hillcrest cores, the Mahnomen Formation consists of slate, phyllite, graywacke, and a minor volcanic component. The Northland and North Hillcrest cores also typically contain beds having as much as 10 percent amphibole. Because the amphibole-rich beds occur within an otherwise epiclastic sequence, we attribute them to a volcanogenic or volcaniclastic source.

A distinctive attribute of the Mahnomen Formation is that it contains authigenic tourmaline layers as much as several centimeters thick. Some layers from the Northland, North Hillcrest, and Merritt sites contain only 1 or 2 modal percent tourmaline and are properly referred to as tourmaline-bearing. However, core drilled on the Gloria property (Fig. 2) by the U.S. Bureau of Mines intersected layers containing as much as 18 modal percent tourmaline. These occurrences have been described in some detail by Cleland and others (in press), as have tourmaline-rich samples collected by Schmidt (1963) from the Feigh, Portsmouth, Sagamore, and Evergreen mines (Fig. 2) that contain as much as 35 modal percent tourmaline. Tourmaline-bearing layers with more than 15 modal percent tourmaline are commonly referred to as tourmalinites (Slack and others, 1984).

GEOCHEMISTRY

The analytical results for 53 selected samples from the North range group are given in Tables 1-4. Data on major, minor, trace, and rare earth elements were obtained from core material derived from the Merritt, North Hillcrest, Northland, and Arko sites. Particular care was taken to ensure that only one rock type was sampled for any given analysis (see footnotes to Tables 1-4). Major element analyses, using a combination of chemical and X-ray fluorescence techniques were completed at XRAL Laboratories, Toronto, Ontario. Trace element and rare earth element (REE) analyses also were performed by XRAL using ICP, ICP/MS, AA spectrophotometry, and neutron activation. The relative accuracy for major element determination is between 1 and 3 percent of the reported values; for minor and trace elements (from low weight percent values to 100 ppm) is between 5 and 10 percent; for lower ppm values it is more variable.

Range of Major Elements

Major element concentrations in the lower and middle members (Fig. 11) of the Trommald Formation are very similar to the average composition of the Biwabik Iron Formation (as calculated by Morey, 1992) on the Mesabi range (Fig. 1). In particular, the total iron content, as well as the oxidation state of the iron, is almost identical. However, on average, the middle and lower members contain appreciably more Mn and slightly more P and Na than average rocks in the Biwabik Iron Formation. This significantly higher Mn content of the Trommald Formation produces Mn/Fe ratios that average 0.21 and have a maximum of 0.67—values considerably larger than an average Mn/Fe ratio of 0.02 in the Biwabik Iron Formation. The average Al content of the Trommald Formation of $X_{Al} = Al/(Al+Fe+Mn) = 0.04$ is also slightly higher than that for the Biwabik of $X_{Al} = 0.02$, which may reflect a greater terrigenous or volcanogenic component.

Major element compositions for the upper member also are broadly similar to average Biwabik values (Fig. 12). However, the upper member is characterized by an even greater Mn enrichment. Also striking is the significant difference in the oxidation state of the iron. The total iron contents of the upper member of the Trommald Formation and the Biwabik Iron Formation are very similar. However, the iron in the upper member of the Trommald Formation is significantly more oxidized than that of the Biwabik. There is also much less CaO, MgO, and CO_2 in this member of the Trommald. This suggests that it contains significantly less carbonate than the Biwabik Iron Formation. Overall the Na content of the upper member of the Trommald Formation is much greater than that of the middle and lower members or that of the Biwabik Iron Formation. The wide range of Na contents shown in Figure 12 reflects the bedded nature of the Na enrichment.

Minor Elements

When compared to an average Biwabik composition, the middle and lower members of the Trommald Formation are enriched in Ba and B, and depleted in Pb, Se, and Sb (Fig. 11). The upper member is even more enriched in Ba and B, and is also enriched in As, Sr, and Mo, and only slightly enriched in Co, Ni and Mo (Fig. 12). Like the other members, it is depleted in Se and Sb, but less so in Pb.

Table 1. Chemical data from the Merritt hole
[Major elements in wt% oxides; minor elements in ppm; Au, ppb]

Depth[1]	Rabbit Lake Fm.		Trommald Formation (oxide iron-formation)					
	90.5	140	150	160	209.4	253.1	255	261.0a
SiO_2	49.9	49.4	29.2	86.8	50.8	52.3	71.6	51.0
TiO_2	1.53	1.2	0.068	0.049	0.06	0.038	0.053	0.045
Al_2O_3	14.2	11	1.87	0.1	0.46	0.71	0.48	2.18
Fe_2O_3	20.78	26.56	65.28	10.59	45.68	21.1	25.0	14.1
FeO	2.9	0.4	0.2	0.1	0.2	< 0.1	< 0.1	< 0.1
MnO	0.03	0.02	0.05	0.06	0.28	19.4	1.19	21.6
MgO	1.7	0.43	0.11	0.09	0.14	0.5	0.58	0.72
CaO	< 0.01	0.15	0.07	< 0.01	< 0.01	0.17	0.11	3.20
Na_2O	0.03	0.04	0.04	< 0.01	0.06	0.23	0.21	4.52
K_2O	5.38	3.15	0.05	< 0.01	0.02	0.66	0.29	1.33
P_2O_5	0.07	0.58	0.44	0.05	0.09	0.05	0.08	0.05
CO_2	< 0.01	0.04	< 0.01	0.04	0.02	0.01	0.01	0.58
Ag	< 0.5	< 0.5	< 0.5	< 0.5	< 0.5	< 0.5	< 0.5	< 0.5
As	7	26	130	7	8	50	37	42
Au	< 5	< 5	< 5	5	< 5	< 5	< 5	< 5
B	128	104	144	35	45	18	14	29
Ba	1660	1450	1240	103	361	4790	2410	9400
Be	7	7	13	3	7	4	5	6
Br	3	2	2	2	2	1	3	2
Cd	< 1	< 1	< 1	< 1	< 1	< 1	< 1	1
Co	36	2	7	4	9	42	18	23
Cr	180	45	22	22	10	9	14	6
Cs	17	1	< 1	< 1	< 1	< 1	< 1	2
Cu	51.6	37.8	6.3	3.9	1.8	2.7	3.7	3.8
Ge	11	< 10	< 10	< 10	< 10	< 10	< 10	< 10
Hf	3.5	2.0	0.6	< 0.5	< 0.5	< 0.5	< 0.5	< 0.6
Mo	< 5	< 5	29	< 5	6	< 5	< 5	< 5
Nb	54	34	26	23	33	26	< 10	12
Ni	71	18	12	10	4	18	13	21
Pb	< 2	6	< 2	< 2	< 2	7	8	6
Rb	199	52	17	< 10	17	20	22	22
Sb	0.6	0.6	0.6	< 0.2	0.4	1.1	1.5	0.3
Sc	26.5	22.6	3.0	0.6	0.6	1.2	0.9	0.5
Se	< 3	< 3	< 3	< 3	< 3	<3	< 3	< 3
Sr	20	1500	518	< 10	< 10	379	< 10	< 10
Ta	2	1	< 1	< 1	< 1	< 1	< 1	< 1
Th	4.6	1.5	0.5	< 0.5	< 0.5	< 0.5	< 0.5	< 0.6
U	2.1	4	5.1	0.7	0.9	0.6	0.7	0.5
V	207	389	759	17	18	< 10	< 10	< 10
W	< 3	3	< 3	< 3	< 3	10	10	< 3
Y	< 10	< 10	< 10	< 10	< 10	13	< 10	22
Zn	111	51.2	29.5	12.6	21.8	61.1	27.6	66.8
Zr	176	86	22	14	28	11	52	< 10
La	28.5	40.8	17.4	1.5	2.4	20.7	9.3	6.5
Ce	57	89	31	3	5	25	17	15
Nd	22	48	18	< 5	<5	10	5	9
Sm	4.0	10.3	3.5	0.2	0.5	2.1	1.1	2.2
Eu	0.8	3.0	1.2	< 0.2	< 0.2	0.9	0.5	0.9
Tb	0.5	0.7	< 0.5	< 0.5	< 0.5	0.5	< 0.5	0.7
Yb	1.2	1.3	0.2	0.2	0.3	1.3	0.6	1.5
Lu	0.16	0.17	n.d.	< 0.05	< 0.05	0.17	0.09	0.21

[1] depth in feet below collar. 90, gray phillite; 140, hematitic phyllite; 150, hematitic iron-formation; 160, quartz vein material; 209, pitted hematitic iron-formation; 253, Mn-oxide zone, massive; 255, red cherty iron-formation with oncolites; 261a, acmite layer.

Table 1. (continued)
[Major elements in wt% oxides; minor elements in ppm; Au, ppb]

Depth	Trommald Fm. (oxide iron-formation)				Trommald Formation (carb.-silicate I.F.)			
	261.0b	278.1	285.3	294	329.9	342.4	380.5	436.6
SiO_2	14.2	77.1	19.9	16.9	21.1	44.6	19.9	49.6
TiO_2	0.161	0.031	0.067	0.102	0.104	0.048	0.190	0.018
Al_2O_3	0.94	4.36	0.89	0.81	2.96	1.60	3.36	0.42
Fe_2O_3	50.7	8.77	31.57	34.67	12.45	3.562	4.574	4.232
FeO	< 0.1	< 0.1	0.3	0.3	26.5	23.7	20.0	8.7
MnO	25.1	0.63	42.4	34.9	8.82	5.27	16.2	4.36
MgO	1.21	0.05	0.46	1.11	4.02	3.21	2.50	3.37
CaO	0.92	0.34	0.80	2.56	1.25	2.55	7.22	11.8
Na_2O	0.19	3.10	0.03	0.07	0.24	0.07	< 0.01	0.04
K_2O	0.58	2.34	0.06	0.53	0.72	0.44	< 0.01	0.10
P_2O_5	0.30	0.01	0.06	0.29	0.06	0.04	0.33	0.08
CO_2	4.84	0.51	3.85	8.6	17.4	10.8	25.1	18
Ag	< 0.5	< 0.5	< 0.5	< 0.5	< 0.5	< 0.5	< 0.5	< 0.5
As	120	3	270	180	6	6	25	4
Au	< 5	< 5	47	8	5	9	6	< 5
B	< 10	17	34	< 10	< 10	10	92	19
Ba	4630	21100	590	3540	199	128	134	62
Be	9	15	8	6	8	6	5	3
Br	2	2	3	2	3	2	2	6
Cd	< 1	< 1	2	2	< 1	< 1	< 1	< 1
Co	49	8	49	52	15	15	23	22
Cr	16	10	21	10	23	11	28	9
Cs	1	< 1	1	< 1	2	5	< 1	< 1
Cu	< 0.5	3.5	20.7	6.0	1.3	1.4	2.0	118.0
Ge	< 10	14	< 10	13	< 10	< 10	< 10	< 10
Hf	0.6	< 0.5	0.5	0.5	0.6	< 0.5	0.9	< 0.5
Mo	< 5	< 5	< 5	< 5	< 5	< 5	< 5	< 5
Nb	34	21	14	11	19	16	27	21
Ni	40	15	38	41	13	15	25	14
Pb	18	< 2	35	17	< 2	< 2	< 2	118
Rb	23	44	30	22	45	< 10	15	23
Sb	2.1	0.3	2.5	2.1	0.2	0.4	< 0.2	2.4
Sc	1.7	0.3	1.3	1.3	3.3	2.0	3.3	0.5
Se	< 3	< 3	< 3	< 3	< 3	< 3	< 3	3
Sr	13	< 10	< 10	18	< 10	< 10	32	25
Ta	< 1	< 1	< 1	< 1	< 1	< 1	< 1	< 1
Th	1.1	< 0.5	0.9	1.2	1.5	0.6	2.0	< 0.5
U	0.5	1.5	1.1	0.6	0.6	0.8	0.8	< 0.5
V	< 10	24	< 10	< 10	16	17	< 10	< 10
W	12	< 3	8	10	< 3	3	4	< 3
Y	< 10	< 10	< 10	12	< 10	< 10	< 10	23
Zn	60.8	17.6	89	85.5	36.2	31.8	45.2	139.0
Zr	54	28	49	41	23	< 10	14	< 10
La	72.7	0.7	48.5	70.1	11.7	9.2	20.9	22.1
Ce	69	< 3	49	68	24	16	43	45
Nd	26	< 5	19	28	8	5	15	17
Sm	4.4	0.2	3.9	5.4	1.6	1.1	2.7	3.0
Eu	1.1	< 0.3	1.1	1.7	0.5	0.4	1.0	1.1
Tb	0.6	< 0.5	0.5	0.6	< 0.5	< 0.5	0.8	0.5
Yb	2.1	< 0.2	2.4	2.7	1.2	0.6	1.3	1.5
Lu	0.31	< 0.05	0.38	0.43	0.18	0.08	0.17	0.22

261b, cherty banded iron-formation; 278, acmite, quartz, Ba-feldspar; 285, very magnetitic iron-formation, magnetite; 294, red cherty banded iron-formation (typical of unit); 329, carbonate-silicate iron formation; 342, white volcanic ash-like layer; 380, carbonate-silicate iron-formation (typical of unit); 436, vein material.

Table 1. (continued)

[Major elements in wt% oxides; minor elements in ppm; Au, ppb]

Depth	Trommald Formation (carbonate-silicate iron-formation)							
	460.1	466.4	488.7	522.7	561.7	593.5	616.9	618.9
SiO_2	29.5	24.4	24.0	29.8	34.2	26.9	29.8	41.9
TiO_2	0.101	0.101	0.085	0.096	0.064	0.093	0.077	0.017
Al_2O_3	2.03	1.56	1.39	1.83	1.15	2.35	1.32	3.32
Fe_2O_3	14.42	9.507	18.45	18.66	9.727	14.37	9.872	15.15
FeO	25.9	20.6	31.9	28.2	31.2	21.8	30.8	11.2
MnO	7.31	9.85	4.82	4.29	4.80	6.77	5.25	2.15
MgO	1.84	1.98	1.87	1.66	1.75	1.9	2.09	3.48
CaO	0.89	6.87	2.57	1.40	2.78	4.59	3.28	7.00
Na_2O	0.22	0.2	0.08	0.18	0.06	0.31	0.1	0.42
K_2O	0.43	0.33	0.36	0.42	0.29	0.51	0.34	0.70
P_2O_5	0.10	0.09	0.06	0.25	1.11	1.13	0.52	0.03
CO_2	14.3	22.5	10.8	9.8	9.4	15.1	12.9	9.8
Ag	< 0.5	< 0.5	< 0.5	< 0.5	< 0.5	< 0.5	< 0.5	< 0.5
As	46	35	4	45	45	56	17	< 2
Au	9	8	< 5	< 5	8	< 5	< 5	48
B	< 10	22	< 10	< 10	< 10	< 10	< 10	< 10
Ba	421	159	225	195	135	132	141	335
Be	7	6	8	8	8	7	9	8
Br	2	2	2	2	3	1	2	5
Cd	< 1	< 1	< 1	< 1	< 1	< 1	< 1	< 1
Co	36	28	13	12	18	32	19	12
Cr	23	20	24	25	20	19	16	6
Cs	1	1	< 1	< 1	1	1	1	1
Cu	30.2	0.8	< 0.5	7.0	21.3	2.0	49.1	1.0
Ge	10	< 10	11	< 10	14	< 10	14	< 10
Hf	< 0.5	< 0.5	< 0.5	< 0.5	< 0.5	< 0.5	< 0.5	< 0.5
Mo	< 5	< 5	< 5	< 5	< 5	< 5	< 5	< 5
Nb	18	22	32	38	19	33	36	26
Ni	20	18	5	5	8	14	8	9
Pb	< 2	< 2	< 2	< 2	< 2	< 2	< 2	< 2
Rb	32	17	< 10	29	36	30	23	33
Sb	1.3	< 0.2	0.5	0.3	1.1	0.6	0.8	0.3
Sc	2.0	1.8	1.5	2.0	1.4	2.2	1.6	0.5
Se	<3	<3	< 3	< 3	< 3	< 3	< 3	< 3
Sr	12	34	< 10	< 10	19	21	< 10	< 10
Ta	<1	<1	< 1	< 1	< 1	< 1	< 1	< 1
Th	1.4	1.2	0.7	1.2	0.8	1.8	1.1	< 0.5
U	0.5	1.4	0.8	1.5	1.1	1.0	1.4	1.5
V	13	<10	12	19	17	13	< 10	16
W	<3	<3	3	< 3	< 3	< 3	< 3	< 3
Y	12	<10	< 10	< 10	< 10	19	< 10	< 10
Zn	29.5	30.5	42.0	27.9	39.6	29.8	32.8	28.1
Zr	28	34	< 10	< 10	35	36	11	12
La	6.2	11.9	4.4	9.3	17.3	35.8	10.3	4.1
Ce	12	19	9	18	29	69	22	8
Nd	<5	7	< 5	5	13	25	8	< 5
Sm	0.9	1.4	0.6	1.3	2.3	4.1	1.5	0.7
Eu	0.3	0.5	< 0.2	0.5	0.5	1.3	0.5	0.4
Tb	<0.5	<0.5	< 0.5	< 0.5	< 0.5	< 0.5	< 0.5	< 0.5
Yb	1.1	1.0	0.9	1.1	1.2	1.7	1.0	0.6
Lu	0.17	0.15	0.12	0.14	0.14	0.22	0.14	0.08

460, carbonate-silicate iron-formation with bands of magnetic; 466, carbonate-silicate iron-formation, non-magnetitic; 488, gray banded iron-formation—magnetic; 522, gray banded iron-formation—magnetic; 561, carbonate-silicate iron-formation—magnetic; 593, carbonate-silicate iron-formation—magnetic; 616, carbonate-silicate iron-formation—magnetic with veining; 618, brown vein material.

Table 1. (continued)
[Major elements in wt% oxides; minor elements in ppm; Au, ppb]

Depth	Trommald Fm.		Mahnomen Formation			
	678.7	700.5	740.8	748.5	754	763.5
SiO_2	38.5	39.4	64.8	84.2	50.3	67.1
TiO_2	0.067	0.090	0.202	0.160	0.884	0.535
Al_2O_3	1.42	1.94	9.15	8.55	26.2	16.5
Fe_2O_3	9.083	23.4	< 0.16	0.214	3.465	1.975
FeO	28.9	19.8	16.7	0.5	3.1	3.1
MnO	3.18	0.57	0.11	0.03	0.03	0.03
MgO	1.97	1.97	1.75	0.18	2.09	1.47
CaO	2.29	0.72	1.14	0.02	< 0.01	0.02
Na_2O	0.06	0.28	< 0.01	3.28	0.08	2.06
K_2O	0.34	0.44	< 0.01	2.52	8.83	4.74
P_2O_5	0.97	0.13	0.03	0.05	0.04	0.04
CO_2	9.61	7.21	0.9	0.12	0.04	0.03
Ag	< 0.5	< 0.5	< 0.5	< 0.5	< 0.5	< 0.5
As	32	3	< 2	4	7	4
Au	< 5	8	7	< 5	< 5	< 5
B	< 10	< 10	37	37	236	120
Ba	145	166	75	1100	2990	1290
Be	7	8	5	< 1	5	2
Br	2	2	1	2	2	3
Cd	< 1	< 1	< 1	< 1	< 1	< 1
Co	12	6	8	4	16	10
Cr	19	23	28	27	180	89
Cs	< 1	1	< 1	1	3	5
Cu	5.4	25.8	2.0	9.0	40.1	30.0
Ge	13	26	< 10	< 10	< 10	< 10
Hf	< 0.5	< 0.5	6.4	4.1	3.3	6.8
Mo	< 5	< 5	< 5	< 5	< 5	< 5
Nb	< 10	14	19	24	38	22
Ni	9	18	18	7	66	42
Pb	< 2	< 2	< 2	20	4	10
Rb	36	28	20	48	265	175
Sb	0.5	0.5	< 0.2	< 0.2	0.3	0.2
Sc	1.3	1.8	3.5	1.8	24.8	11.4
Se	< 3	< 3	< 3	< 3	< 3	< 3
Sr	< 10	< 10	< 10	132	35	136
Ta	< 1	< 1	< 1	< 1	1	< 1
Th	0.7	1.3	7.1	4.0	13.0	11.0
U	0.5	0.9	1.5	1.5	3.5	2.5
V	18	17	22	10	158	72
W	< 3	< 3	< 3	< 3	3	< 3
Y	< 10	< 10	< 10	< 10	< 10	23
Zn	38.0	19.9	66.2	12.0	68.9	49.4
Zr	19	40	956	179	158	306
La	15.8	4.0	13.3	10.4	54.7	27.9
Ce	29	10	27	20	101	55
Nd	12	< 5	10	9	41	22
Sm	2.2	0.6	1.8	1.9	6.2	3.8
Eu	0.7	< 0.2	0.3	< 0.2	1.6	0.9
Tb	< 0.5	< 0.5	< 0.5	< 0.5	0.5	0.5
Yb	1.1	0.6	0.9	0.6	1.9	1.5
Lu	0.15	0.07	0.12	0.12	0.21	0.21

678, carbonate-silicate iron-formation; 700, carbonate-silicate iron-formation; 740, sheared tourmalinite; 748, gray quartzite—possibly contains tourmaline; 754, gray banded cherty rock—possibly tourmalines; 763, quartz-rich phyllitic rock.

Table 2. Chemical data from the Arko hole
[Major elements in wt% oxides; minor elements in ppm; Au, ppb]

Depth[1]	Trommald Formation (carbonate-silicate iron-formation)					
	85	125	170	200	232	275
SiO_2	33.4	29.2	24.4	29.6	44.1	31.0
TiO_2	0.103	0.131	0.099	0.129	0.123	0.169
Al_2O_3	2.87	2.83	2.34	2.79	2.93	3.29
Fe_2O_3	16.11	16.51	15.54	19.3	10.82	13.37
FeO	17.0	19.7	19.4	16.2	9.7	21.8
MnO	5.41	8.45	10.1	7.09	5.31	6.78
MgO	5.19	3.63	3.81	3.92	4.11	3.60
CaO	4.03	2.32	3.27	3.36	6.94	2.56
Na_2O	0.19	0.16	0.18	0.33	0.19	0.06
K_2O	0.71	0.32	0.42	0.66	0.44	< 0.01
P_2O_5	0.38	0.38	1.18	0.27	0.04	0.04
CO_2	10.3	13.9	16.4	11.8	12	14.1
Ag	< 0.5	< 0.5	< 0.5	< 0.5	< 0.5	< 0.5
As	4	7	4	24	9	8
Au	< 5	< 5	< 5	< 5	< 5	< 5
B	< 10	< 10	< 10	24	22	< 10
Ba	130	185	202	161	99	127
Be	7	8	9	8	6	9
Br	3	3	2	1	2	1
Cd	1	2	3	2	1	2
Co	21	26	19	32	19	24
Cr	23	28	18	27	23	33
Cs	1	1	2	3	2	< 1
Cu	4.5	3.6	4.3	9.7	4.5	2.0
Ge	< 10	< 10	17	< 10	< 10	< 10
Hf	< 0.5	0.6	< 0.5	0.8	< 0.5	1.1
Mo	< 5	< 5	< 5	< 5	< 5	< 5
Nb	17	23	< 10	< 10	13	29
Ni	14	16	18	21	18	16
Pb	< 2	< 2	< 2	< 2	< 2	< 2
Rb	20	< 10	33	22	25	17
Sb	0.3	0.2	< 0.2	< 0.2	< 0.2	0.2
Sc	3.2	2.8	2.3	2.6	2.7	3.1
Se	< 3	< 3	< 3	< 3	< 3	< 3
Sr	26	16	15	18	25	< 10
Ta	< 1	< 1	< 1	< 1	< 1	< 1
Th	1.6	1.8	1.7	1.5	1.4	2.2
U	< 0.5	< 0.5	0.5	0.5	< 0.5	< 0.5
V	41	21	17	39	38	28
W	< 3	< 3	< 3	< 3	< 3	< 3
Y	< 10	< 10	< 10	13	11	< 10
Zn	78.6	40.3	53.5	43	50.7	49.7
Zr	25	13	35	29	49	55
La	27.8	12.3	42.4	11.9	5.7	5.3
Ce	50	22	68	21	10	11
Nd	20	9	26	8	< 5	< 5
Sm	3.7	1.6	4.0	1.4	0.8	0.7
Eu	0.7	0.5	1.0	0.4	0.3	0.3
Tb	< 0.5	< 0.5	0.5	< 0.5	< 0.5	< 0.5
Yb	1.2	0.9	1.0	1.0	0.7	0.7
Lu	0.16	0.14	0.13	0.13	0.10	0.11

[1] depth in feet below collar. 85, greenish-black slate; 125, black slate; 170, black slate; 200, greenish-black slate; 232, greenish-black slate; 275, black slate with laminations.

17

Table 3. Chemical data from the North Hillcrest hole
[Major elements in wt% oxides; minor elements in ppm; Au, ppb]

Depth[1]	Trommald Formation				Mahnomen Formation			
	18.2	29.3	35.2	52.7	142.5	181	230.5	375
SiO_2	27.8	27	47.3	79.2	63.6	64.6	69.2	62.6
TiO_2	0.057	0.182	0.043	0.065	0.596	0.550	0.089	0.629
Al_2O_3	1.04	3.19	0.56	3.15	18.0	11.6	3.64	18.2
Fe_2O_3	1.783	2.131	9.44	8.01	43.44	15.39	2.317	2.089
FeO	28.9	10.5	23.9	7.1	0.5	0.1	3.8	5.4
MnO	8.45	6.38	0.14	0.05	0.04	0.13	0.28	0.05
MgO	3.07	4.20	0.12	0.10	1.63	2.14	1.82	1.90
CaO	1.27	0.60	< 0.01	< 0.01	0.04	0.58	3.08	0.01
Na_2O	< 0.01	0.10	0.02	< 0.01	1.54	0.63	< 0.01	0.40
K_2O	0.04	0.78	< 0.01	< 0.01	4.85	2.18	0.14	4.74
P_2O_5	0.45	0.10	0.82	0.06	0.06	0.04	0.20	0.05
CO_2	25.2	0.84	17.6	4.16	0.04	52.7	0.14	0.01
Ag	< 0.5	< 0.5	< 0.5	< 0.5	< 0.5	< 0.5	0.5	< 0.5
As	60	26	6	4	8	2	2	2
Au	< 5	8	< 5	< 5	< 5	< 5	16	<5
B	< 10	< 10	< 10	50	72	66	16	134
Ba	228	1540	143	111	1170	761	115	666
Be	7	9	15	4	4	6	5	3
Br	3	3	3	2	2	2	2	2
Cd	2	1	1	< 1	< 1	< 1	< 1	< 1
Co	25	37	6	2	15	28	77	17
Cr	18	33	14	17	110	100	24	110
Cs	1	2	< 1	1	3	5	< 1	4
Cu	17.7	13.3	5.2	3.2	27.8	16.0	350.	51.1
Ge	< 10	< 10	< 10	10	12	11	13	< 10
Hf	< 0.5	1.2	< 0.5	1.0	4.3	6.0	1.2	4.8
Mo	6	< 5	< 5	< 5	< 5	< 5	< 5	< 5
Nb	22	22	15	18	26	18	11	14
Ni	9	15	18	5	49	30	26	59
Pb	< 2	< 2	< 2	< 2	15	< 2	30	16
Rb	24	19	20	14	161	103	< 10	172
Sb	0.2	< 0.2	0.7	< 0.2	< 0.2	< 0.2	0.4	0.3
Sc	1.2	3.4	0.9	1.3	13.5	12.0	3.5	12.8
Se	<3	< 3	<3	< 3	< 3	< 3	< 3	< 3
Sr	< 10	< 10	< 10	< 10	95	72	150	51
Ta	<1	< 1	< 1	< 1	< 1	< 1	< 1	< 1
Th	0.8	2.4	0.6	1.4	11.0	10.0	2.2	11.0
U	< 0.5	0.5	< 0.5	< 0.5	3.3	1.3	1.4	2.3
V	20	33	11	13	69	53	18	66
W	< 3	< 3	< 3	< 3	< 3	< 3	< 3	< 3
Y	< 10	< 10	< 10	18	20	< 10	18	< 10
Zn	24.3	55.0	49.5	9.4	133	65.9	82.6	162
Zr	35	59	19	31	175	248	72	204
La	14.9	7.3	6.4	7.2	30.3	23.7	11.1	31.8
Ce	28	16	11	16	58	45	33	59
Nd	11	6	< 5	6	20	15	15	24
Sm	1.8	1.0	0.7	1.0	3.5	2.7	3.1	4.0
Eu	0.4	0.3	0.4	0.5	1.0	0.6	0.6	0.8
Tb	< 0.5	< 0.5	< 0.5	< 0.5	< 0.5	< 0.5	< 0.5	0.6
Yb	1.2	1.1	0.6	0.3	1.3	0.8	0.5	1.1
Lu	0.16	0.15	0.07	< 0.05	0.18	0.16	0.06	0.15

[1]depth in feet below collar. 18, laminated tan shale; 29, greenish brown slate; 35, brown iron-formation with quartz; 52, red oxidized iron-formation; 142, gray slaty; 181, gray schist; 230, gray schist; 375, gray phyllite.

Table 4. Chemical data from the Northland hole
[Major elements in wt% oxides; minor elements in ppm; Au, ppb]

Depth[1]	368.4	440	514.2	552	592.8	632.4	676.7	772.1	795.5
SiO_2	63.0	61.0	60.0	59.6	61.2	59.0	57.4	76.9	80.0
TiO_2	0.662	0.706	0.637	0.642	0.424	0.878	0.789	0.174	0.206
Al_2O_3	18.4	21	19.8	19.2	6.93	18	21	9.08	9.16
Fe_2O_3	3.039	2.508	5.591	5.307	3.153	2.454	2.15	0.949	0.817
FeO	3.6	2.8	2.6	2.9	13.0	6.7	4.4	5.4	2.0
MnO	0.11	0.10	0.04	0.05	0.17	0.08	0.05	0.04	0.06
MgO	2.24	1.83	1.46	1.71	1.82	2.43	2.08	1.55	0.89
CaO	0.1	0.05	0.03	0.16	4.09	0.89	0.75	0.54	0.86
Na_2O	0.07	0.1	0.08	0.12	1.08	0.66	1.06	2.78	2.79
K_2O	4.61	5.75	6.18	6.14	0.22	4.32	5.33	0.41	1.19
P_2O_5	0.05	0.06	0.07	0.06	0.04	0.05	0.05	0.19	0.09
CO_2	0.09	0.17	0.04	0.25	5.61	1.3	1.11	0.43	1.08
Ag	< 0.5	< 0.5	< 0.5	< 0.5	< 0.5	< 0.5	< 0.5	< 0.5	< 0.5
As	< 2	2	< 2	< 2	< 2	21	26	< 2	< 2
Au	< 5	< 5	< 5	< 5	< 5	6	< 5	< 5	39
B	130	195	210	168	30	90	126	35	47
Ba	881	818	1110	3940	143	820	906	187	259
Be	4	4	5	5	6	4	4	3	2
Br	2	2	2	2	2	1	2	2	2
Cd	< 1	< 1	< 1	1	< 1	1	< 1	< 1	< 1
Co	15	12	12	19	43	34	31	12	6
Cr	110	130	120	100	61	120	140	37	39
Cs	4	10	11	11	8	7	9	1	2
Cu	8.0	7.7	8.2	4.8	19.2	35.6	28.0	44.2	22.0
Ge	23	22	24	< 10	< 10	< 10	< 10	14	< 10
Hf	4.2	3.6	3.3	2.7	1.7	2.6	4.2	2.8	3.8
Mo	< 5	< 5	< 5	< 5	< 5	< 5	< 5	< 5	< 5
Nb	25	16	15	25	16	23	12	< 10	11
Ni	53	45	51	50	160	62	69	21	16
Pb	2	2	2	< 2	33	12	7	6	5
Rb	201	215	261	260	25	181	223	15	41
Sb	< 0.2	0.2	< 0.2	0.3	0.2	0.2	0.2	< 0.2	< 0.2
Sc	13.6	15.5	15.5	15.4	15.8	23.7	17.3	4.4	5.4
Se	< 3	< 3	< 3	< 3	< 3	< 3	< 3	< 3	< 3
Sr	63	64	54	61	319	103	138	133	142
Ta	< 1	< 1	< 1	< 1	< 1	< 1	< 1	< 1	< 1
Th	10.0	11.0	13.0	12.0	4.5	8.7	11.0	4.1	5.6
U	1.1	1.2	1.9	2.7	0.9	1.7	2.1	0.8	1.1
V	66	76	72	62	67	139	98	27	33
W	< 3	< 3	< 3	< 3	< 3	< 3	< 3	< 3	< 3
Y	< 10	14	15	< 10	< 10	< 10	< 10	27	20
Zn	106	83.9	107	86.5	124	129	105	88.3	38.8
Zr	168	125	146	123	77	123	172	130	201
La	25.4	37.7	38.3	36.3	11.2	30.2	38.9	11.6	18.9
Ce	49	66	69	63	21	64	78	42	58
Nd	19	24	26	23	8	24	30	16	22
Sm	3.4	3.7	4.0	3.8	1.4	3.9	5	4.6	3.9
Eu	0.6	1.0	1.1	1.0	0.5	0.6	1.5	0.8	0.9
Tb	0.5	< 0.5	0.5	< 0.5	< 0.5	< 0.5	0.6	< 0.5	< 0.5
Yb	1.2	1.1	1.1	1.1	0.8	1.7	1.4	0.9	0.9
Lu	0.18	0.15	0.15	0.16	0.13	0.26	0.20	0.12	0.13

[1]depth in feet below collar. 368, gray phyllite; 440, gray phyllite; 514, gray phyllite; 552 gray phyllite; 592, gray phyllite with quartz; 632, gray phyllite; 676, gray phyllite; 772, gray phyllite; 795, quartz-rich rock.

Figure 11. (A) Major and (B) minor element chemistry of the middle and lower carbonate-silicate members of the Trommald Formation compared to chemistry of the Biwabik Iron Formation.

Rare Earth Elements

REE patterns of various rock types in the Trommald Formation normalized to the chondrite values of Evensen and others (1978) are shown in Figure 13. The REE data from the lower and middle members of the Trommald Formation (carbonate-silicate iron-formation) and the Biwabik Iron Formation are very similar (Table 5). The slope between the light REEs and the heavy REEs is nearly the same, as is the lack of Eu and Ce anomalies. In contrast, the upper member of the Trommald Formation—oxide iron-formation—is quite different in a number of parameters. The average slope between light REEs and heavy REEs (La/Yb) is almost twice that of the lower part of the Trommald Formation and the Biwabik Iron Formation. Also there is a small negative Ce anomaly in the upper member of the Trommald Formation which is lacking in the lower members and in the Biwabik Iron Formation.

Stratigraphic Distribution

To better understand the compositional variations of the strata in the North range group, selected oxides are plotted in Figures 14-17 as a function of depth. The data

Table 5. Summary REE data for the Trommald and the Biwabik Formations.

[All data normalized to chondrites. Ce/Ce* = Ce/((La-Nd)0.666); Eu/Eu* = Eu/((Sm-Tb)0.666)]

	Trommald Fm. Oxide I.F.	Trommald Fm. Carb-Silc I.F.	Biwabik Iron Fm.
Ce/Ce*	0.73	0.96	0.96
range	(0.50-0.98)	(0.80-1.28)	(0.8-1.5)
Eu/Eu*	0.99	0.92	1.08
range	(0.45-1.34)	(0.40-1.18)	(0.71-3.08)
La/Yb	17.54	9.06	8.38
range	(2.88-57.72)	(3.24-28.13)	(5.0-25)
Sm/Yb	4.06	1.85	2.29
range	(1.60-19.05)	(0.73-4.35)	(1.07-6.44)
Eu/Sm	0.89	0.81	0.96
range	(0.53-1.21)	(0.44-1.14)	(0.53-2.1)

of Tables 1-4 are combined with the wet chemical data reported by Grout and Wolff (1955), which are based on the analysis of sample intervals 1 to 5 feet thick. The combined whole-rock chemical data clearly differentiate among the various stratigraphic units that have been recognized. The Trommald Formation stands out most clearly

20
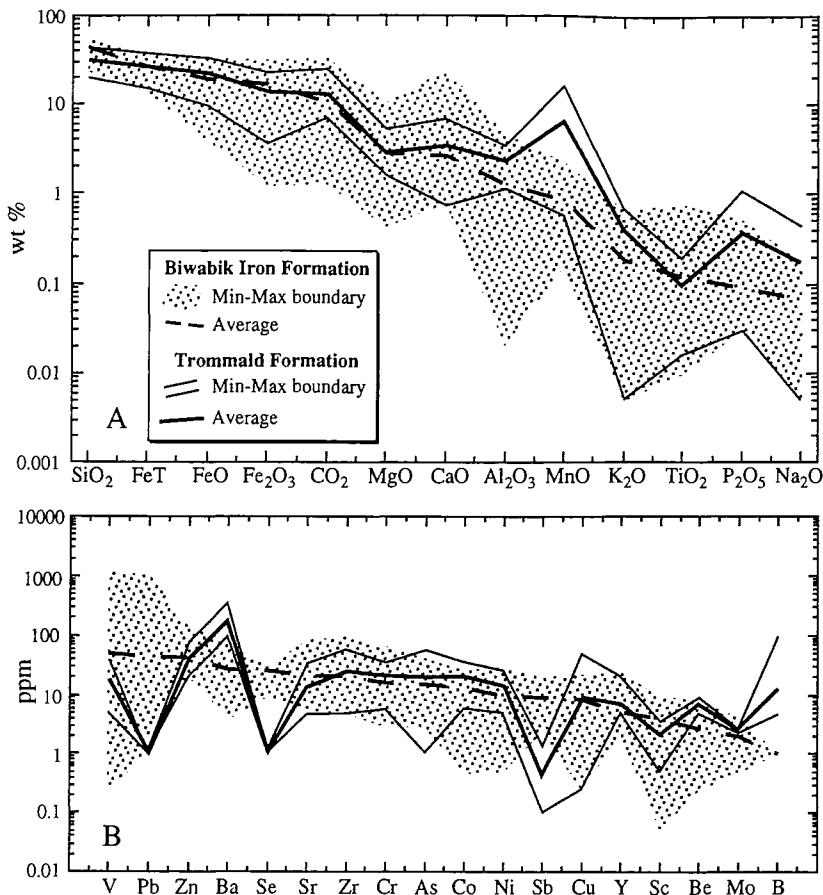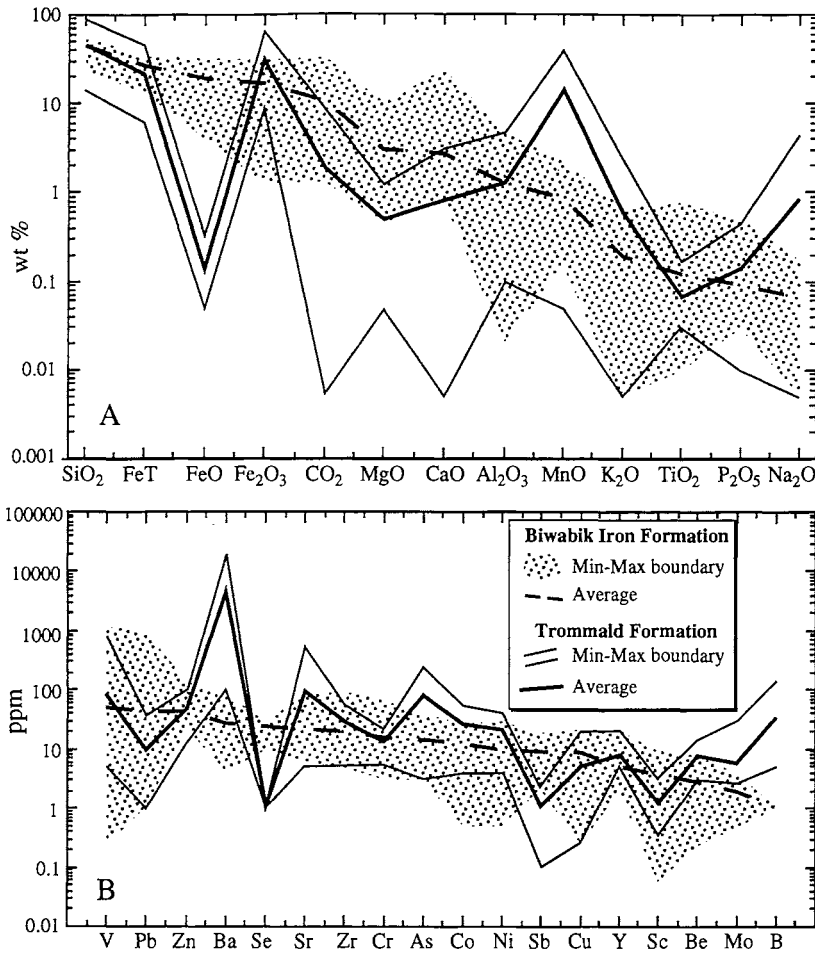
Figure 12. (A) Major and (B) minor element chemistry of the upper oxide member of the Trommald Formation compared to chemistry of the Biwabik Iron Formation.

(Fig. 14). It contains an average 2 to 3 weight percent Al_2O_3, whereas the Rabbit Lake and Mahnomen Formations contain about 15 weight percent Al_2O_3. Members within the Trommald Formation also can be distinguished by their bulk compositions. Hematite iron-formation in the upper member can be differentiated readily from the carbonate- and silicate-rich middle and lower members by the presence of less CO_2, CaO, and MgO, but more MnO.

The middle and lower members have only subtly different whole-rock compositions. The lower member has slightly more SiO_2, but less MnO, CaO, and CO_2 than does the middle member. This reflects the greater abundance of silicates in the former and carbonates in the latter. However, the absence of a sharp break between the compositions of middle and lower members implies a gradual transition from the deposition of silicates to deposition of carbonates. It also is interesting to note that the total iron content, reported as Fe_2O_3, generally ranges between 30 and 50 weight percent in all three members. Even though they contain markedly different iron minerals, their total iron contents are remarkably similar.

The boundary between the middle and upper members, however, marks a radical change in the whole-rock composition of the Trommald Formation (Fig. 14). Carbon dioxide all but disappears in the upper member with a corresponding decrease in CaO and MgO and an increase in MnO and variable iron content.

A plot of the MnO versus CO_2 contents of the lower and middle members shows a pronounced correlation (Fig. 18b), which strongly implies that manganese in thin-bedded strata is largely in a carbonate phase, an idea first proposed by Grout and Wolff (1955). The absence of a similar correlation in the upper member (Fig. 18a) implies that the Mn is probably present as an oxide or silicate phase. This is consistent with the identified presence of manganese oxides and rhodonite in the upper member.

MINERAL CHEMISTRY OF THE TROMMALD FORMATION

The major minerals contained in the Trommald Formation were analyzed using a Cameca SX50 electron microprobe at the University of Chicago. The results are summarized below.

21
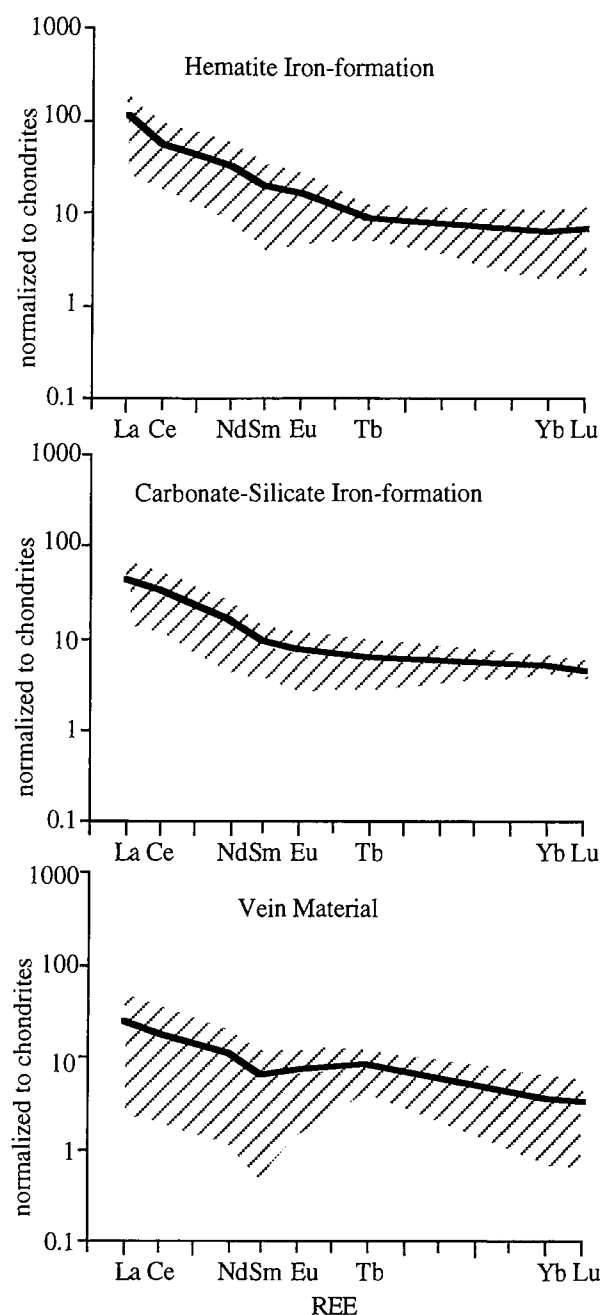
Figure 13. Rare earth element plots for the Trommald Formation normalized to chondrites. The central line represents the average value; the shaded areas represent one standard deviation from the mean.

Aegirine

Aegirine was first recognized in the Trommald Formation in 1941 and described in detail by Grout (1941, 1946) who referred to it as acmite. He suggested that this sodic pyroxene was of hypogene hydrothermal origin involving the reaction of hematite and chert with a Na-rich

solution. This pyroxene, now termed aegirine, has been described in some detail by McSwiggen and others (1994a) and the analytical data are summarized in Table 6. To date we have found aegirine only in the upper member where it occurs as core grains in micronodules, as very fine grained material in the groundmass of various stratigraphic layers, as bladed euhedral grains enclosed within the groundmass, as rims and various kinds of appendages on micronodules, and as vein material that transects these textures. The chemical data, however, show that the aegirine—regardless of textural setting—has a remarkably consistent composition.

Aegirine can form under a wide range of conditions. In addition to being a high-temperature phase, it also can form as a low-temperature authigenic mineral. It has been shown experimentally that it can form via a reaction between quartz and hematite in the presence of a NaCl-rich solution at fairly low temperatures (Likhoydov, 1981). Its presence in the upper member implies that a saline solution permeated sediments rich in ferric iron and silica at temperatures higher than those encountered under normal seafloor conditions.

Rhodonite

Rhodonite also has been found only in the upper member of the Trommald Formation, where it has textural attributes similar to those of aegirine. It occurs as core grains within micronodules (Fig. 9a and 9d), as mineral coatings around the core grains (Fig. 9b), as groundmass material, and as vein fillings. Electron microprobe analyses are summarized in Table 7. These data show that rhodonite compositions deviate from the pure end-member composition ($MnSiO_3$) only in their MgO and CaO content. Typically they contain less than 1.5 weight percent MgO and between 1.3 and 6.3 weight percent CaO. They fall within the range reported by Deer and others (1978) as the most manganese-rich examples known. According to Deer and others (1978), rhodonite occurs in many manganese ore deposits and is typically associated with metasomatic activities. It occurs in deposits such as those at Broken Hill, New South Wales; Långban, Sweden; Franklin, New Jersey; and the Wabush Iron Formation of the Labrador Trough, Canada.

Hyalophane

Hyalophane [(K, Ba)$Al_{1-2}Si_{3-2}O_8$]is one of the Ba-feldspars. It too has been found only in the upper member of the Trommald Formation. Like aegirine and rhodonite, it has several textural attributes that imply that it formed at different times in the paragenetic history of the rock. A more detailed summary is given in McSwiggen and others (1994b). Electron microprobe results are summarized in Table 8.

Table 6a. Electron microprobe analyses of aegirine core grains from the upper member of the Trommald Formation, Merritt hole
[Major elements in wt% oxides; n.d., not detected]

Sample	core grains									
	M262.6	M262.6	M262.6	M262.6	M278.8	M262.4R	M262.4R	M262.4R	M262.4R	M262.4R
SiO_2	55.00	52.82	51.51	52.65	53.41	52.83	52.44	51.97	52.82	52.44
TiO_2	0.02	0.02	0.03	0.02	0.05	n.d.	n.d.	0.01	0.03	0.04
Al_2O_3	0.51	0.40	0.43	0.20	0.22	0.77	0.60	0.81	0.85	0.51
Cr_2O_3	n.d.	0.04	n.d.	n.d.	0.03	0.04	0.01	0.02	n.d.	0.04
Fe_2O_3*	29.45	31.28	30.56	31.59	28.19	32.67	30.04	32.29	33.03	31.77
FeO*	1.00	1.89	1.73	2.50	0.77	0.74	2.61	0.49	0.37	1.07
$FeO_{(t)}$^	27.50	30.04	29.23	30.92	26.13	30.14	29.64	29.54	30.09	29.66
MnO	1.96	0.65	2.11	0.53	3.14	0.44	0.69	0.67	0.42	0.75
MgO	0.03	n.d.	0.08	n.d.	1.03	n.d.	n.d.	n.d.	n.d.	0.02
CaO	0.65	1.43	0.76	0.98	3.02	0.20	1.48	0.59	0.20	0.82
Na_2O	11.43	12.14	11.86	12.26	10.94	12.68	11.66	12.53	12.82	12.33
K_2O	0.02	0.02	n.d.	0.01	n.d.	n.d.	n.d.	0.03	n.d.	0.01
Total	100.07	100.69	99.07	100.73	100.79	100.37	99.53	99.40	100.54	99.80

Table 6b. Electron microprobe analyses of fine-grained aegirine groundmass and bladed aegirine from the upper member of the Trommald Formation, Merritt hole [Major elements in wt% oxides; n.d., not detected]

Sample	fine ground mass									blades
	M262.6	M262.6	M264.4	M278.8	M277	M277	M288	M288	M288	M288
SiO_2	53.07	52.66	52.15	52.97	53.07	53.62	52.64	53.49	53.01	52.59
TiO_2	0.02	0.04	0.03	0.03	0.04	0.02	0.01	n.d.	0.01	0.07
Al_2O_3	0.35	0.31	0.06	0.42	0.46	0.53	0.49	0.42	0.54	0.13
Cr_2O_3	n.d.	n.d.	0.03	0.01	0.03	n.d.	n.d.	n.d.	n.d.	n.d.
Fe_2O_3*	32.23	30.87	31.02	30.12	27.88	28.42	31.15	32.62	31.95	31.00
FeO*	1.09	1.16	1.11	1.25	1.45	0.45	1.61	0.80	1.66	1.16
$FeO_{(t)}$^	30.09	28.94	29.02	28.35	26.54	26.02	29.64	30.15	30.41	29.05
MnO	0.74	1.96	2.19	1.44	2.67	2.37	0.51	0.30	0.42	1.89
MgO	0.06	0.11	0.44	1.03	1.68	1.55	0.48	0.19	0.05	0.03
CaO	0.53	1.53	1.72	1.70	2.41	2.22	0.73	0.45	0.63	1.28
Na_2O	12.51	11.98	12.04	11.69	10.82	11.03	12.09	12.66	12.40	12.03
K_2O	0.01	0.01	0.01	0.02	0.01	n.d.	n.d.	n.d.	0.01	n.d.
Total	100.61	100.63	100.80	100.68	100.52	100.21	99.71	100.93	100.68	100.18

* Estimated from stoichiometry
^ Total measured iron represented as FeO.

Table 6c. Electron microprobe analyses of aegirine rims and appendages on micronodules from the upper member of the Trommald Formation, Merritt hole [Major elements in wt% oxides; n.d., not detected]

Sample	micronodule rims							appendages	
	M262.6	M262.6	M262.6	M262.6	M264.4	M264.4	M264.4	M262.4R	M262.4R
SiO_2	53.30	52.97	53.30	53.25	52.59	52.77	52.38	52.55	53.09
TiO_2	0.03	0.05	0.02	0.05	n.d.	0.04	0.03	0.01	0.01
Al_2O_3	0.28	0.52	0.34	0.51	0.32	0.22	0.40	0.34	0.59
Cr_2O_3	n.d.	0.02	n.d.	n.d.	0.04	0.03	0.01	0.02	n.d.
Fe_2O_3*	30.38	32.65	31.25	31.67	31.51	30.92	31.80	30.43	32.29
FeO*	1.73	0.40	1.25	0.45	1.64	0.99	0.96	2.91	1.91
$FeO_{(t)}$^	29.06	29.78	29.37	28.94	30.00	28.81	29.57	30.29	30.96
MnO	1.22	0.68	1.09	1.19	0.70	1.41	0.56	1.01	0.15
MgO	0.30	0.16	0.29	0.15	0.26	0.33	0.25	0.01	0.08
CaO	1.24	0.53	0.99	0.95	0.67	1.35	0.62	1.58	0.21
Na_2O	11.79	12.67	12.13	12.29	12.23	12.00	12.34	11.81	12.53
K_2O	0.02	0.01	n.d.	0.01	0.01	0.01	n.d.	0.02	0.01
Total	100.28	100.66	100.66	100.51	99.98	100.07	99.35	100.69	100.86

Table 6d. Electron microprobe analyses of aegirine vein filling from the upper member of the Trommald Formation, Merritt hole [Major elements in wt% oxides; ---, not analyzed; n.d., not detected]

Sample	vein fillings												
	M262.6	M264.4	M262.4	M262.4	M262.4	M278.1	M278.1	M278.1	M278.1	M278.1	M278.1	M278.1	M278.1
SiO_2	53.12	52.79	53.00	52.87	53.27	53.04	52.50	52.73	52.40	53.11	52.98	53.49	53.09
TiO_2	0.04	0.02	0.13	0.03	0.07	0.05	n.d.	n.d.	n.d.	0.03	0.02	0.03	0.02
Al_2O_3	0.79	0.80	0.64	0.73	0.81	0.42	0.41	0.36	0.51	0.50	0.43	0.44	0.43
Cr_2O_3	n.d.	n.d.	n.d.	0.02	0.01	—	—	—	—	---	—	—	—
Fe_2O_3*	29.66	30.95	28.65	31.00	30.77	31.99	32.95	32.57	33.27	32.06	32.75	32.59	32.28
FeO*	0.74	0.73	2.78	1.16	1.81	1.82	1.36	1.57	0.23	1.49	1.12	1.40	2.12
$FeO_{(t)}$^	27.43	28.58	28.56	29.05	29.49	30.60	31.02	30.87	30.16	30.34	30.59	30.73	31.17
MnO	1.15	1.07	0.94	0.75	0.77	0.07	0.09	0.14	0.16	0.27	0.06	0.09	0.09
MgO	1.13	0.60	0.56	0.21	0.42	0.08	0.09	0.14	0.25	0.33	0.08	0.09	0.09
CaO	2.24	1.38	1.34	0.80	1.02	0.14	0.18	0.19	0.38	0.53	0.16	0.14	0.15
Na_2O	11.51	12.01	11.12	12.03	11.94	12.41	12.79	12.64	12.91	12.44	12.71	12.65	12.53
K_2O	0.01	n.d.	0.12	n.d.	n.d.	n.d.	0.01	0.01	0.02	0.03	n.d.	n.d.	n.d.
Total	100.39	100.35	99.28	99.60	100.88	100.01	100.40	100.35	100.13	100.79	100.31	100.92	100.80

* Estimated from stoichiometry
^ Total measured iron represented as FeO.

Table 7a. Electron microprobe analyses of rhodonite clasts in the upper member of the Trommald Formation, Merritt hole
[Major elements in wt% oxides; n.d., not detected]

Sample	M264.4	M294.7	M294.7	M294.7	M294.7	M264.4	M294.7	M294.7	M294.7	M294.7
SiO_2	46.58	46.95	47.05	46.13	46.75	46.70	46.45	47.10	46.83	45.77
TiO_2	0.02	n.d.	0.01	n.d.	n.d.	0.04	n.d.	0.01	0.05	0.02
Al_2O_3	n.d.	0.01	n.d.	n.d.	n.d.	n.d.	0.02	0.13	n.d.	0.01
Cr_2O_3	0.01	0.03	n.d.	n.d.	n.d.	n.d.	n.d.	0.05	n.d.	0.04
FeO	n.d.	n.d.	n.d.	n.d.	n.d.	n.d.	n.d.	0.01	n.d.	2.81
MnO	48.87	49.90	49.95	48.21	48.75	47.18	50.59	49.62	50.03	47.03
MgO	0.36	1.60	1.66	1.15	1.33	0.19	0.69	1.10	1.17	1.20
CaO	3.84	1.88	1.86	4.29	3.71	6.36	1.83	1.62	2.04	3.38
Na_2O	n.d.	0.01	n.d.	n.d.	n.d.	0.01	0.01	n.d.	0.01	n.d.
K_2O	n.d.	n.d.	n.d.	n.d.	n.d.	0.01	0.01	n.d.	0.01	0.01
Total	99.66	100.37	100.54	99.78	100.54	100.48	99.60	99.63	100.14	100.25

Table 7b. Electron microprobe analyses of rhodonite rims around micronodules and rhodonite vein filling in the upper member of the Trommald Formation, Merritt hole
[Major elements in wt% oxides; ---, not analyzed; n.d., not detected]

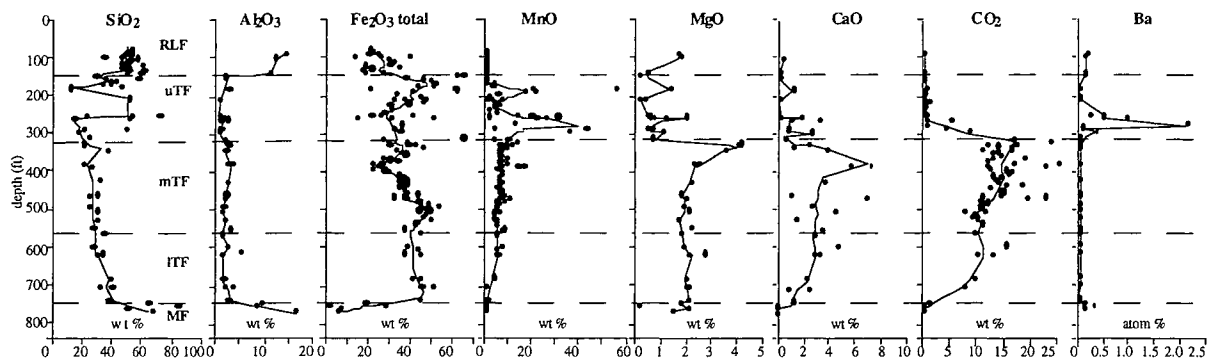|	rim			vein
Sample	M294.0	M294.0	M294.0	M278.8
SiO_2	47.46	47.30	47.23	47.36
TiO_2	---	---	---	n.d.
Al_2O_3	0.03	0.01	n.d.	n.d.
Cr_2O_3	---	---	---	0.01
FeO	0.07	0.18	n.d.	n.d.
MnO	48.20	49.21	48.56	46.51
MgO	1.52	1.67	1.07	0.46
Na_2O	0.01	n.d.	n.d.	0.01
CaO	1.78	1.347	2.952	6.29
K_2O	0.02	0.04	0.02	n.d.
Total	99.09	99.75	99.82	100.64

Figure 14. Compositional profiles through the Rabbit Lake Formation (RLF), the upper (uTF), middle (mTF), and lower (lTF) members of the Trommald Formation, and the Mahnomen Formation (MF) from drill core at the Merritt mine. Analyses are from this study and from Grout and Wolff (1955). Profiles are weighted curves fit to the data to illustrate compositional trends.

Hyalophane and other Ba-silicates have a very restricted paragenesis. Typically they are associated with sediment-hosted exhalative manganese deposits and deposits associated with Cu-Pb-Zn-Ba mineralization.

Carbonates

The Trommald Formation contains abundant carbonates, some of which have compositions that are rare in nature. Electron microprobe analyses of the carbonates are listed in Table 9. All of the carbonates fall in the four-component compositional space defined by $CaCO_3$-$FeCO_3$-$MnCO_3$-$MgCO_3$. This carbonate system is very complex and many details are still unclear. However, a summary of the phase relationships in the four ternary systems is shown in Figure 19. These diagrams were constructed using information from a number of sources. The $MgCO_3$-$FeCO_3$-$CaCO_3$ diagram is from Rosenberg (1967) and McSwiggen (1993). The $MgCO_3$-$MnCO_3$-$CaCO_3$ diagram is modified from Goldsmith and Graf (1960). The ternary carbonate field $MgCO_3$-$FeCO_3$-$MnCO_3$ is assumed to be continuous solid solution, inasmuch as it is bounded on all three sides by binary solid solutions. A compilation of natural carbonate compositions by Essene (1983) suggests that a miscibility gap exists for carbonates along the $MnCO_3$-$MgCO_3$ binary. However, Goldsmith and Graf (1960) have shown experimentally that complete solid solution exists along this binary. Therefore the gap in Essene's data may result from the lack of appropriate bulk compositions in the rocks being studied. The ternary field $CaCO_3$-$MnCO_3$-$FeCO_3$ was constructed using the natural assemblages of this study and the other ternary systems.

Because of the moderately low Mg-contents of most of the carbonates in this study, they can be approximated using ternary $CaCO_3$-$MnCO_3$-$FeCO_3$ diagrams (Figs. 20-22). It is obvious that carbonates in the upper member are different from those in the middle and lower members. In the upper member, the carbonates contain little or no iron and consequently most analyses lie along the calcite-rhodochrosite binary (Fig. 20). Most of the data fall along the zone of solid solution extending from calcite to kutnahorite [$CaMn(CO_3)_2$]. The remaining data plot in the rhodochrosite field. A gap in the data set occurs between $X_{MnCO_3} = 0.78$ and 0.55. The width of this gap based on the experimental work of Goldsmith and Graf (1957) suggests an equilibrium metamorphic temperature of 480° to 490°C.

The middle and lower members of the Trommald Formation commonly contain two coexisting carbonates, a manganiferous siderite and a dolomite-like carbonate that occurs over a range in composition from ferroan dolomite to ferroan kutnahorite or manganiferous ankerite. From the plots in Figures 20-22, the compositions of these dolomite-like carbonates appear to shift toward the $CaCO_3$ component with increasing MgO content. This shift is an artifact of the projection used. On a quaternary $CaCO_3$-$MgCO_3$-$MnCO_3$-$FeCO_3$ plot, the dolomite-like, $R\bar{3}$, carbonates fall very near the $CaMg(CO_3)_2$-$CaMn(CO_3)_2$-$CaFe(CO_3)_2$ plane (Fig. 23). For clarity, the data from the Merritt and Arko holes were plotted separately. If the two data sets were overlain, the Arko carbonates would cut across the tie lines from the Merritt hole and thus indicate that the Arko and the Merritt sites represent two different sets of equilibrium conditions.

The carbonates from the middle and lower members that lie near the $CaMg(CO_3)_2$-$CaMn(CO_3)_2$-$CaFe(CO_3)_2$ plane have been plotted separately in Figure 24a. A published (Essene, 1983) compilation of natural carbonates in this compositional range is shown in Figure 24b. Some of the Cuyuna data fall within compositional space not previously reported. However, our data do not answer the questions as to the extent of the miscibility gap along the $CaFe(CO_3)_2$-$CaMn(CO_3)_2$ join. Experimental work and

26

Table 8a. Electron microprobe analyses of authigenic hyalophane from the upper member of the Trommald Formation, Merritt hole
[Major elements in wt% oxides; ---, not analyzed; n.d., not detected]

Sample	M271.1	M271.1	M271.1	M271.1	M271.1	M271.1	M262.6	M262.6	M264.4	M264.4	M264.4
SiO_2	59.77	60.94	60.72	61.58	57.57	61.31	57.45	64.54	57.30	57.35	57.75
Al_2O_3	19.93	19.83	20.36	19.40	20.35	19.86	20.48	18.35	20.54	19.67	20.49
FeO	n.d.	0.10	0.12	0.11	0.07	0.09	---	---	---	---	---
MgO	n.d.	n.d.	n.d.	n.d.	n.d.	n.d.	---	---	---	---	---
CaO	n.d.	n.d.	0.01	n.d.	n.d.	0.01	n.d.	n.d.	n.d.	n.d.	n.d.
Na_2O	0.61	0.62	0.56	0.45	0.66	0.64	0.31	0.31	0.63	0.40	0.58
K_2O	13.58	13.93	12.02	14.37	12.18	13.78	11.46	16.48	11.00	11.25	11.42
BaO	6.48	5.10	6.66	4.49	9.13	5.09	10.41	0.14	10.74	10.91	9.96
SrO	---	---	---	---	---	---	---	---	---	---	---
Total	100.37	100.53	100.44	100.40	99.97	100.78	100.11	99.81	100.21	99.57	100.19

Table 8b. Electron microprobe analyses of hyalophane core grains and hyalophane rims of micronodules from the upper member of the Trommald Formation, Merritt hole [Major elements in wt% oxides; ---, not analyzed; n.d., not detected]

	core grains								rims		
Sample	M294	M294	M294	M294.0	M294.0	M294.7	M294.7	M294.7	M294.7	M294.7	M294.7
SiO_2	59.21	59.13	58.27	57.03	59.16	58.95	59.19	59.54	59.22	57.22	61.44
Al_2O_3	20.18	19.97	20.18	20.54	20.12	19.86	19.74	19.41	20.38	20.83	20.06
FeO	0.13	0.06	0.12	0.32	0.17	---	---	---	---	---	---
MgO	n.d.	n.d.	n.d.	n.d.	n.d.	---	---	---	---	---	---
CaO	0.01	n.d.	n.d.	n.d.	n.d.	0.03	n.d.	n.d.	0.03	0.03	0.13
Na_2O	0.64	0.64	0.66	0.61	0.67	0.69	0.66	0.64	0.42	0.48	0.42
K_2O	12.94	13.11	12.76	12.07	12.91	13.32	13.28	12.81	11.04	10.95	11.39
BaO	7.57	7.04	7.99	10.21	7.65	6.79	7.05	6.97	9.09	10.14	6.15
SrO	---	---	---	---	---	n.d.	n.d.	---	---	---	---
Total	100.66	99.94	99.98	100.77	100.67	99.63	99.92	99.36	100.18	99.64	99.59

Table 8c. Electron microprobe analyses of hyalophane vein filling in the upper member of the Trommald Formation, Merritt hole
[Major elements in wt% oxides; ---, not analyzed; n.d., not detected]

Sample	M278.8	M278.8	M278.8	M278.8	M278.8	M278.8	M278.8	M278.8	M278.8	M278.8	M278.8
SiO_2	60.54	60.92	60.35	60.88	60.59	61.40	60.82	58.90	57.76	58.40	56.63
Al_2O_3	19.65	19.54	19.59	19.30	19.59	19.49	19.52	19.89	20.70	20.01	20.37
FeO	---	---	---	---	---	---	---	---	---	---	---
MgO	---	---	---	---	---	---	---	---	---	---	---
CaO	n.d.	n.d.	n.d.	n.d.	n.d.	n.d.	n.d.	n.d.	0.02	n.d.	n.d.
Na_2O	0.39	0.52	0.60	0.45	0.63	0.57	0.60	0.36	0.44	0.44	0.33
K_2O	14.15	14.05	14.26	14.08	13.91	14.16	14.03	13.48	12.00	12.55	11.99
BaO	5.02	4.56	4.69	4.36	5.12	4.53	4.86	6.81	8.79	8.11	10.61
SrO	n.d.	n.d.	n.d.	n.d.	n.d.	n.d.	n.d.	n.d.	n.d.	n.d.	n.d.
Total	99.75	99.60	99.50	99.06	99.84	100.16	99.84	99.44	99.71	99.51	99.93

Table 8c. (continued)
[Major elements in wt% oxides; ---, not analyzed; n.d., not detected]

Sample	M278.8	M278.8	M278.1	M278.1	M278.1	M278.1	M294.7	M278.8	M278.8	M259
SiO_2	57.73	57.86	54.85	55.47	55.15	53.93	57.30	60.20	57.31	56.15
Al_2O_3	20.35	19.96	20.73	20.66	20.77	21.06	20.53	19.31	20.39	20.41
FeO	---	---	---	---	---	---	---	---	---	---
MgO	---	---	---	---	---	---	---	---	---	---
CaO	n.d.	n.d.	n.d.	n.d.	n.d.	n.d.	n.d.	n.d.	0.01	n.d.
Na_2O	0.40	0.31	0.31	0.39	0.30	0.50	0.63	0.63	0.54	0.55
K_2O	12.44	12.45	11.65	11.65	11.81	10.66	11.98	13.34	10.51	11.69
BaO	9.22	9.17	12.56	12.20	12.07	13.31	10.21	6.50	11.18	10.96
SrO	n.d.	n.d.	n.d.	n.d.	n.d.	n.d.	---	---	---	---
Total	100.14	99.75	100.10	100.37	100.10	99.47	100.64	99.98	99.95	99.74

Table 9a. Electron microprobe analyses of carbonate rims of micronodules in the upper member of the Trommald Formation, Merritt hole [Major elements in wt% oxides; ---, not analyzed; n.d., not detected]

Sample	M294.7	M294.7	M294.7	M294.7	M294.7	M294.7	M294.7	M294.7	M294.7
CaO	23.79	23.32	23.21	6.23	1.84	7.02	6.92	2.86	8.75
MgO	1.10	1.03	1.17	1.22	0.40	0.66	0.62	0.51	0.68
FeO	n.d.	n.d.	n.d.	n.d.	n.d.	n.d.	n.d.	n.d.	n.d.
MnO	35.10	34.48	35.77	55.89	60.06	54.30	54.24	58.36	52.15
BaO	---	---	---	---	---	---	---	---	---
SrO	---	---	---	---	---	---	---	---	---
Total	59.99	58.83	60.15	63.34	62.30	61.98	61.78	61.73	61.58
X_{CaCO_3}	0.448	0.448	0.437	0.120	0.037	0.138	0.137	0.057	0.172
X_{MgCO_3}	0.029	0.027	0.031	0.033	0.011	0.018	0.017	0.014	0.018
X_{FeCO_3}	0.000	0.000	0.000	0.000	0.000	0.000	0.000	0.000	0.000
X_{MnCO_3}	0.523	0.524	0.532	0.848	0.952	0.844	0.846	0.928	0.810

Table 9a. (continued)
[Major elements in wt% oxides; ---, not analyzed; n.d., not detected]

Sample	M294.7	M294.7	M294.7	M294.7	M294.7	M294.7	M294.7	M262B	M266B	M266B
CaO	6.47	10.20	30.06	25.32	10.11	30.17	7.44	4.75	6.28	4.63
MgO	0.61	0.67	0.93	1.35	0.97	0.88	0.66	2.36	3.69	2.02
FeO	n.d.	n.d.	n.d.	n.d.	n.d.	0.62	n.d.	7.98	0.02	5.94
MnO	54.78	47.53	29.08	33.70	49.53	28.82	53.55	44.94	47.39	45.88
BaO	---	---	---	---	---	---	---	---	---	---
SrO	---	---	---	---	---	---	---	---	---	---
Total	61.86	58.40	60.07	60.37	60.61	60.49	61.65	60.02	57.39	58.47
X_{CaCO_3}	0.128	0.209	0.553	0.470	0.200	0.552	0.147	0.095	0.128	0.096
X_{MgCO_3}	0.017	0.019	0.024	0.035	0.027	0.022	0.018	0.066	0.105	0.058
X_{FeCO_3}	0.000	0.000	0.000	0.000	0.000	0.009	0.000	0.125	0.000	0.096
X_{MnCO_3}	0.855	0.771	0.423	0.495	0.774	0.417	0.835	0.714	0.766	0.750

Table 9b. Electron microprobe analyses of carbonate cores of micronodules in the upper member of the Trommald Formation, Merritt hole
[Major elements in wt% oxides; ---, not analyzed; n.d., not detected]

Sample	M264.4	M264.4	M277	M277	M277	M277	M277
CaO	5.98	6.93	43.73	42.77	4.55	44.40	39.97
MgO	0.37	0.90	0.46	0.41	1.54	0.36	0.47
FeO	n.d.	n.d.	n.d.	n.d.	n.d.	n.d.	n.d.
MnO	54.85	53.27	20.92	18.64	52.38	17.67	23.39
BaO	---	---	---	---	---	---	---
SrO	---	---	---	---	---	---	---
Total	61.20	61.10	65.11	61.82	58.47	62.43	63.83
X_{CaCO_3}	0.120	0.138	0.718	0.736	0.095	0.754	0.676
X_{MgCO_3}	0.010	0.025	0.011	0.010	0.045	0.008	0.011
X_{FeCO_3}	0.000	0.000	0.000	0.000	0.000	0.000	0.000
X_{MnCO_3}	0.870	0.837	0.272	0.254	0.861	0.237	0.313

Table 9c. Electron microprobe analyses of carbonate vein filling in the Trommald Formation, Merritt hole
[Major elements in wt% oxides; ---, not analyzed; n.d., not detected]

Sample	M262.6	M262.6	M259	M259	M436.6	M436.6	M436.6	M436.6	M436.6	M436.6	M436.6
CaO	35.79	36.65	2.88	3.96	31.96	29.80	28.91	31.48	1.99	1.52	1.62
MgO	0.93	0.86	1.69	1.68	12.94	10.91	8.29	12.76	2.33	1.67	1.14
FeO	n.d.	n.d.	n.d.	n.d.	11.34	9.31	6.60	7.12	37.46	42.13	44.36
MnO	22.70	23.36	57.04	55.67	5.03	10.66	11.53	7.84	15.33	13.17	11.33
BaO	---	---	---	---	---	---	---	---	---	---	---
SrO	---	---	---	---	---	---	---	---	---	---	---
Total	59.42	60.87	61.61	61.31	61.27	60.68	55.34	59.20	57.12	58.48	58.45
X_{CaCO_3}	0.650	0.651	0.057	0.079	0.509	0.491	0.528	0.516	0.043	0.032	0.035
X_{MgCO_3}	0.023	0.021	0.047	0.047	0.287	0.250	0.211	0.291	0.070	0.049	0.034
X_{FeCO_3}	0.000	0.000	0.000	0.000	0.141	0.120	0.094	0.091	0.628	0.698	0.740
X_{MnCO_3}	0.326	0.328	0.896	0.875	0.063	0.139	0.167	0.102	0.260	0.221	0.191

Table 9c. (continued)
[Major elements in wt% oxides; ---, not analyzed; n.d., not detected]

Sample	M436.6	M618.9	M618.9	M618.9	M618.9	M618.9	M618.9	M618.9	M618.9	M618.9	M618.9
CaO	1.20	29.27	28.90	29.94	28.77	31.08	28.72	30.16	28.36	33.01	1.73
MgO	2.36	13.60	13.22	13.59	15.05	12.59	6.02	13.74	7.57	11.66	2.39
FeO	41.54	8.68	8.37	8.93	8.48	7.76	8.93	8.83	9.55	8.68	39.62
MnO	13.02	4.76	3.95	4.56	3.53	4.15	13.29	3.84	9.71	4.51	13.83
BaO	---	n.d.	n.d.	n.d.	0.01	n.d.	0.02	n.d.	0.01	n.d.	n.d.
SrO	---	0.01	0.08	n.d.	n.d.	0.06	0.01	n.d.	0.04	n.d.	0.05
Total	58.12	56.33	54.51	57.02	55.83	55.64	56.97	56.57	55.24	57.86	57.62
X_{CaCO_3}	0.025	0.498	0.508	0.504	0.487	0.537	0.526	0.509	0.525	0.554	0.037
X_{MgCO_3}	0.070	0.322	0.323	0.318	0.354	0.302	0.153	0.323	0.195	0.272	0.071
X_{FeCO_3}	0.687	0.115	0.115	0.117	0.112	0.105	0.128	0.116	0.138	0.114	0.659
X_{MnCO_3}	0.218	0.064	0.055	0.061	0.047	0.057	0.193	0.051	0.142	0.060	0.233

Table 9c. (continued)
[Major elements in wt% oxides; n.d., not detected]

Sample	M618.9	M630.1	M630.1	M630.1	M630.1	M630.1	M630.1	M634.0	M634.0	M634.0	M634.0
CaO	1.52	28.83	29.84	30.27	30.22	31.98	27.15	29.60	28.90	2.18	1.91
MgO	2.39	8.45	12.37	12.62	10.43	10.55	1.86	7.15	7.62	2.70	2.34
FeO	39.30	9.10	7.36	7.07	7.11	7.66	16.79	8.91	9.69	45.22	42.53
MnO	14.19	7.56	5.40	5.28	7.92	7.00	9.74	10.75	10.58	8.61	12.09
BaO	0.05	n.d.	n.d.	0.02	n.d.	n.d.	n.d.	0.04	n.d.	n.d.	n.d.
SrO	0.07	0.15	0.05	0.09	0.12	n.d.	0.05	0.09	0.08	0.03	n.d.
Total	57.52	54.08	55.01	55.35	55.79	57.19	55.59	56.54	56.87	58.73	58.87
X_{CaCO_3}	0.032	0.537	0.523	0.526	0.535	0.550	0.537	0.538	0.521	0.045	0.040
X_{MgCO_3}	0.071	0.219	0.302	0.305	0.257	0.252	0.051	0.181	0.191	0.078	0.068
X_{FeCO_3}	0.656	0.132	0.101	0.096	0.098	0.103	0.259	0.126	0.136	0.735	0.693
X_{MnCO_3}	0.240	0.111	0.075	0.073	0.111	0.095	0.152	0.155	0.151	0.142	0.199

Table 9d. Electron microprobe analyses of carbonate groundmass in the upper member of the Trommald Formation, Merritt hole
[Major elements in wt% oxides; ---, not analyzed; n.d., not detected]

Sample	M288	M288	M288	M288	M264.9	M264.9	M264.9	M271.1	M271.1	M271.1	M271.1	M271.1
CaO	7.24	6.85	27.95	26.33	6.12	3.68	5.42	7.75	4.91	5.24	1.61	3.18
MgO	0.43	0.49	0.88	0.88	1.90	1.50	1.90	0.70	0.60	0.69	0.82	1.20
FeO	n.d.	n.d.	n.d.	n.d.	0.23	0.55	0.16	n.d.	n.d.	n.d.	n.d.	n.d.
MnO	53.93	54.09	32.41	33.22	52.35	54.83	51.22	50.57	54.55	53.80	57.66	56.68
BaO	---	---	---	---	n.d.	n.d.	n.d.	0.05	0.03	0.08	n.d.	n.d.
SrO	---	---	---	---	0.22	0.17	0.09	0.05	n.d.	n.d.	0.03	0.05
Total	61.60	61.43	61.24	60.43	60.81	60.72	58.79	59.13	60.09	59.81	60.12	61.10
X_{CaCO_3}	0.143	0.136	0.510	0.489	0.122	0.074	0.111	0.159	0.101	0.108	0.033	0.064
X_{MgCO_3}	0.012	0.014	0.022	0.023	0.053	0.042	0.054	0.020	0.017	0.020	0.024	0.034
X_{FeCO_3}	0.000	0.00	0.000	0.000	0.004	0.009	0.003	0.000	0.000	0.000	0.000	0.000
X_{MnCO_3}	0.845	0.850	0.468	0.488	0.822	0.875	0.832	0.821	0.883	0.873	0.943	0.902

Table 9e. Electron microprobe analyses of carbonate groundmass in the middle and lower members of the Trommald Formation, Merritt hole
[Major elements in wt% oxides; n.d., not detected]

Sample	M326.6	M326.6	M326.6	M326.6	M326.6	M326.6	M326.6	M326.6	M326.6	M351.2	M351.2	M351.2
CaO	24.60	1.52	24.77	24.74	1.47	23.62	1.29	2.01	1.50	1.40	1.90	1.35
MgO	3.62	4.73	3.89	3.89	4.50	3.48	4.56	5.05	4.52	3.21	3.26	3.49
FeO	13.81	34.01	14.71	14.64	33.96	12.82	32.84	33.55	33.64	38.17	38.61	40.38
MnO	12.90	17.59	12.02	12.23	18.80	15.40	19.13	17.76	17.92	14.25	13.71	12.44
BaO	0.02	n.d.	n.d.	n.d.	n.d.	n.d.	0.01	0.03	n.d.	0.02	n.d.	0.02
SrO	0.10	0.02	0.09	0.03	n.d.	0.06	n.d.	n.d.	0.01	n.d.	n.d.	0.01
Total	55.05	57.86	55.48	55.54	58.73	55.37	57.84	58.39	57.58	57.05	57.48	57.69
X_{CaCO_3}	0.486	0.031	0.484	0.483	0.030	0.467	0.027	0.041	0.031	0.030	0.040	0.028
X_{MgCO_3}	0.099	0.135	0.106	0.106	0.128	0.095	0.131	0.142	0.130	0.095	0.095	0.102
X_{FeCO_3}	0.213	0.547	0.224	0.223	0.540	0.198	0.530	0.532	0.545	0.635	0.636	0.663
X_{MnCO_3}	0.202	0.286	0.186	0.189	0.303	0.240	0.312	0.285	0.294	0.240	0.229	0.207

Table 9e. (continued)
[Major elements in wt% oxides; n.d., not detected]

Sample	M351.2	M435	M435	M435	M503.4	M503.4	M503.4	M503.4	M529.2	M529.2	M529.2	M529.2
CaO	1.91	26.54	1.44	25.94	30.68	25.76	27.57	21.98	23.76	27.37	1.76	3.58
MgO	3.24	1.72	2.61	2.07	9.71	3.29	8.29	1.87	3.35	7.25	2.31	1.71
FeO	38.74	16.29	40.80	16.79	12.90	16.50	13.61	18.78	15.02	10.35	41.12	41.92
MnO	14.18	10.85	13.63	10.91	4.12	9.92	8.52	12.43	13.76	12.69	12.73	10.25
BaO	n.d.	n.d.	n.d.	n.d.	n.d.	n.d.	0.01	0.01	n.d.	0.01	n.d.	0.07
SrO	n.d.	0.10	0.08	0.11	0.09	0.09	0.08	0.08	0.10	0.08	0.02	n.d.
Total	58.07	55.50	58.55	55.82	57.50	55.55	58.08	55.15	56.00	57.75	57.93	57.53
X_{CaCO_3}	0.040	0.528	0.030	0.513	0.533	0.505	0.488	0.448	0.466	0.493	0.037	0.076
X_{MgCO_3}	0.094	0.048	0.076	0.057	0.235	0.090	0.204	0.053	0.091	0.181	0.068	0.051
X_{FeCO_3}	0.632	0.253	0.668	0.259	0.175	0.252	0.188	0.299	0.230	0.145	0.681	0.699
X_{MnCO_3}	0.234	0.171	0.226	0.171	0.057	0.154	0.119	0.200	0.213	0.181	0.213	0.173

Table 9e. (continued)
[Major elements in wt% oxides; n.d., not detected]

Sample	M570	M570	M595	M595	M595	M626.8	M626.8	M685.2	M685.2	M685.2	M685.2	M685.2
CaO	24.91	28.01	25.80	2.29	24.72	1.65	30.86	27.67	27.83	1.12	1.08	28.01
MgO	1.62	6.51	2.24	2.09	2.25	2.44	8.54	10.51	10.12	3.24	3.10	10.10
FeO	14.41	11.18	18.02	43.11	15.93	41.40	7.99	12.85	11.58	46.58	46.50	14.04
MnO	15.25	10.78	11.14	11.48	13.10	12.66	8.39	4.79	6.44	7.47	7.97	6.13
BaO	0.03	0.01	n.d.	0.01	0.02	n.d.	0.03	n.d.	n.d.	n.d.	n.d.	n.d.
SrO	0.09	0.15	0.03	n.d.	0.03	n.d.	n.d.	n.d.	n.d.	n.d.	0.12	n.d.
Total	56.30	56.63	57.23	58.98	56.05	58.15	55.80	55.82	55.97	58.42	58.77	58.28
X_{CaCO_3}	0.494	0.516	0.498	0.048	0.488	0.035	0.555	0.493	0.497	0.023	0.023	0.484
X_{MgCO_3}	0.045	0.167	0.060	0.061	0.062	0.072	0.214	0.261	0.251	0.094	0.090	0.243
X_{FeCO_3}	0.223	0.161	0.272	0.702	0.246	0.682	0.112	0.179	0.161	0.759	0.756	0.189
X_{MnCO_3}	0.239	0.157	0.170	0.189	0.204	0.211	0.119	0.068	0.091	0.123	0.131	0.084

Table 9f. Electron microprobe analyses of carbonate groundmass in the middle member of the Trommald Formation, Arko hole

[Major elements in wt% oxides; n.d., not detected]

Sample	A102	A102	A102	A102	A117	A117	A117	A122	A122	A122	A122	A122
CaO	24.47	2.02	24.15	1.62	2.09	23.91	1.70	25.86	24.95	24.56	1.49	1.64
MgO	4.62	5.83	5.38	5.52	5.41	4.44	6.04	4.97	4.75	4.53	5.55	4.85
FeO	11.87	26.27	13.31	29.07	27.96	12.41	31.08	14.39	12.93	12.74	29.84	27.30
MnO	14.01	22.50	11.96	21.39	22.13	14.27	18.29	13.68	12.88	13.81	18.93	22.20
BaO	0.01	n.d.	0.04	n.d.	n.d.	n.d.	n.d.	n.d.	n.d.	n.d.	n.d.	0.02
SrO	0.01	0.11	n.d.	0.03	n.d.	n.d.	n.d.	n.d.	n.d.	0.05	n.d.	0.04
Total	54.99	56.73	54.83	57.62	57.59	55.03	57.11	58.90	55.51	55.69	55.81	56.04
X_{CaCO_3}	0.478	0.042	0.469	0.033	0.043	0.468	0.035	0.472	0.481	0.475	0.031	0.035
X_{MgCO_3}	0.125	0.167	0.145	0.157	0.154	0.121	0.172	0.126	0.127	0.122	0.163	0.143
X_{FeCO_3}	0.181	0.424	0.202	0.464	0.446	0.190	0.497	0.205	0.195	0.192	0.491	0.451
X_{MnCO_3}	0.216	0.367	0.184	0.346	0.358	0.221	0.296	0.197	0.196	0.211	0.315	0.371

Table 9f. (continued)

[Major elements in wt% oxides; n.d., not detected]

| Sample	A140	A140	A140	A140	A181	A181	A181	A181	A25	A25	A25	A25
CaO	1.09	21.47	1.36	22.96	2.08	24.27	23.86	2.04	24.90	25.13	2.16	2.25
MgO	7.08	5.06	5.95	4.14	5.44	4.75	4.39	5.12	3.89	5.38	4.87	5.31
FeO	36.73	15.50	32.80	13.29	26.57	13.18	12.57	26.51	11.69	10.89	25.82	25.73
MnO	12.68	13.70	16.74	14.48	23.18	13.55	13.54	23.87	15.95	14.45	23.26	23.51
BaO	n.d.	n.d.	0.02	n.d.	0.01	n.d.	n.d.	0.01	0.05	n.d.	0.03	0.04
SrO	0.04	0.04	0.04	0.17	n.d.	n.d.	0.03	n.d.	n.d.	n.d.	0.02	n.d.
Total	57.62	55.77	56.90	55.04	57.28	55.76	54.40	57.56	56.48	55.84	56.15	56.84
X_{CaCO_3}	0.022	0.417	0.028	0.454	0.043	0.468	0.473	0.042	0.478	0.478	0.045	0.047
X_{MgCO_3}	0.198	0.137	0.171	0.114	0.155	0.127	0.121	0.146	0.104	0.142	0.143	0.153
X_{FeCO_3}	0.578	0.235	0.528	0.205	0.426	0.198	0.194	0.425	0.175	0.162	0.425	0.416
X_{MnCO_3}	0.202	0.211	0.273	0.227	0.376	0.206	0.212	0.387	0.242	0.217	0.387	0.385
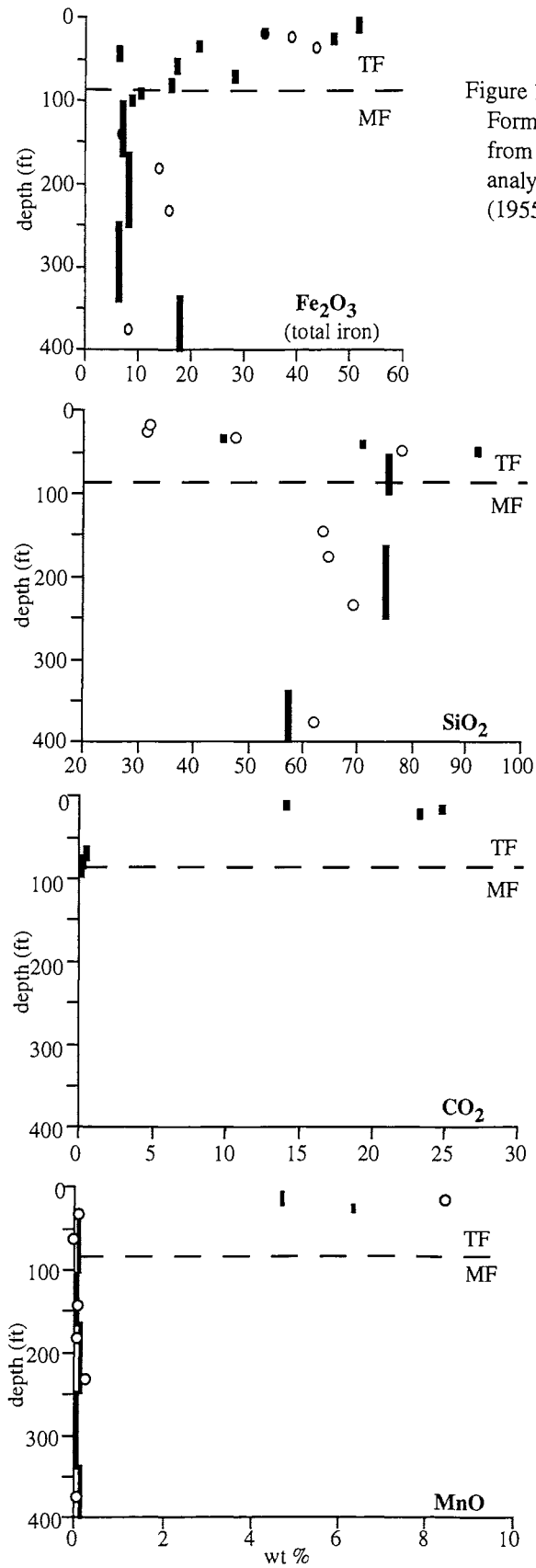
Figure 15. Compositional profiles through the Trommald Formation (TF) and the Mahnomen Formation (MF) from drill core at the North Hillcrest mine. Circles are analyses from this study; lines are from Grout and Wolff (1955).
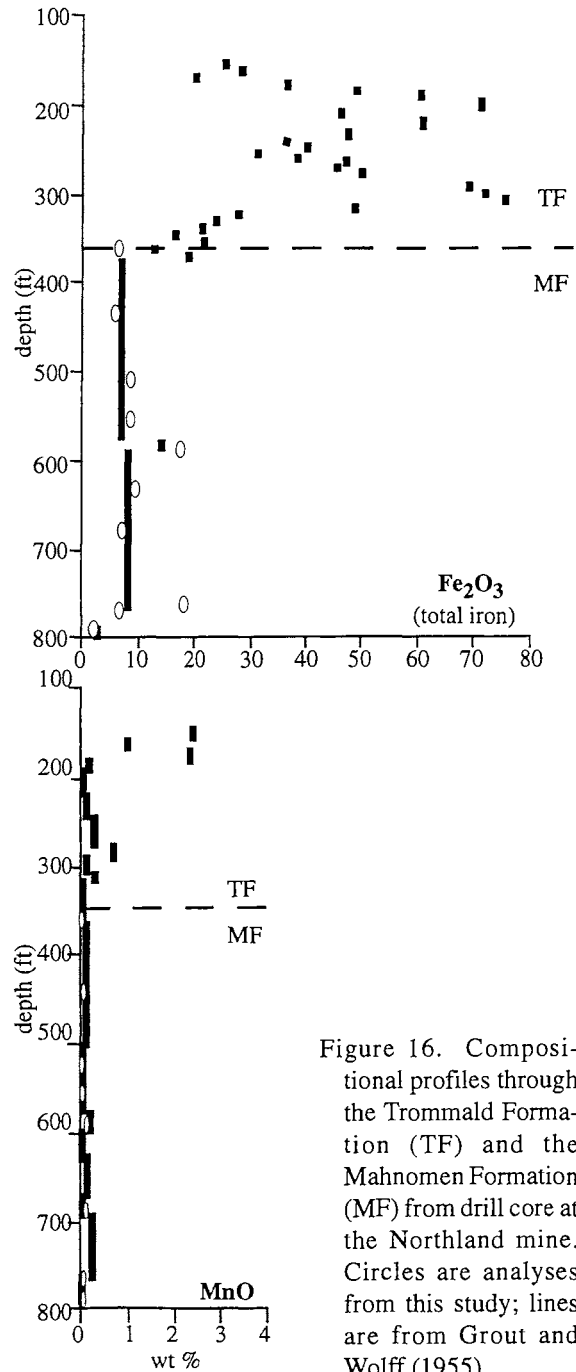
Figure 16. Compositional profiles through the Trommald Formation (TF) and the Mahnomen Formation (MF) from drill core at the Northland mine. Circles are analyses from this study; lines are from Grout and Wolff (1955).
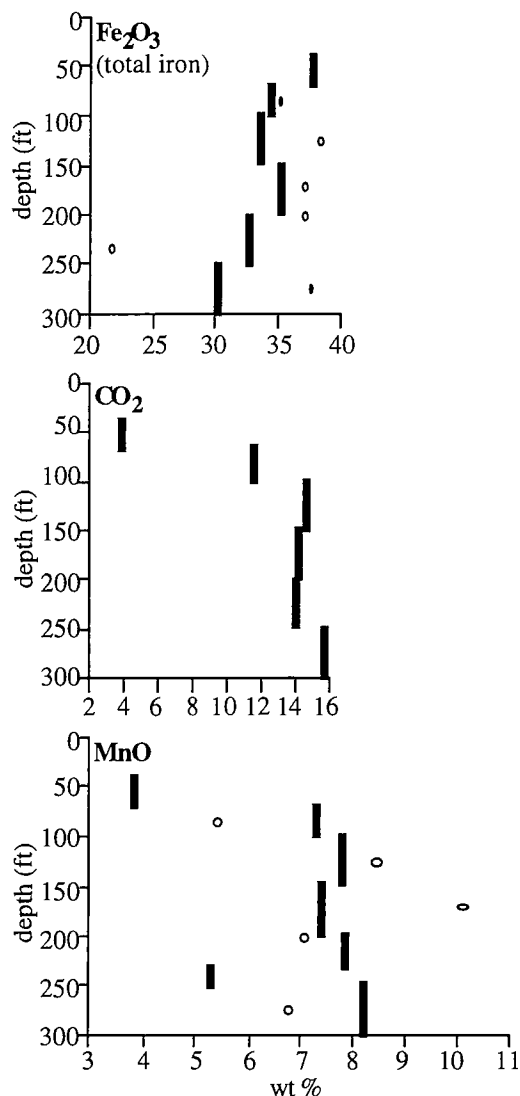
Figure 17. Compositional profiles through the Trommald Formation (TF) from drill core at the Arko mine. Circles are analyses from this study; lines are from Grout and Wolff (1955).

Figure 18. MnO versus CO_2 plots for the Trommald Formation. (A) Upper member hematite iron-formation. (B) Middle and lower members carbonate-silicate iron-formation. Data from Grout and Wolff (1955), Morey and others (1985), and this study. Note difference in scales.

observations of natural assemblages have shown that pure ankerite is a metastable phase (Rosenberg, 1967) According to Essene (1983), this immiscibility extends well toward kutnahorite. It would appear that units of the carbonate-silicate iron-formation of the Trommald Formation are the perfect rocks for investigating the extent of this miscibility gap.

Minnesotaite, Chamosite, and Stilpnomelane

The three iron silicates minnesotaite, chamosite, and stilpnomelane occur in abundance only in the middle and lower members of the Trommald Formation. Chamosite and minnesotaite a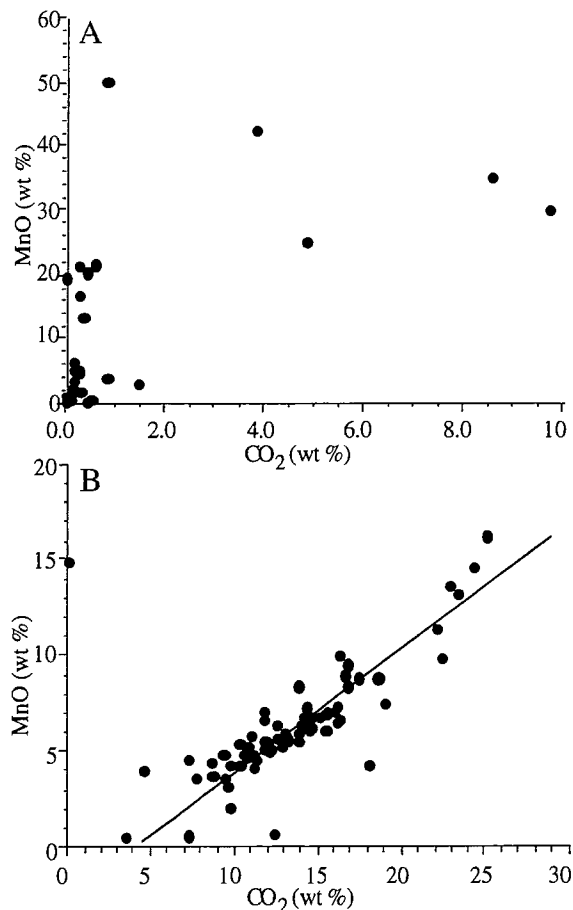re mutually exclusive. Assemblages containing minnesotaite and stilpnomelane occur in the Merritt core, whereas the assemblage chamosite + stilpnomelane occurs only in the Arko core. We have not yet determined if this mutually exclusive relationship is controlled by bulk composition or by metamorphic conditions. However, it is clear that the compositions of the individual phases are controlled by the bulk composition of the rock. Selected electron microprobe analyses of these minerals are summarized in Tables 10-12. Using those data, plots of the Mg/(Fe+Mg+Mn) and Mn/(Fe+Mg+Mn) ratios against stratigraphic positions for stilpnomelane and minnesotaite (Fig. 25) show a clear correlation with the whole rock chemistry for the Merritt hole (Fig. 14). The Mg content of both phases is highest at the upper contact of the middle member and drops sharply downward, a pattern reflected in the whole rock compositions. A similar pattern is seen in the Mn content of the two minerals and the bulk composition of the core (Fig. 14). The data

36

Table 10. Electron microprobe analyses of chamosite in the middle member
of the Trommald Formation, Arko hole
[Major elements in wt% oxides; n.d., not detected]

Sample	A102	A102	A117	A140	A140
SiO_2	25.98	28.53	29.31	32.34	25.68
TiO_2	0.04	0.03	0.02	0.02	0.08
Al_2O_3	17.57	17.09	16.43	15.09	19.38
FeO	36.55	34.98	35.09	35	36.29
MnO	0.82	0.69	0.92	1.29	1.09
MgO	9.59	8.71	8.25	6.99	7.74
CaO	0.05	0.02	0.05	0.7	0.3
Na_2O	n.d.	n.d.	n.d.	n.d.	n.d.
K_2O	0.01	0.1	0.21	0.4	0.03
Total	90.6	90.14	90.28	91.83	90.59

Table 11. Electron microprobe analyses of minnesotaite in middle and lower members of the Trommald Formation, Merritt hole
[Major elements in wt% oxides; n.d., not detected]

Sample	M326.6	M326.6	M326.6	M326.6	M326.6	M326.6	M351.2	M351.2	M351.2	M351.2	M435	M435
SiO_2	49.69	51.07	50.42	52.35	51.87	52.33	51.71	53.46	50.43	49.76	50.97	49.61
TiO_2	0.03	0.03	n.d.	0.01	n.d.	0.01	n.d.	0.06	n.d.	0.02	n.d.	n.d.
Al_2O_3	2.01	1.66	2.29	1.79	1.93	2.04	1.76	1.74	1.77	1.88	2.90	2.50
FeO	35.04	35.08	34.73	34.2	35.5	34.84	39.63	37.72	37.42	37.72	38.31	37.23
MnO	1.63	1.42	1.80	1.64	1.60	1.45	1.16	1.33	1.31	1.30	1.56	1.43
MgO	5.06	5.42	4.88	5.16	4.87	4.98	3.26	3.51	3.58	3.29	2.16	2.34
CaO	0.03	n.d.	0.05	0.07	0.06	0.03	0.02	0.02	n.d.	0.01	0.02	0.01
Na_2O	0.02	n.d.	0.03	0.03	0.01	0.02	0.03	0.02	n.d.	0.04	0.01	0.02
K_2O	0.69	0.61	0.63	0.56	0.55	0.70	0.55	0.53	0.43	0.63	0.79	0.72
Total	94.21	95.30	94.83	95.81	96.39	96.40	98.12	98.38	94.95	94.64	96.72	93.85

Table 11. (continued)
[Major elements in wt% oxides; n.d., not detected]

Sample	M435	M435	M435	M435	M435	M435	M503.4	M503.4	M529.2	M529.2	M529.2	M529.2
SiO_2	49.22	51.92	52.28	51.77	47.32	52.31	52.62	52.25	51.74	52.06	52.84	52.24
TiO_2	n.d.	n.d.	0.02	0.01	n.d.	n.d.	n.d.	0.01	n.d.	0.02	0.01	n.d.
Al_2O_3	2.05	2.24	2.10	2.60	2.05	2.14	1.99	2.04	2.43	2.43	1.80	2.31
FeO	37.93	37.49	38.40	38.88	39.63	38.74	39.49	39.50	38.11	38.08	38.30	38.36
MnO	1.42	1.49	1.50	1.48	2.71	1.46	1.31	1.35	1.37	1.39	1.51	1.48
MgO	2.61	2.57	2.33	2.42	2.36	2.54	2.61	2.50	2.22	2.34	2.56	2.39
CaO	0.01	n.d.	0.02	0.01	0.23	0.03	0.04	0.04	n.d.	0.03	0.01	0.05
Na_2O	n.d.	0.02	n.d.	0.01	n.d.	n.d.	0.04	n.d.	0.05	0.05	n.d.	0.02
K_2O	0.52	0.54	0.55	0.66	0.52	0.60	0.51	0.50	0.62	0.56	0.44	0.55
Total	93.76	96.27	97.20	97.84	94.81	97.82	98.60	98.21	96.53	96.95	97.48	97.38

Table 11. (continued)
[Major elements in wt% oxides; n.d., not detected]

Sample	M570	M570	M570	M570	M570	M618.9	M626.8	M626.8	M630.1	M630.1	M685.2
SiO_2	52.64	52.19	52.01	52.52	48.33	52.38	52.28	52.18	52.55	52.84	50.95
TiO_2	n.d.	0.02	n.d.	n.d.	0.02	n.d.	n.d.	n.d.	0.06	n.d.	0.02
Al_2O_3	1.40	2.29	2.32	1.61	2.02	1.87	2.08	2.30	1.64	1.90	2.57
FeO	38.99	38.06	38.55	39.09	38.98	38.56	38.38	38.49	38.63	38.67	38.04
MnO	1.34	1.22	1.18	1.30	1.34	1.26	1.27	1.33	1.08	1.10	0.51
MgO	2.59	2.62	2.45	2.61	2.52	2.42	2.40	2.36	2.52	2.42	2.49
CaO	0.07	0.05	0.03	0.03	n.d.	n.d.	0.01	0.04	0.01	0.01	0.01
Na_2O	0.02	0.03	0.06	0.04	0.02	0.01	0.03	n.d.	n.d.	0.07	0.04
K_2O	0.32	0.60	0.59	0.41	0.56	0.46	0.54	0.54	0.45	0.45	0.74
Total	97.37	97.06	97.19	97.62	93.79	96.97	96.99	97.24	96.94	97.46	95.38

Table 12a. Electron microprobe analyses of stilpnomelane from the middle member of the Trommald Formation, Arko hole

[Major elements in wt% oxides; n.d., not detected]

Sample	A25	A102	A102	A117	A122	A122	A122	A140	A140	A181	A181	A272
SiO_2	49.56	50.50	50.75	46.24	50.00.	49.98	49.38	45.55	50.41	49.94	50.28	50.34
TiO_2	n.d.	0.03	0.02	0.05	n.d.	0.01	n.d.	0.03	n.d.	0.01	0.02	n.d.
Al_2O_3	5.31	5.22	5.34	7.46	5.55	5.52	5.61	7.30	5.46	5.27	5.30	5.06
FeO	29.66	29.94	30.16	31.36	30.69	30.57	31.03	32.08	30.69	28.92	30.26	30.21
MnO	1.57	1.58	1.49	1.34	1.76	1.85	1.59	1.21	1.13	1.62	1.90	1.80
MgO	4.90	5.54	5.22	6.21	4.87	4.88	4.45	5.43	5.14	5.20	4.89	5.37
CaO	0.43	0.37	0.41	0.20	0.30	0.27	0.29	0.30	0.46	0.16	0.16	0.31
Na_2O	n.d.	n.d.	n.d.	0.06	n.d.	0.05	0.07	n.d.	n.d.	0.07	0.05	0.02
K_2O	0.39	0.34	0.42	0.43	0.26	0.49	0.67	0.87	0.40	0.69	0.58	0.54
Total	91.83	93.52	93.80	93.34	93.42	93.60	93.10	92.77	93.69	91.87	93.43	93.64

Table 12b. Electron microprobe analyses of stilpnomelane from the middle member of the Trommald Formation, Merritt hole

[Major elements in wt% oxides; n.d., not detected]

| Sample	M326.6	M326.6	M326.6	M351.2	M351.2	M435	M435	M595	M618.9	M630.1	M634	M685.2
SiO_2	48.05	49.28	47.75	50.57	50.98	48.66	48.13	48.32	48.34	48.61	48.40	47.76
TiO_2	0.02	n.d.	0.01	0.01	n.d.	n.d.	n.d.	0.03	n.d.	n.d.	0.01	n.d.
Al_2O_3	5.12	5.46	5.34	5.43	5.39	5.48	5.71	5.69	5.84	5.58	5.67	5.60
FeO	31.11	32.17	32.04	32.48	32.88	35.27	34.94	33.43	35.17	35.59	33.69	33.16
MnO	1.12	1.47	1.17	0.83	0.90	1.27	1.12	0.98	0.97	0.73	0.66	0.37
MgO	4.34	4.33	4.34	2.72	3.03	2.16	2.11	2.13	2.12	2.16	2.10	2.25
CaO	0.03	0.04	0.09	0.04	0.03	0.07	0.07	0.07	0.06	0.05	n.d.	n.d.
Na_2O	0.27	0.04	0.01	0.44	0.21	0.32	0.43	0.42	0.26	0.40	0.75	0.31
K_2O	1.28	0.36	0.54	1.92	1.06	1.26	1.39	1.20	0.92	1.19	1.84	0.97
Total	91.33	93.15	91.29	94.43	94.48	94.49	93.90	92.26	93.65	94.30	93.12	90.42
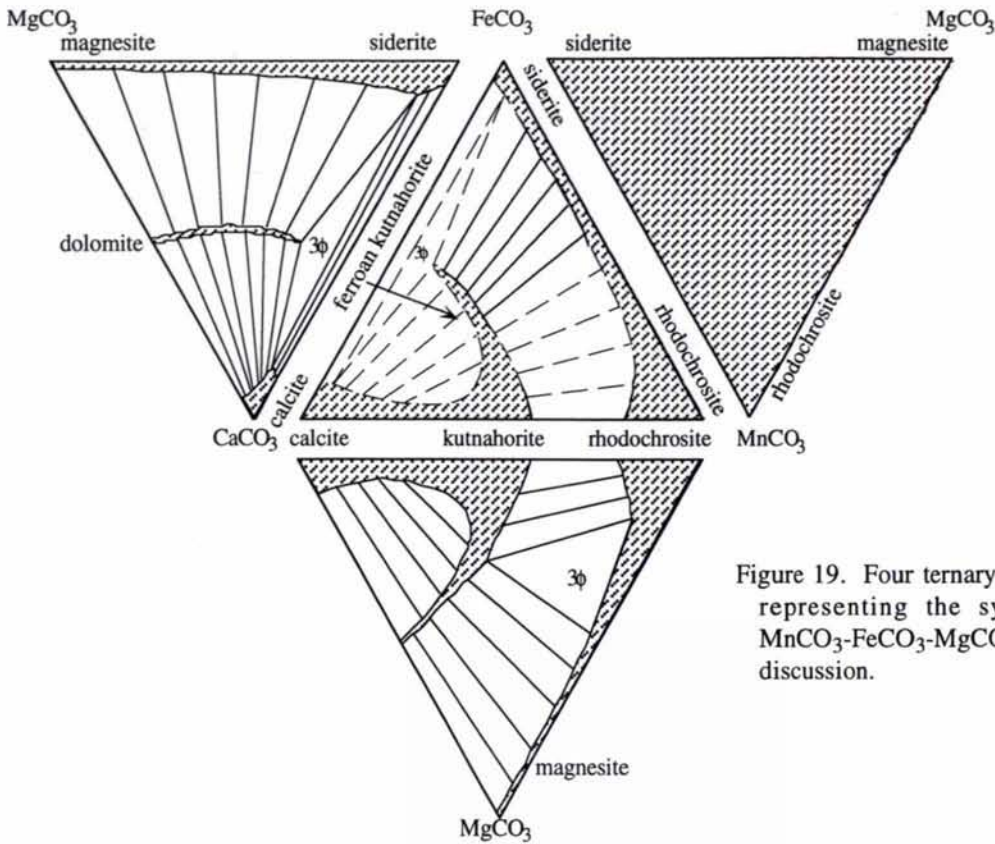
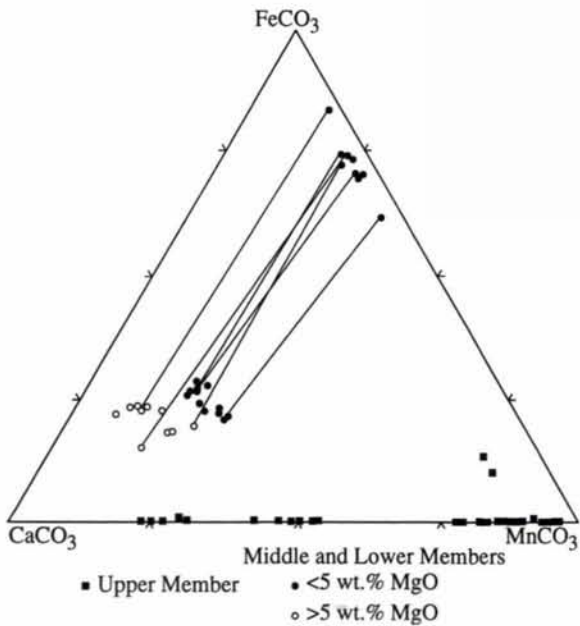Figure 19. Four ternary phase diagrams representing the system $CaCO_3$-$MnCO_3$-$FeCO_3$-$MgCO_3$. See text for discussion.

Figure 20. Ternary $CaCO_3$-$MnCO_3$-$FeCO_3$ phase diagram projected through $MgCO_3$ for the carbonates in the Trommald Formation from the Merritt drill hole exclusive of carbonate vein filling. The MgO content of the ferroan kutnahorite causes them to plot away from the kutnahorite-ankerite binary.
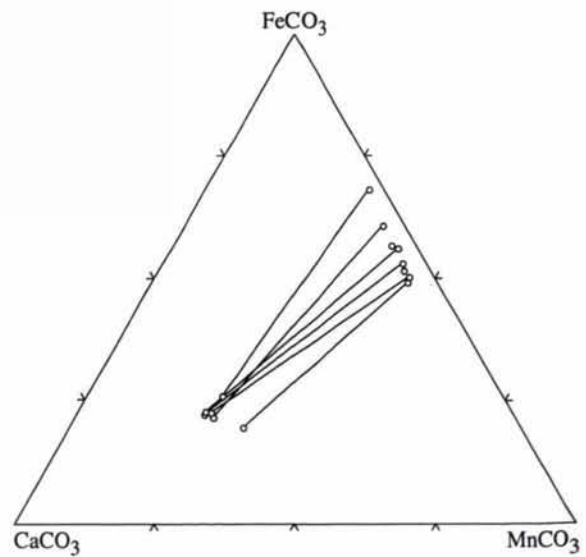
Figure 21. Ternary $CaCO_3$-$MnCO_3$-$FeCO_3$ phase diagram projected through $MgCO_3$ for carbonates between 3 and 7 weight percent MgO in the middle member of the Trommald Formation from the Arko drill hole.
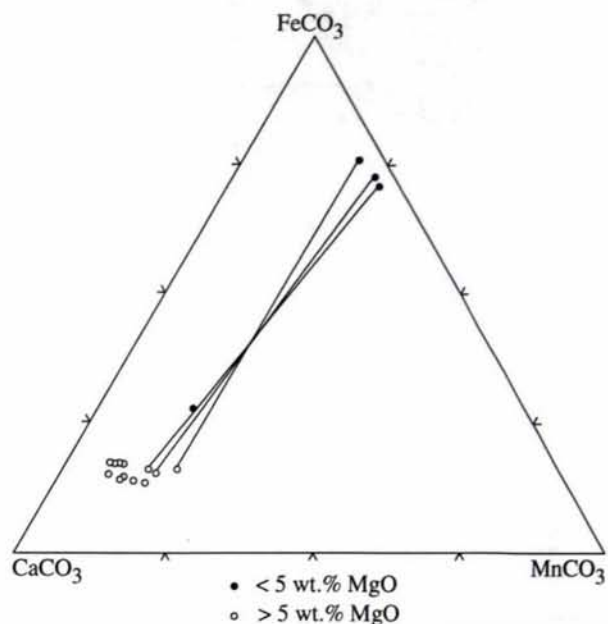
Figure 22. Ternary $CaCO_3$-$MnCO_3$-$FeCO_3$ phase diagram projected through $MgCO_3$ for the carbonates in veins in the middle and lower members of the Trommald Formation from the Merritt drill hole

in Table 12 also show that, contrary to Schmidt's (1963) suggestion, Mn is not a significant constituent of the stilpnomelane.

Oxides

Both magnetite (Table 13) and hematite (Table 14) occur in the Trommald Formation. Hematite dominates in the upper member. It occurs both as a disseminated phase associated with a variety of other minerals, and as near-monomineralic beds 0.5 to 2 cm thick. Magnetite is also present in the upper member in discrete beds, mainly as very small, disseminated octahedral grains. The beds are best detected from their magnetic signature. In contrast, hematite is only sparingly present in the middle member where it occurs as relatively minor secondary coatings. Magnetite is the principal iron oxide in the middle and lower members. It occurs in the lower half of the middle member and throughout the lower member as disseminated euhedral grains or in thin layers composed of aggregates of interlocking grains. Its stratigraphic distribution is clearly shown in Figure 3.

Manganite occurs in the upper member of the Trommald Formation. It is typically intermixed with the iron oxide. Compositionally it is nearly pure Mn oxide (Table 15).
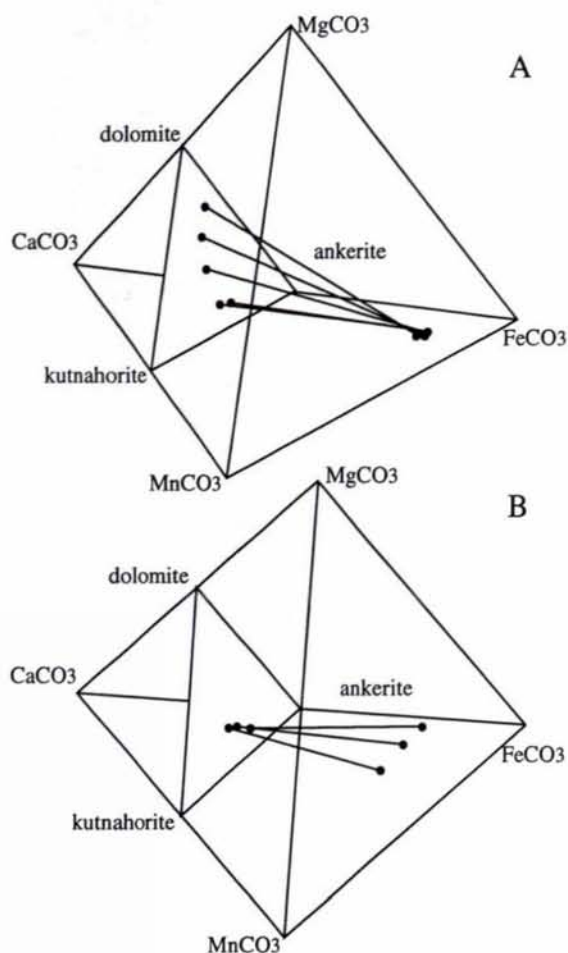
Figure 23. $CaCO_3$-$MnCO_3$-$FeCO_3$-$MgCO_3$ plots of coexisting carbonate compositions from the middle and lower members of the Trommald Formation from the Merritt hole (A) and the Arko hole (B).

Jacobsite

Jacobsite is an Fe-Mn spinel that has been found in one layer of the upper member of the Trommald Formation in the Merritt core at a depth of 285.3 feet. It occurs as groundmass material intergrown with rhodonite. Selected electron microprobe analyses are summarized in Table 16. These data show that the Jacobsite contains very few cations other than Mn and Fe.

Tourmaline

Tourmaline occurrences are widespread throughout the study area. It has been identified in samples from pits and core in the lower Trommald Formation and the Mahnomen Formation. Electron microprobe analyses are summarized in Table 17. These data show that the tourmaline has a fairly constant composition falling along the schorl-dravite (Fe-Mg) solid solution join (Fig. 26), even

Table 13a. Electron microprobe analyses of magnetite in the middle member of the Trommald Formation, Arko hole
[Major elements in wt% oxides; n.d., not detected]

Sample	A102	A117	A117	A122	A140	A140	A181	A25,	A272,	A90
SiO_2	1.42	1.80	1.51	0.25	2.19	0.04	0.89	2.48	2.38	2.17
TiO_2	0.02	0.01	0.08	0.02	0.04	0.01	0.06	0.04	0.03	0.02
Al_2O_3	0.03	0.04	0.05	0.02	0.08	0.02	0.04	0.03	0.04	0.02
Cr_2O_3	0.05	0.09	0.04	0.01	0.01	n.d.	0.01	n.d.	n.d.	n.d.
Fe_2O_3*	67.87	67.15	67.43	67.99	67.44	69.05	68.22	66.36	67.25	66.74
FeO*	30.49	30.17	30.29	30.54	30.30	31.02	30.65	29.81	30.21	29.98
MgO	0.27	0.28	0.29	0.04	0.23	n.d.	0.09	0.45	0.51	0.54
MnO	0.12	0.25	0.13	0.12	0.09	0.02	0.16	0.32	0.10	0.23
CaO	n.d.	0.05	0.02	0.03	0.05	n.d.	0.03	0.11	0.03	0.04
Total	100.27	99.83	99.84	99.01	100.43	100.16	100.14	99.61	100.55	99.75

* FeO/Fe_2O_3 ratio calculated from stoichiometry.

42

Table 13b. Electron microprobe analyses of magnetite in the middle member of the Trommald Formation, Merritt hole
[Major elements in wt% oxides; n.d., not detected]

Sample	M435	M435	M435	M503.4	M503.4	M529.2	M570	M570	M595	M595	M626.8	M634.0	M685.2
SiO_2	0.06	0.53	0.10	0.55	0.76	0.45	0.75	1.01	0.37	0.35	1.16	0.22	0.16
TiO_2	0.07	0.10	0.10	0.11	0.13	0.14	0.10	0.08	0.08	0.06	0.11	0.10	0.07
Al_2O_3	0.03	0.05	0.04	0.04	0.04	0.05	0.06	0.02	0.04	0.03	0.05	0.03	0.04
Cr_2O_3	0.01	n.d.	0.03	0.02	n.d.	0.02	0.05	n.d.	n.d.	n.d.	0.03	0.10	0.02
Fe_2O_3*	69.49	68.38	68.99	68.63	68.52	68.35	68.72	68.20	68.96	68.93	68.34	69.07	68.68
FeO*	31.22	30.72	30.99	30.83	30.78	30.70	30.87	30.64	30.98	30.97	30.70	31.03	30.85
MgO	n.d.	n.d.	n.d.	0.01	n.d.	0.01	n.d.	0.03	0.01	n.d.	n.d.	0.01	n.d.
MnO	0.05	0.02	0.10	0.03	n.d.	0.02	0.09	n.d.	0.08	0.06	0.10	0.17	0.05
CaO	n.d.	n.d.	n.d.	0.06	n.d.	n.d.	n.d.	n.d.	0.01	0.01	0.02	0.02	0.28
Total	100.93	99.79	100.33	100.27	100.22	99.73	100.65	99.98	100.53	100.41	100.52	100.75	100.15

* FeO/Fe_2O_3 ratio calculated from stoichiometry.

Table 14. Electron microprobe analyses of hematite in the
Trommald Formation, Merritt hole
[Major elements in wt% oxides; n.d., not detected]

Sample	M271.1	M271.1	M294.0	M294.0	M634.0
SiO_2	0.01	0.04	0.08	0.05	0.91
TiO_2	0.24	0.11	0.22	0.28	0.02
Al_2O_3	0.02	0.02	0.01	n.d.	n.d.
Cr_2O_3	n.d.	n.d.	0.01	n.d.	n.d.
Fe_2O_3	99.87	99.17	99.78	99.15	99.52
MgO	0.01	n.d.	n.d.	n.d.	n.d.
MnO	0.43	0.55	0.05	0.71	0.17
CaO	n.d.	0.01	0.01	0.03	0.02
Total	100.58	99.89	100.15	100.23	100.65

Table 15. Electron microprobe analyses of manganite in the
upper member of the Trommald Formation, Merritt hole
[Major elements in wt% oxides; n.d., not detected]

Sample	M264.9	M271.1	M271.1	M271.1	M271.1
SiO_2	0.74	0.60	0.47	1.31	0.55
TiO_2	n.d.	n.d.	n.d.	0.03	0.01
Al_2O_3	0.03	0.02	0.06	n.d.	0.03
Cr_2O_3	0.03	0.01	0.02	n.d.	n.d.
FeO	n.d.	n.d.	n.d.	n.d.	n.d.
MgO	n.d.	0.03	n.d.	n.d.	0.01
MnO	76.75	78.11	78.11	78.20	79.12
CaO	0.01	0.04	0.04	0.03	0.02
Total	77.56	78.81	78.70	79.57	79.73

Table 16. Electron microprobe analyses of jacobsite in the upper member of the
Trommald Formation, Merritt hole
[Major elements in wt% oxides; n.d., not detected]

| Sample	M285.3	M285.3	M285.3	M285.3	M285.3	M285.3	M285.3	M285.3
SiO_2	2.60	0.11	0.19	0.45	0.25	0.23	0.61	0.66
TiO_2	0.06	0.06	0.03	0.09	0.05	0.07	0.04	0.07
Al_2O_3	0.21	0.13	0.13	0.15	0.12	0.16	0.23	0.23
Cr_2O_3	0.04	n.d.	0.01	0.03	0.02	n.d.	n.d.	n.d.
Fe_2O_3	67.96	70.92	68.92	70.55	71.26	70.44	69.37	69.20
MgO	0.15	0.04	0.07	0.03	0.09	0.04	0.10	0.10
MnO	26.67	26.66	28.07	27.17	26.85	27.90	28.47	28.50
CaO	0.03	0.01	n.d.	0.04	0.01	n.d.	0.02	0.03
Total	97.72	97.92	97.40	98.51	98.64	98.84	98.85	98.79
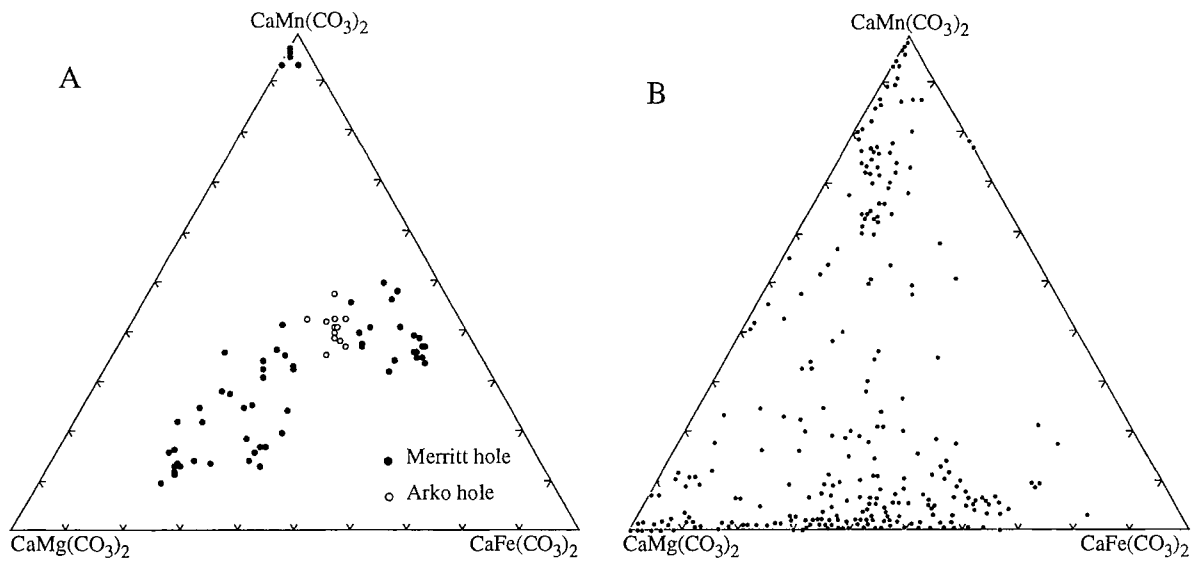
Figure 24. Variation in composition of R3̄ (dolomite-like) carbonates in the middle and lower members of the Trommald Formation (A), as compared to those previously reported by Essene, 1983 in the literature (B).
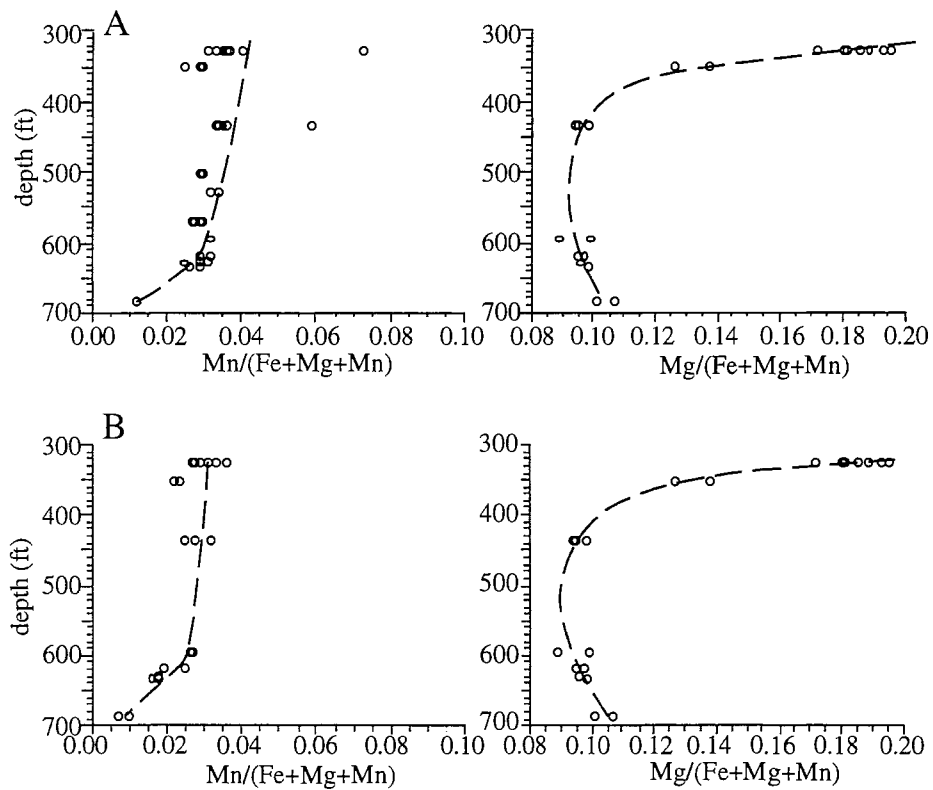

Figure 25. Compositional variation with depth of (A) minnesotaite and (B) stilpnomelane in the Merritt drill core.
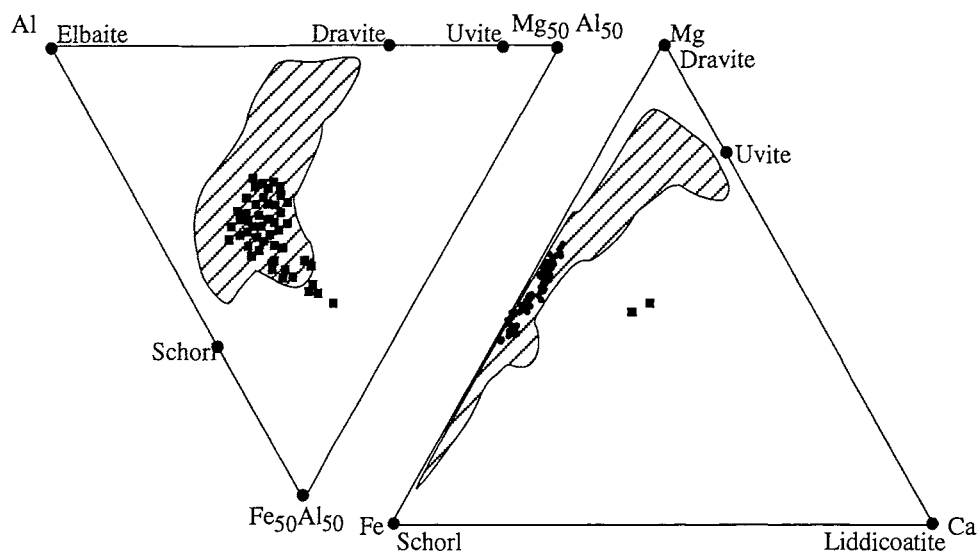
Figure 26. Ternary Fe-Al-Mg and Ca-Al-Mg plots showing compositional fields of tourmalines from several massive sulfide deposits. Tourmaline compositions from Cuyuna district are overlaid on these fields (modified from Slack and Coad, 1989).

though sample localities are scattered and individual grains vary in size and modal abundance. Individual tourmaline grains from the Northland, North Hillcrest, and Merritt cores are very small, generally less 0.05 mm in diameter, and account for approximately 1 or 2 modal percent of the rocks. In contrast, samples collected from several open pit mines contain as much as 35 modal percent, with grains that average 1.0 mm in length. Some grains are as much as 7.0 mm long. Most grains are zoned from blue-green cores to brown rims, with several having light-yellow-brown cores and darker yellow-brown rims. This color zonation is the result of small increases in TiO_2 content from core to rim. Other grains, especially from the Northland, North Hillcrest, and Merritt cores, are dark green from core to rim without color zonation.

The formation of tourmaline is dependent upon abundant boron. A likely source of boron in the sedimentary environment is hydrothermal fluids. The fluids typically leach the boron from the country rock and then transport it to a favorable depositional environment, typically at or below the interface between sediment (or rock) and water (Palmer and Slack, 1989). It appears that the bulk composition and especially the alumina content of the host sediment is an important factor in the formation of tourmaline from boron-rich solutions. Inasmuch as alumina is not typically carried in hydrothermal fluids, it must be supplied at the depositional site. This explains the restriction of tourmaline in the North range to host rocks that are Al-rich.

Barite

Samples of barite veins were collected by R.G. Schmidt from a number of mines while he was working on the Cuyuna range in the 1950s. The size of the samples indicates that some of the veins were at least 8 cm wide. Selected electron microprobe analyses of two such samples are summarized in Table 18. The analyses show that the samples have a simple composition, and that they contain significant but variable amounts of Sr, ranging from near zero to almost 3 weight percent within a given sample. The Sr content of barite is an important indicator of hydrothermal processes. For example, Bonatti and others (1972) have shown that the Sr content of barite in the Chiatur manganese deposits in Georgia (former U.S.S.R.) was greatest at sites close to a hydrothermal vent.

DISCUSSION

The abundance of manganese oxides on the North range has long been an enigma. Because the manganese and iron oxides are closely associated, early studies assumed that both assemblages formed at the same time by the same processes. Those processes were thought to involve the modification of some primary protolith through several generations of events (e.g., Morey, 1983). Such models typically involved oxidizing and leaching solutions that moved along structural channelways. There is less agreement as to the source of fluids or when they moved through the rocks. Both ascending hydrothermal fluids and descending supergene fluids have been proposed. Schmidt (1963), who suggested that both kinds of fluids

Table 17a. Electron microprobe analyses of tourmaline grains from the Portsmouth pit
[Major elements in wt% oxides; n.d., not detected]

Sample	P244,1R	P244,1M	P244,1R	P244,1M	P529,1R	P529,1M	P529,2R	P529,R/M	P529,M
SiO_2	36.97	37.17	56.66	41.98	36.00	37.01	36.96	36.30	36.67
TiO_2	1.14	0.41	0.70	0.43	1.15	0.55	0.64	0.68	0.65
Al_2O_3	31.62	33.68	21.92	30.95	31.01	33.63	31.36	32.28	32.29
FeO	8.54	7.66	5.58	7.10	8.36	7.44	7.96	8.00	7.94
MnO	0.02	0.03	0.01	0.02	0.02	0.02	0.05	0.02	n.d.
MgO	6.00	5.78	3.83	5.37	6.21	5.87	6.33	5.86	6.15
CaO	0.39	0.30	0.26	0.26	0.48	0.35	0.26	0.31	0.36
Na_2O	2.17	2.04	1.34	1.81	2.15	2.01	2.14	1.97	2.16
K_2O	0.02	0.02	0.01	0.01	0.01	0.01	0.02	0.02	0.01
F	0.11	0.04	0.09	0.04	0.06	0.04	0.05	0.04	0.02
Total	87.00	87.13	90.41	87.98	85.46	86.92	85.76	85.47	86.26

46

Table 17b. Electron microprobe analyses
of tourmaline grains from the Merritt core
[Major elements in wt% oxides]

Sample	M741-1	M741-3	M741-4
SiO_2	36.53	35.89	37.21
TiO_2	0.29	0.63	0.65
Al_2O_3	31.68	31.37	31.03
FeO	11.95	7.71	7.27
MnO	0.01	0.02	0.03
MgO	2.81	5.35	6.06
CaO	0.13	0.35	0.46
Na_2O	1.43	1.96	2.09
K_2O	0.03	0.03	0.02
F	0.05	0.15	0.13
Total	84.90	83.46	84.95

Table 17c. Electron microprobe analyses of tourmaline grains from Northland and North Hillcrest cores
[Major elements in wt% oxides; n.d., not detected]

Sample	N368,1R	N368,1M	N368,2R	N368,2-M	N440,1-R	N440,1M
SiO_2	36.25	36.09	41.71	35.01	36.36	37.21
TiO_2	0.50	0.47	0.67	1.21	0.82	1.56
Al_2O_3	31.54	31.83	26.68	29.79	31.92	30.18
FeO	9.86	9.18	8.79	11.02	9.30	9.45
MnO	n.d.	n.d.	n.d.	n.d.	0.01	0.03
MgO	4.73	4.89	4.56	4.74	5.06	5.26
CaO	0.10	0.27	0.19	0.19	0.14	0.40
Na_2O	1.93	1.91	1.79	2.24	2.10	2.12
K_2O	0.02	0.02	0.03	0.03	0.03	0.04
F	0.08	0.05	0.12	0.13	0.17	0.11
Total	85.00	84.70	84.53	84.36	85.91	86.34

Table 17c. (continued)
[Major elements in wt% oxides; n.d., not detected]

Sample	N552,2R	N552,2	MN637,1-R	N637,1-M	H142,1
SiO_2	35.10	38.84	37.34	33.92	40.56
TiO_2	0.94	0.69	n.d.	n.d.	1.10
Al_2O_3	28.31	26.96	20.46	24.05	28.33
FeO	10.78	11.63	9.77	10.67	8.33
MnO	0.01	0.01	0.01	n.d.	0.02
MgO	6.01	5.28	4.92	5.04	5.13
CaO	0.25	0.14	n.d.	n.d.	0.46
Na_2O	2.43	2.37	1.62	2.01	2.08
K_2O	0.02	0.03	n.d.	n.d.	0.76
F	0.18	0.11	0.14	0.21	0.13
Total	84.02	86.06	74.24	75.89	87.00

Table 17d. Electron microprobe analyses of tourmaline grains from the Evergreen pit
[Major elements in wt% oxides; n.d., not detected]

Sample	E146,1R	E146,1M	E146,2R	E146,2M	E146,3R	E146,3M	E1190,1-R	E1190,1M	E1190,2R	E1190,2M
SiO_2	38.33	34.52	36.82	37.54	36.46	36.90	36.80	36.48	37.38	36.88
TiO_2	0.66	0.50	0.65	0.44	0.72	0.46	0.89	0.44	0.55	0.48
Al_2O_3	31.98	31.43	32.55	32.87	32.82	33.14	32.33	33.19	32.50	32.56
FeO	7.87	7.47	8.06	7.66	8.08	7.49	8.27	8.12	8.28	8.11
MnO	0.02	0.02	0.01	0.02	0.01	0.02	0.02	0.01	0.01	0.01
MgO	5.78	5.56	5.97	5.93	5.78	6.01	5.98	5.77	6.1	5.99
CaO	0.29	3.60	0.30	0.27	0.32	0.41	0.52	0.38	0.33	0.37
Na_2O	2.08	1.87	2.15	2.17	2.14	2.08	2.08	2.12	2.22	2.13
K_2O	0.01	0.01	0.01	0.02	0.01	0.01	0.01	0.01	0.01	0.01
F	0.08	0.17	0.10	0.05	0.08	0.08	0.11	0.11	0.08	0.10
Total	87.10	85.14	86.62	86.96	86.43	86.60	86.99	86.61	87.45	86.63

Table 17e. Electron microprobe analyses of tourmaline grains from the Feigh pit.
[Major elements in wt% oxides; n.d., not detected]

Sample	F1405,1R	F1405,1R/M	F1405,1M	F1405,2R	F1405,2R/M	F1405,2M	F1405,3R	F1405,3M
SiO_2	36.96	36.01	34.65	36.27	35.36	35.2	41.99	35.88
TiO_2	0.54	0.80	0.99	1.27	0.63	0.54	0.82	0.72
Al_2O_3	31.99	32.13	31.90	31.31	32.83	32.69	28.88	32.54
FeO	8.68	8.54	9.11	8.95	8.18	8.13	8.01	8.27
MnO	0.12	0.12	0.15	0.09	0.13	0.13	0.07	0.10
MgO	5.75	5.59	5.49	5.77	5.60	5.75	5.35	5.75
CaO	0.55	0.53	0.60	0.52	0.37	0.43	0.37	0.43
Na_2O	2.09	1.98	1.92	2.00	2.17	2.22	1.95	2.18
K_2O	0.02	0.02	0.02	0.03	0.03	0.02	0.02	0.02
F	0.05	n.d.	0.08	0.01	n.d.	n.d.	0.03	n.d.
Total	86.74	85.708	84.91	86.21	85.29	85.11	87.47	85.893

Table 17f. Electron microprobe analyses of tourmaline grains from the Sagamore pit
[Major elements in wt% oxides; n.d., not detected]

Sample	S976,1R	S976,1M	S976,2R	S976,2R/M	S976,2M	S976,3R	S976,4R	S976,4R/M	S978,1R	S976,1M	S978,2R
SiO_2	36.20	36.51	34.74	35.46	35.20	34.74	36.34	34.55	35.23	35.04	36.93
TiO_2	0.77	0.37	0.98	0.22	0.52	0.76	0.78	0.80	0.61	0.70	0.59
Al_2O_3	32.72	33.67	31.81	34.29	32.99	32.30	32.31	32.40	32.53	33.00	33.16
FeO	9.79	9.48	10.01	9.75	9.69	10.40	9.68	9.94	8.70	8.71	8.63
MnO	0.09	0.11	0.09	0.10	0.06	0.12	0.09	0.11	0.07	0.11	0.11
MgO	4.40	3.90	4.57	3.73	4.23	4.06	4.39	4.33	5.19	5.13	5.10
CaO	0.32	0.25	0.34	0.10	0.24	0.14	0.27	0.27	0.91	0.25	0.22
Na_2O	1.93	1.64	2.06	1.47	1.79	1.70	1.94	1.91	2.09	2.06	1.93
K_2O	0.01	0.01	0.01	0.01	n.d.	0.02	0.01	0.02	0.02	0.02	0.02
F	0.02	0.02	0.06	n.d.	0.05	0.03	0.05	0.10	0.13	0.05	0.06
Total	86.28	85.97	84.66	85.12	84.78	84.27	85.86	84.43	85.52	85.06	86.74

49

Table 17f. (continued)
[Major elements in wt% oxides n.d., not detected]

Sample	S978,2M	S978,3R	S978,3M	S978,4R	S978,4M	S978,5R	S978,5M	S1406,2R	S1406,2M	S1406,3R	S1406,3M
SiO_2	37.89	36.53	37.16	35.77	37.03	38.85	36.03	34.39	34.98	34.65	34.18
TiO_2	0.50	0.58	0.54	0.83	0.19	1.01	1.46	1.44	1.32	1.03	1.24
Al_2O_3	32.35	32.76	33.53	32.29	34.52	31.95	31.41	29.90	28.65	30.20	29.52
FeO	8.37	8.59	8.47	8.61	8.74	8.75	9.69	11.42	11.13	11.20	11.60
MnO	0.09	0.09	0.09	0.09	0.09	0.10	0.12	0.11	0.12	0.13	0.10
MgO	5.07	5.16	4.84	5.28	4.49	5.35	5.11	4.85	4.83	4.82	4.95
CaO	0.25	0.20	0.16	0.24	0.07	0.28	0.40	0.46	0.47	0.41	0.58
Na_2O	1.98	2.03	1.79	2.08	1.43	2.10	2.01	2.24	2.16	2.19	2.18
K_2O	0.01	0.02	0.01	0.02	0.01	0.03	0.02	0.01	0.02	0.01	0.02
F	0.11	0.06	0.09	0.09	0.01	0.12	0.08	0.14	0.16	0.10	0.13
Total	86.61	86.02	86.67	85.27	86.57	88.54	86.32	84.96	83.83	84.72	84.53

Table 18. Electron microprobe analyses of barite from veins within the Trommald Formation [Major elements in wt% oxides; n.d., not detected]

Sample	539A	539A	539A	539A	539A	539A	539A	1353	1354	1354	539B	539B
BaO	65.77	62.88	63.86	64.04	62.59	62.16	63.44	63.01	64.16	64.16	64.87	64.52
CaO	0.01	0.03	0.01	0.02	n.d.	0.02	0.01	n.d.	n.d.	n.d.	0.03	0.01
SrO	n.d.	2.20	1.38	1.31	2.75	2.52	2.51	2.06	1.48	0.99	0.42	0.32
SO₃	33.95	34.75	34.26	34.37	34.56	35.20	34.25	34.75	33.87	34.82	34.95	34.72
Total	99.72	99.85	99.51	99.74	99.90	99.90	100.21	99.82	99.51	99.97	100.27	99.57

were responsible for the iron ore deposits of the North range, believed that the fluids were considerably younger than the rocks through which they flowed.

There is little systematic evidence as to the sources of manganiferous components in the Trommald Formation. Harder and Johnston (1918), Thiel (1924), and Grout and Wolff (1955) have suggested that the manganese protolith was a "green carbonate slate" in which the manganese resided in a carbonate phase. The precise stratigraphic position of the "green carbonate slate" was never established, but it appears to be more or less equivalent to the part of the lower member that lacks appreciable magnetite. These early workers believed that manganese carbonate was dissolved and the manganese remobilized upward to where it was precipitated as oxides. The abundance of hematite in what we call the upper member was considered to be the result of oxidation and leaching of primary iron-formation.

Schmidt (1963) established that the bulk of the manganese in the Trommald protolith occurs at or near the transition zone between the upper and middle members. The rock types of these units were presumably deposited in considerably different regimes, i.e., one having shallow-water attributes and the other deeper-water attributes. Thus Morey (1990) suggested that the manganese protolith was preferentially deposited in a relatively specific sedimentological regime, the geometry of which was constrained by the paleogeographic configuration of the depositional basin. We now challenge this suggestion. Although the upper member of the Trommald Formation at the Merritt locality is somewhat oxidized and leached, its textural and mineralogical attributes clearly show that much of the hematite is a primary mineral and that the protolith was an iron-formation. The fact that hematite is closely associated with manganese oxides having similar textural attributes, we believe, suggests that the manganese oxides also are primary phases. Indeed, given their restricted stratigraphic distribution, it would be difficult to believe that the iron oxides are primary phases and the manganese oxides secondary phases.

We have confirmed earlier observations that manganese in the lower member occurs chiefly in the carbonate phases. However, the manganese oxides first appear at a stratigraphic level that includes the presence of hyalophane, aegirine, rhodonite, and hematite. Of these minerals, hyalophane has a very restricted paragenesis; it is associated typically with either sedimentary manganese and ferromanganese deposits or with Cu-Pb-Zn-Ba deposits (McSwiggen and others, 1994b). The presence of hyalophane supports the view that the iron-formation, at least in part, consists of chemical sediments precipitated from a hydrothermal fumerolic system. Other evidence for such a system includes the presence of aegirine in the hyalophane-rich interval. In addition, tourmaline-bear-

50

ing layers, as well as tourmalinites, at stratigraphic levels below, within, and above the iron-formation, together with Sr-rich barite veins that transect the iron-formation, are all indicative of a submarine exhalative system that vented complex brine solutions onto or just beneath a sediment-water interface on the ocean floor.

Lastly, ordinary seawater deposits typically have a strongly positive Ce anomaly that distinguishes them from hydrothermal deposits. The upper member of the Trommald Formation is marked by a slightly negative Ce anomaly. Thus the evidence collectively indicates that the Trommald Formation was not formed entirely by simple sedimentary processes, but rather is partly the product of a long-lived hydrothermal system.

Bonatti (1975) has proposed a number of chemical criteria that distinguish metals formed by the slow precipitation in ordinary seawater from those formed by hydrothermal processes in tectonically active areas. Among these criteria are a high Si/Al ratio, which is observed in the deposits associated with modern seafloor vents. The Trommald Formation has Si/Al ratios that place it within this hydrothermal field (Fig. 27). Of course most iron-formations do, by the fact that they are very low in Al_2O_3 and high in SiO_2. Some workers have concluded that the source of the Fe in all iron-formations is exhalative in nature (e.g., Kimberley, 1989). However, this does not address the question of the proximity of the exhalative vent relative to the deposits. Was the vent adjacent to the deposits or in another part of the basin? Modern proximal hydrothermal deposits also have only minor concen-

trations of Ni+Co+Cu relative to Fe and Mn, but the Fe/Mn ratios can range from >1.0 to <0.1. This relationship is also observed in the Trommald Formation (Fig. 28). Lastly deposits of hydrothermal origin typically have U/Th ratios greater than 1. The Trommald has U/Th ratios that cluster around equal amounts of U and Th, but are more akin to a field defined by modern sea-floor deposits (Fig. 29).

In summary, similarities in bulk composition, elemental distribution patterns, and mineralogy of the Trommald Formation and modern, submarine, exhalative iron- and manganese-rich deposits suggest a development by similar genetic processes. There are also various spatial and genetic relationships between the deposition of iron- and manganese-rich materials in modern exhalative environments and various kinds of polymetallic sulfide deposits. These spatial and genetic relationships open up the possibility for the presence of a variety of sulfide deposits in the Cuyuna range. The model by Large (1980) suggests that sediment-hosted, submarine exhalative sulfide deposits are typically centered on a fracture or fault system that allows venting to take place. Surrounding the area of the vent are the stratiform massive sulfide deposits, which are capped and surrounded by stratiform barite deposits, which are in turn surrounded by stratiform ferromanganese (Fig. 30). Beneath the ore zones are fracture zones typically altered and mineralized with sulfides, tourmalinite, chlorite, and dolomite. If this model can be applied to the North range, it suggests that the iron-formations may represent the outer part of this system, and that the inner part of this system is yet to be discovered.
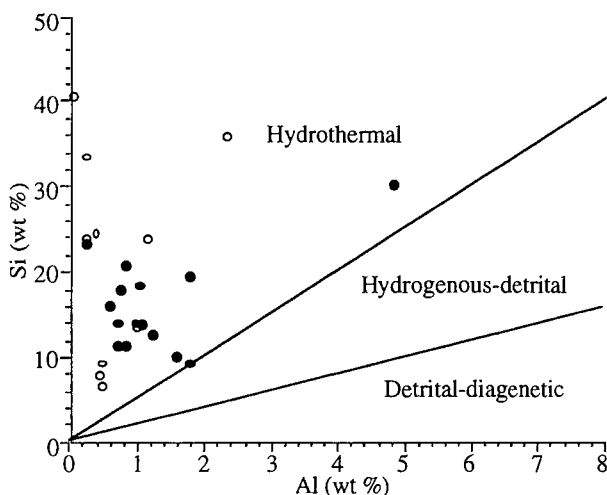

Figure 27. Ratio of Si/Al in the Trommald Formation as compared to ratios from marine sediments that are hydrothermal, hydrogenous-detrital, or detrital-diagenetic in origin (modified from Bonatti, 1975; Crerar and others, 1982). Open circles represent hematite iron-formations; closed circles represent carbonate-silicate iron-formation.
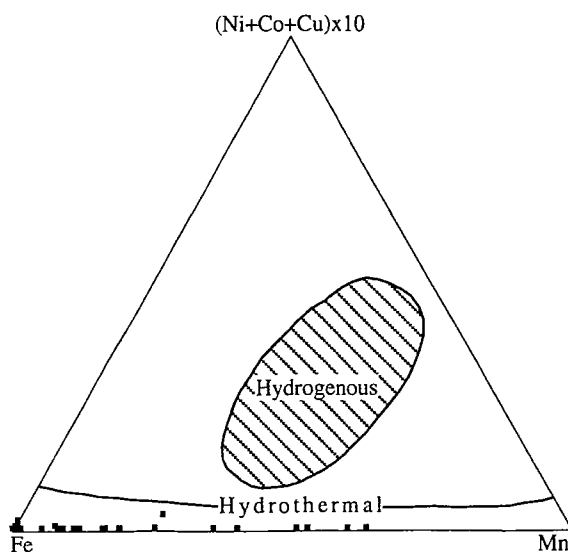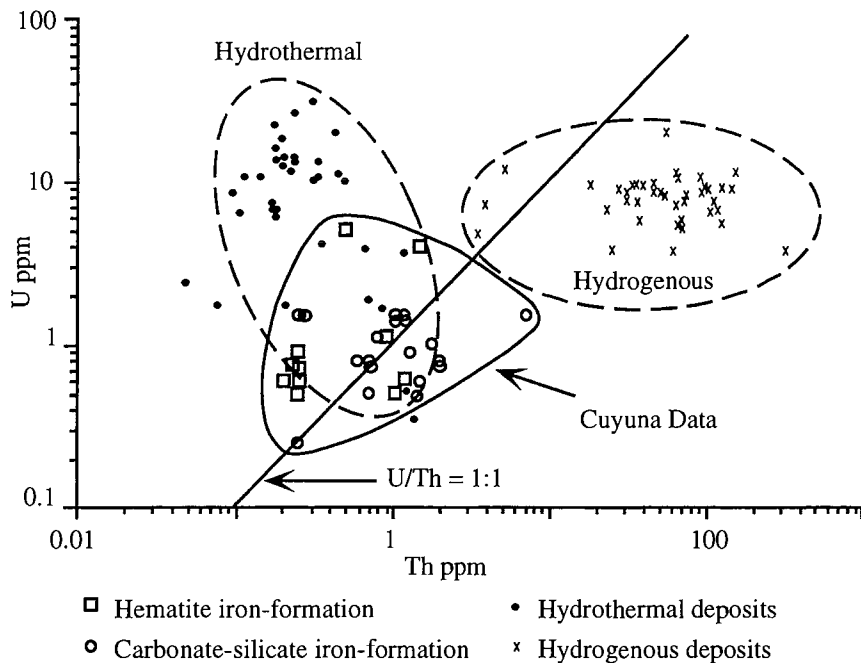

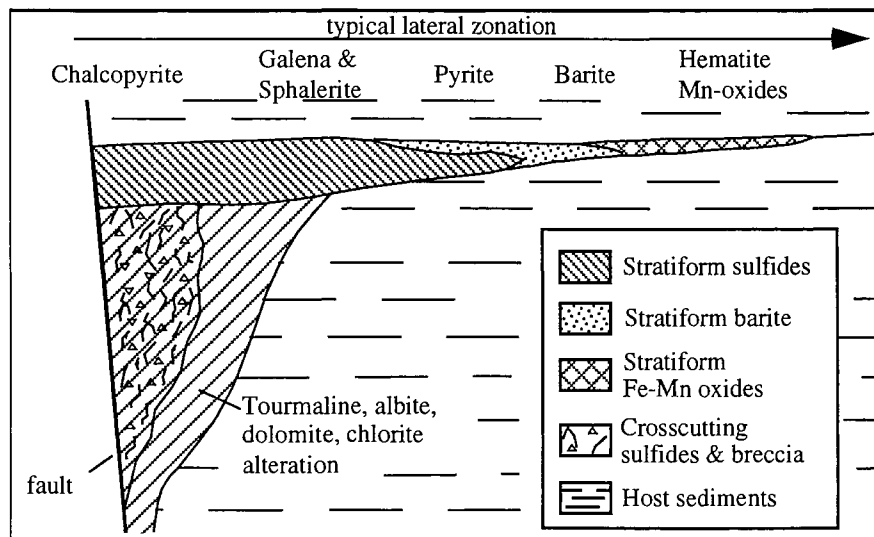Figure 28. Ratio of Fe/Mn/Ni+Co+Cu in the Trommald Formation (modified from Bonatti, 1975).

51

Figure 29. Ratio of U/Th in the Trommald Formation as compared to other metalliferous deposits from the ocean floor (modified from Bonatti, 1975).

□ Hematite iron-formation   • Hydrothermal deposits

○ Carbonate-silicate iron-formation   ˣ Hydrogenous deposits

CONCLUSIONS

The Cuyuna North range contains manganiferous deposits that are enormous in size, but low in grade in terms of extractable manganese content. Original models for the Trommald Formation assumed that it was one of several classic Lake Superior-type iron-formations of the Lake Superior region. The occurrence of aegirine and hyalophane in the iron-formation and associated barite and tourmalinites implies that the protoliths to the manganese iron ores have a marked exhalative hydrothermal component. It is possible that these rocks could be prime exploration targets for Pb-Zn-Ag deposits. Though the area has undergone extensive mineral exploration in the past,

the exploration has been mostly limited to iron ore. Very little is known about the geology stratigraphically beneath the iron-formation itself.

REFERENCES CITED

Beltrame, R.J., Holtzman, R.C., and Wahl, T.E., 1981, Manganese resources of the Cuyuna range, east-central Minnesota: Minnesota Geological Survey Report of Investigations 24, 22 p.

Bonatti, E., 1975, Metallogenesis at oceanic spreading centers: Earth and Planetary Sciences Annual Review, v. 3, p. 401-431.

Figure 30. Model for sediment-hosted, submarine exhalative sulfide deposits (after Large, 1980; Brisky, 1986).

52

Briskey, J.A., 1986, Descriptive model of sedimentary exhalative Zn-Pb, *in* Cox, D.P., and Singer, D.A., eds., Mineral Deposit Models: U.S. Geological Survey Bulletin 1693, p. 211-213.

Cleland, J.M., Morey, G.B., and McSwiggen, P.L., in press, Significance of tourmaline-rich rocks in the North range group of the Cuyuna iron range, east-central Minnesota: Economic Geology.

Crerar, D.A., Namson, J., Chyi, M.S., Williams, L., and Feigenson, M.D., 1982, Manganiferous cherts of the Franciscan assemblages: I. General geology, ancient and modern analogues, and implications for hydrothermal convection at oceanic spreading centers: Economic Geology, v. 77, p. 519-540.

Darby, D., 1972, Evidence of Precambrian life in Minnesota, *in* Sims, P.K., and Morey, G.B., eds., Geology of Minnesota: A centennial volume: Minnesota Geological Survey, p. 264-271.

Deer, W.A., Howie, R.A., and Zussman, J., 1978, An introduction to the rock forming minerals (2nd ed.): New York, Wiley, 528 p.

Door, J.V.N., II, Crittenden, M.D., Jr., and Worl, R.G., 1973, Manganese, *in* Probst, D.A., and Pratt, W.P., eds., United States Mineral Resources: U.S. Geological Survey Professional Paper 820, p. 385-399.

Essene, E.J., 1983, Solid solution and solvi among metamorphic carbonates with applications to geologic thermobarometry, *in* Reeder, R.J., ed., Carbonates: Mineralogy and chemistry: Reviews in Mineralogy, v. 11, p. 77-96.

Evensen, N.M., Hamilton, P.J., and O'Nions, R.K., 1978, Rare-earth abundances in chondritic meteorites: Geochimica et Cosmochimica Acta, v. 42, p. 1199-1212.

Goldich, S.S., Nier, A.O.C., Baadsgaard, Halfdan, Hoffman, J.H., and Krueger, H.W., 1961, The Precambrian geology and geochronology of Minnesota: Minnesota Geological Survey Bulletin 41, 193 p.

Goldsmith, J.R., and Graf, D.L., 1957, The system CaO-MnO-CO$_2$; solid solution and decomposition relations: Geochimica et Cosmochimica Acta, v. 11, p. 310-334.

_____1960, Subsolidus relations in the system CaCO$_3$-MgCO$_3$-MnCO$_3$: Journal of Geology, v. 68, p. 324-335.

Grout, F.F., 1941, Emergency reserves of manganese on the Cuyuna Range, Minnesota [abs.]: Economic Geology, v. 36, p. 848.

_____1946, Acmite occurrences on the Cuyuna Range, Minnesota: American Mineralogist, v. 31, p. 125-130.

Grout, F.F., and Wolff, J.F., 1955, The geology of the Cuyuna district, Minnesota: A progress report: Minnesota Geology Survey Bulletin 36, 144 p.

Harder, E. C., and Johnston, A.W., 1918, Preliminary report on the geology of east-central Minnesota, including the Cuyuna iron-ore district: Minnesota Geological Survey Bulletin 15, 178 p.

Heath, G.R., 1981, Ferromanganese nodules of the deep sea, *in* Skinner, B.J., ed., Economic Geology Seventy-Fifth Anniversary Volume, p. 736-765.

Holst, T.B., 1984, Evidence for nappe development during the early Proterozoic Penokean orogeny, Minnesota: Geology, v. 12, no. 3, p. 135-138.

Kimberley, M.M., 1989, Exhalative origin of iron-formations: Ore Geology Reviews, v. 5, p. 13-145.

Large, D.E., 1980, Geological parameters associated with sediment-hosted submarine exhalative Pb-Zn deposits: An empirical model for mineral exploration: Geologisches Jahrbuch, v. 40, p. 59-129.

Lewis, W.E., 1951, Relationship of the Cuyuna manganiferous resources to others in the United States, *in* Geology of the Cuyuna Range—Mining Geology Symposium, 3rd, Hibbing, Minnesota, 1951, [Proceedings]: Minneapolis, University of Minnesota, Center for Continuation Study, p. 30-43.

Likhoydov, G.G., 1981, Stability of the aegirine-quartz-hematite association, as shown by experimental data: Doklady Akademiya Nauk SSSR, v. 242, p. 174-176.

McSwiggen, P.L., 1993, Alternative solution model for the ternary carbonate system CaCO$_3$-MgCO$_3$-FeCO$_3$; II. Calibration of a combined ordering model and mixing model: Physics and Chemistry of Minerals, v. 20, p. 42-55.

McSwiggen, P.L., Morey, G.B., and Cleland, J.M., 1994a, The origin of aegirine in iron formation of the Cuyuna Range, east-central Minnesota: Canadian Mineralogist, v. 32, p. 589-598.

_____1994b, Occurrence and genetic implications of hyalophane in manganese-rich iron-formation, Cuyuna iron range, Minnesota, USA: Mineralogical Magazine, v. 58, p. 387-399.

Melcher, F., Morey, G.B., McSwiggen, P.L., Cleland, J.M., and Brink, S.E., 1996, Hydrothermal systems in manganese-rich iron-formation of the Cuyuna North range, Minnesota: Geochemical and mineralogical study of the Gloria drill core: Minnesota Geological Survey Report of Investigations 46 (in press).

Morey, G.B., 1990, Geology and manganese resources of the Cuyuna iron range, east-central Minnesota: Minnesota Geological Survey Information Circular 32, 28 p.

Morey, G.B., McSwiggen, P.L., Kuhns, M.J.P., and Jirsa, M.A., 1985, Analytical results of the public geologic sample program, 1983-1985 biennium: Minnesota Geological Survey Information Circular 22, 56 p.

Morey, G.B., and Morey D.D., 1986, Distribution of iron-formations in the main Cuyuna range, east-central Minnesota: Minnesota Geological Survey Miscellaneous Map M-60, scale 1:48,000.

Palmer, M.R., and Slack, J.F., 1989, Boron isotopic composition of tourmaline from massive sulfide deposits and tourmalinites: Contributions to Mineralogy and Petrology, v. 103, p. 434-451.

Rosenberg, P.E., 1967, Subsolidus relations in the system $CaCO_3$-$MgCO_3$-$FeCO_3$ between 350° and 550°C: American Mineralogist, v. 52, p. 787-796.

Schmidt, R.G., 1963, Geology and ore deposits of the Cuyuna North range, Minnesota: U.S. Geological Survey Professional Paper 407, 96 p.

Slack, J.F., and Coad, P.R., 1989, Multiple hydrothermal and metamorphic events in the Kidd Creek volcanogenic massive sulphide deposit, Timmins, Ontario: Evidence from tourmalines and chlorites: Canadian Journal of Earth Sciences, v. 26, p. 694-715.

Slack, J.F., Herriman, N., Barnes, R.G., and Plimer, I.R., 1984, Stratiform tourmalinites in metamorphic terranes and their geologic significance: Geology, v. 12, p. 713-716.

Southwick, D.L., and Morey, G.B., 1991, Tectonic imbrication and foredeep development in the Penokean orogen, east-central Minnesota—An interpretation based on regional geophysics and the results of test drilling: U.S. Geological Survey Bulletin 1904-C,D, p. C1-C17.

Southwick, D.L., Morey, G.B., and McSwiggen, P.L., 1988, Geologic map (scale 1:250,000) of the Penokean orogen, central and eastern Minnesota, and accompanying text: Minnesota Geological Survey Report of Investigations 37, 25 p.

Thiel, G.A., 1924, The manganese minerals; Their identification and paragenesis: Economic Geology, v. 19, p. 466-472.

Trendall, A.F., 1968, Three great basins of Precambrian banded iron formation deposition: A systematic comparison: Geological Society of America Bulletin, v. 79, p. 1527-1544.